A pilot study of seasonal and interannual patterns in the distribution of chlorophyll *a* and temperature over three areas of the southwest Indian Ocean: northeast Madagascar, southeast Madagascar and the Mascarene Islands.

KOMUL BHAVNAH

KMLBHA001

SUPERVISORS: EMERITUS PROFESSORS JOHN FIELD and FRANK SHILLINGTON and MR BEENESH MOTAH

Submitted in the partial fulfilment of the requirements for the degree of Master of Science (Applied Marine Science)

DEPARTMENT OF BIOLOGICAL SCIENCES

FACULTY OF SCIENCE

UNIVERSITY OF CAPE TOWN

JULY 2016

PLAGIARISM DECLARATION

- I know that plagiarism is wrong. Plagiarism is to use another's work and pretend that it is one's own.
- I have used the required convention for citation and referencing. Each contribution to and quotation in this assignment from the work(s) of other people has been attributed, and has been cited and referenced.
- This assignment is my own work.
- I have not allowed, and will not allow, anyone to copy my work with the intention of passing it off as his or her own work.
- I acknowledge that copying someone else's work, or part of it, is wrong, and declare that this is my own work.

SIGNATURE: Signed

DATE: 13/07/16

ACKNOWLEDGEMENT

To devise, write and construct this project was very demanding and challenging but also very interesting and instructive. I would like to thank the University of Cape Town and everyone who have helped and inspired me during this project.

Firstly, I would like to express my sincere gratitude to my supervisors Emeritus Professors John Field and Frank Shillington and Mr Beenesh Motah for their excellent guidance, supervision, valuable advice, patience and support which made this an enjoyable and interesting project and also for believing in me. Also, my most sincere thanks to Emeritus Professor John Field for arranging funding for my work.

Much appreciation goes to Charine Colins and Fehmi Dilmahamod who remained extremely patient throughout numerous questions of Matlab and guidance into scripts. Thank you to Emeritus Professor Derry Devine, Ms. Pavs Pillay and Dr. Cecile Reed for their constant support throughout the AMS course and project; to Christo Whitle, Sannassy Pilly Jyodee, Kevin Veerapen, Yuneeda Oozeerally, Ronie Francois, Brandon Foor, Yakshi Kistnah, Akshay Jankee, all my friends from both the AMS class 2014 and 2015 and everyone else for the valuable discussions, kind assistance and awesome company and support during the writing-up of this thesis.

I would also like to express my gratitude to the NATIONAL RESEARCH FOUNDATION (NRF) and the Postgraduate centre and Funding office of UCT for their financial support through the NRF Innovation Masters Scholarship that was awarded to me.

Most importantly, none of this would have been possible without the love and patience of my mum Deoranee Koossool, my brother Dharvesh Komul and my grandma Bhagwatee Koossool. They have been a constant source of love, support, encouragement and strength and I would like to express my heart-felt gratitude to them. Also, without God's grace and love, I would not have reached so far.

ABSTRACT

Remotely sensed weekly MODIS data of chlorophyll a (Chl-a) concentration, sea surface temperature (SST) and satellite altimetry data of Absolute Dynamic Topography (ADT) and geostrophic velocities are used to examine the seasonal and interannual patterns in the Chl-a concentration and SST over three pilot study areas of the southwest Indian Ocean, namely Northeast Madagascar, Southeast Madagascar and Mascarene Islands. The weekly and monthly climatology and the weekly means of each variables are assessed using image displays and time series from 2003 to 2014. It is found that there is a seasonal cycle of phytoplankton blooms occurring twice a year across northeast and southeast Madagascar. The two blooms occur during the summer monsoon and during the winter monsoon, respectively. Unlike these two areas, the Mascarene Islands area has only one bloom during the summer monsoon. There is a negative correlation between SST and Chl-a concentration across all three areas; when SST is high, Chl-a concentration is low and vice versa. Also, the current patterns showed that the two Madagascar study areas, are more physically dynamic than the Mascarene Islands region. Unlike the Masacarene region, the Madagascar regions are more affected by the forcing of the South Equatorial Current that splits into the Southeast Madagascar Current and Northeast Madagascar Current, thus causing displacement of surface water. New outcomes of this study are that the north Indian Ocean (north of 10^0S) is not the only area that is affected by the summer and winter monsoons but the areas south of 10^0S may also be indirectly affected by the monsoons. Across Northeast Madgascar region, the summer monsoon bloom is well spread over the area while the winter monsoon bloom is mostly coastal. Across the Southest Madagascar region, the summer monsoon bloom spreads from east to west while, the winter monsoon bloom spreads from west to east. The Mascarene region is less productive with higher sea surface height and weaker eddies compared to the other areas and the mixed layer depth is greater across the Mascarene region, thus less nutrients are injected to the euphotic zone and the weaker eddies result in less mixing and consequently in weak Chl-a production. This study should improve our understanding of the seasonal and interannual variability of the SST and Chl-a and the dynamics of the ADT and geostrophic velocities in these regions for improved management of fishery resources using an ecosystem approach to fisheries.

TABLE OF CONTENTS

CHAPTER 1: INTRODUCTION 1

1.1 INDIAN OCEAN 2

1.2 GEOSTROPHIC FLOW AND EDDY CHARACTERISTICS IN THE SOUTH INDIAN OCEAN 4

1.3 THE WIND REGIME IN THE INDIAN OCEAN: THE MONSOONAL CLIMATE 8

1.4 THE STUDY AREAS 9

1.4.1 THE MASCARENE ISLANDS 9

1.4.2 MADAGASCAR 11

1.5 Chl-a AS INDICATOR OF PHYTOPLANKTON CONCENTRATION 13

1.6 RESEARCH AIMS 17

1.7 SPECIFIC OBJECTIVES 18

CHAPTER 2: METHODOLOGY 19

2.1 DATA SOURCES 19

2.2 SOFTWARE USED 25

2.3 DATA PROCESSING 26

CHAPTER 3: RESULTS 29

SECTION 1. Northeast Madagascar, NEM (AREA 1) 30

SECTION 2. Southeast Madagascar, SEM (AREA 2) 46

SECTION 3. Mascarene Islands, MI (AREA 3) 63

CHAPTER 4: DISCUSSION 74

Northeast Madagascar, NEM (AREA 1) 74

Southeast Madagascar, SEM (AREA 2) 77

Mascarene Islands, MI (AREA 3) 78

CHAPTER 5: CONCLUSION 81

CHAPTER 6: REFERENCES: 83

CHAPTER 7: APPENDIX 92

CHAPTER 1 INTRODUCTION

In aquatic systems primary productivity is mostly contributed by unicellular organisms, namely phytoplankton which manufacture organic compounds through photosynthesis. Phytoplankton constitute the basis of the marine food web and are major drivers in the cycling of various elements. One major factor affecting phytoplankton production is the ocean-atmosphere interaction. The ocean and the atmosphere interact with each other by exchanging heat, moisture and momentum causing the ocean's surface circulation and that of the lower atmosphere to be closely coupled (Raymont 1980). Furthermore, the most dynamic and changing portion of the marine environment is the mixed layer given that it links the ocean to the atmosphere and is also a determining factor of primary productivity (Narvekar and Kumar 2014).

According to Kantha and Clayson (2003), the mixed layer depth (MLD) is usually tens of meters deep and has uniform temperature, salinity and density as it is well mixed; below the mixed layer, are found the thermocline, halocline, and pycnocline where these variables change quickly with depth. The mixed layer is further important for the production of phytoplankton in that it receives strong enough solar insolation to drive photosynthesis (Kantha and Clayson 2003). The supply of macronutrients such as nitrates and phosphates from below the thermocline usually determines the spatial patterns of primary productivity (Pennington et al. 2006) and the depth of the thermocline varies with the strength of winds (Hermes and Reason 2008), hence influencing the primary productivity. In addition to the variations in thermocline depth, the surface temperature is also often associated with variations in phytoplankton production (Fiedler and Talley 2006). Thus, the analysis of the patterns in surface temperature and Chl-*a* can give us a good idea of the productivity of an area.

Since the wind drives the upper layer current circulation across the ocean, the latter also determines the patterns of primary productivity in the ocean. This study is concerned with the westward flowing Indian Ocean South Equatorial Current (SEC) (Fig 1.2) which splits at the east coast of Madagascar near 17^0 S to form the Northeast and Southeast Madagascar Currents (NEMC and SEMC) (Tomczak & Godfrey 2003; Schott et al. 2009) which in turn

affects the present study areas (Northeast Madagascar, Southeast Madagascar and Mascarene Islands).

Space based remote sensing is important for this study as it provides broad scale measurements of ocean properties with high spatial (down to 1 km pixels) and temporal (daily to weekly composites) resolution, allowing the highly dynamic nature of the ocean surface and its properties to be observed and studied. Remote sensing has allowed scientists to study the variability of surface Chl-*a*, hence primary productivity, on a global and regional scale for nearly two decades. In this study, the influences of the absolute dynamic topography (ADT) and geostrophic velocities on the ecosystem will be considered and ultimately emphasis will be put on how the Chl-*a* and the sea surface temperature in the Northeast Madagascar, Southeast Madagascar and Mascarene Islands regions varies seasonally and interannually.

Marine phytoplankton plays an important role in sustaining the world's marine ecosystems and fisheries given that primary productivity is a good indicator of the health of the marine ecosystem and the fisheries' stock. Hence, this study will be beneficial for the successful management of the marine ecosystems and ecological processes in the studied regions.

1.1 INDIAN OCEAN

The Indian Ocean (IO) being the smallest of all the Oceans has a north-south stretch of 9600km from Antarctica to the inner Bay of Bengal and a stretch of 7800km in east-west direction between southern Africa and western Australia (Fig. 1.1) (Tomczak & Godfrey 2003). Additionally, the IO is divided into three fragments of about the same size by two ridge systems, which are the *Central Indian Ridge*, a northward extension of the interoceanic ridge system between the western and central part of the IO and the *Ninety East Ridge* which extends in an approximately perfect north-south orientation from the Andaman Islands to 33^0 S (Fig. 1.1) and they run through the IO in a roughly meridional direction (Tomczak & Godfrey 2003).

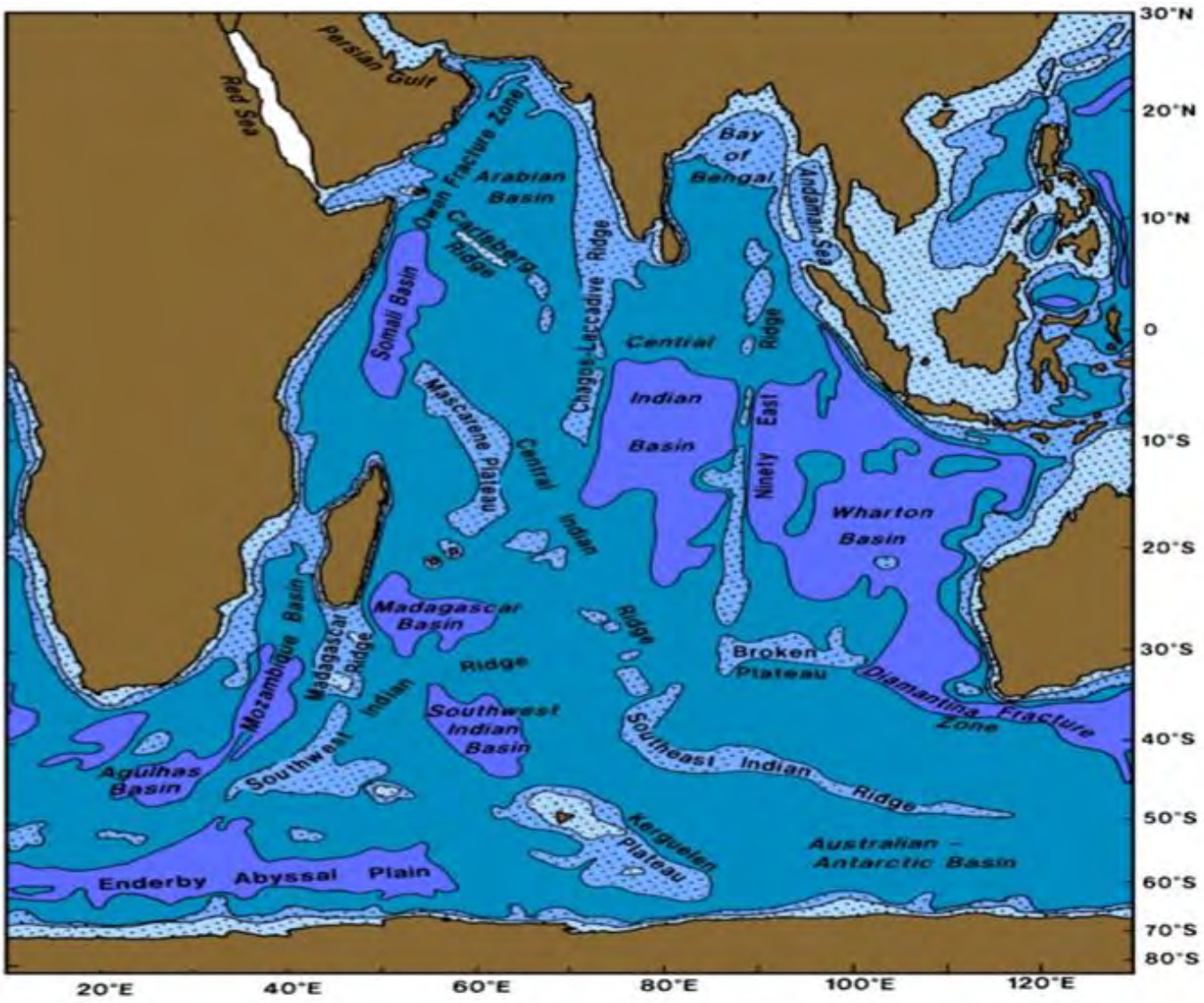

Fig. 1.1 Topography of the Indian Ocean (from Tomczak & Godfrey, 2003)

Unlike in the Atlantic and Pacific Oceans, it does not connect to both the North and South poles but only to the South through the Southern Ocean, as it is land-locked by the presence of Asia as its northern boundary, thus preventing northward heat export from the tropics to the high latitudes resulting in the highest mean sea surface temperature on Earth. The irregularity in the Indian Ocean's structure and circulation caused by this exceptional topography (Qasim 1999) drives the strong monsoon circulation which in turn drives the seasonal evolution of the Indian Ocean's currents and the location of the upwelling regions (Hong et al. 2012).

The interactions with the atmosphere display numerous modes of climate variability both regionally and worldwide in tropical Indian Ocean (Schott et al. 2009). The rising branch of the IO Walker circulation is the cause of the absence of steady equatorial easterlies in the IO (Schott et al. 2002) and it is the only ocean which has annual-mean westerly winds on the equator which results in a flat and deep equatorial thermocline (Xie et al. 2002), producing no climatic equatorial upwelling in the eastern ocean (Schott et al. 2002). However, upwelling occurs in the Northern Hemisphere, more precisely off the coast of Somalia, Arabia and India which usually occurs only during the summer monsoon while in the Southern Hemisphere upwelling occurs near the expiration of the south-east trades as well as along the Sumatran/Javan west coast (Schott et al. 2002).

1.2 GEOSTROPHIC FLOW AND EDDY CHARACTERISTICS IN THE SOUTH INDIAN OCEAN

The South Indian Ocean (SIO) has unique current systems which is characterised by the South Equatorial Current (SEC) which is supplied by the Indonesian Through flow (ITF) as shown in Fig. 1.2 below. When the SEC reaches the east coast of Madagascar near 17^0S, it splits into the Northeast Madagascar Current (NEMC) and Southeast Madagascar Current (SEMC) (Schott et al. 2001, 2009). The NEMC splits into the northward and southward flows at about 12^0S after flowing from the north tip of Madagascar at Cape Amber to the coast of Tanzania. The northward branch of NEMC then splits into the East African Coast Current (EACC) and the southward branch that connects the Mozambique Channel through flow with anticyclonic eddies (Schouten et al. 2003).

The SEMC travels to the southern tip of Madagascar, where it casts a succession of eddies and dipoles migrating to the African coast where further south they generate eddies of the Agulhas retroflection, affecting the transmission of IO waters into the Atlantic (Tomczak & Godfrey 2003, Schott et al. 2009, Quartly et al. 2006). It has further been suggested by Lutjeharms et al. (1981) that the SEMC does not seem to continue over to the east coast of Africa but appears to end in a retroflection regime with high eddy energy and weak mean flow to the southwest of Madagascar which might even supply the NEMC. The SEMC alters the

transportation of IO waters into the Atlantic since it is observed to retroflect and discharge eddies and filaments, which act as a source for the Agulhas Current System. The eastward outflow from the Agulhas retroflection re-enters the IO as an extensive north-eastward flow, which extends mostly to the west coast of Australia and part of it also recirculates north-westward into the SEC.

The East Gyral Current (EGC) is a persistent eastward current that is supplied by the recirculation of the ITF and the SEC as well as by the northeastward flow which extends to the Agulhas retroflection. The two seasonally reversing currents in the IO are the Somali current which occurs due to changes in the wind stress curl over the tropical Indian Ocean associated with the monsoon (Schott et al. 2009) and the Southwest/Northeast Monsoon Current (Tomczak & Godfrey 2003, Schott et al. 2009) south of India/Sri Lanka. The Somali current flows towards the north during the summer monsoon (austral winter) and turns into a southward flow during the winter monsoon (austral summer) which then supplies the South Equatorial Countercurrent (SECC) which flows east across the whole Indian Ocean (Schott et al. 2009). Additionally, the semiannual westerly equatorial winds gives rise to Wyrtki Jets (WJs) which are the manifestation of strong eastward surface jets during the intermonsoon periods (Tomczak & Godfrey 2003, Schott et al. 2009) and are unique to the IO. Their impact are felt well off the equator when they reflect from the eastern boundary of the basin as they create bursts of coastal Kelvin and Rossby waves and further influence the upwelling regime off Sumatra. (Schott et al. 2009).

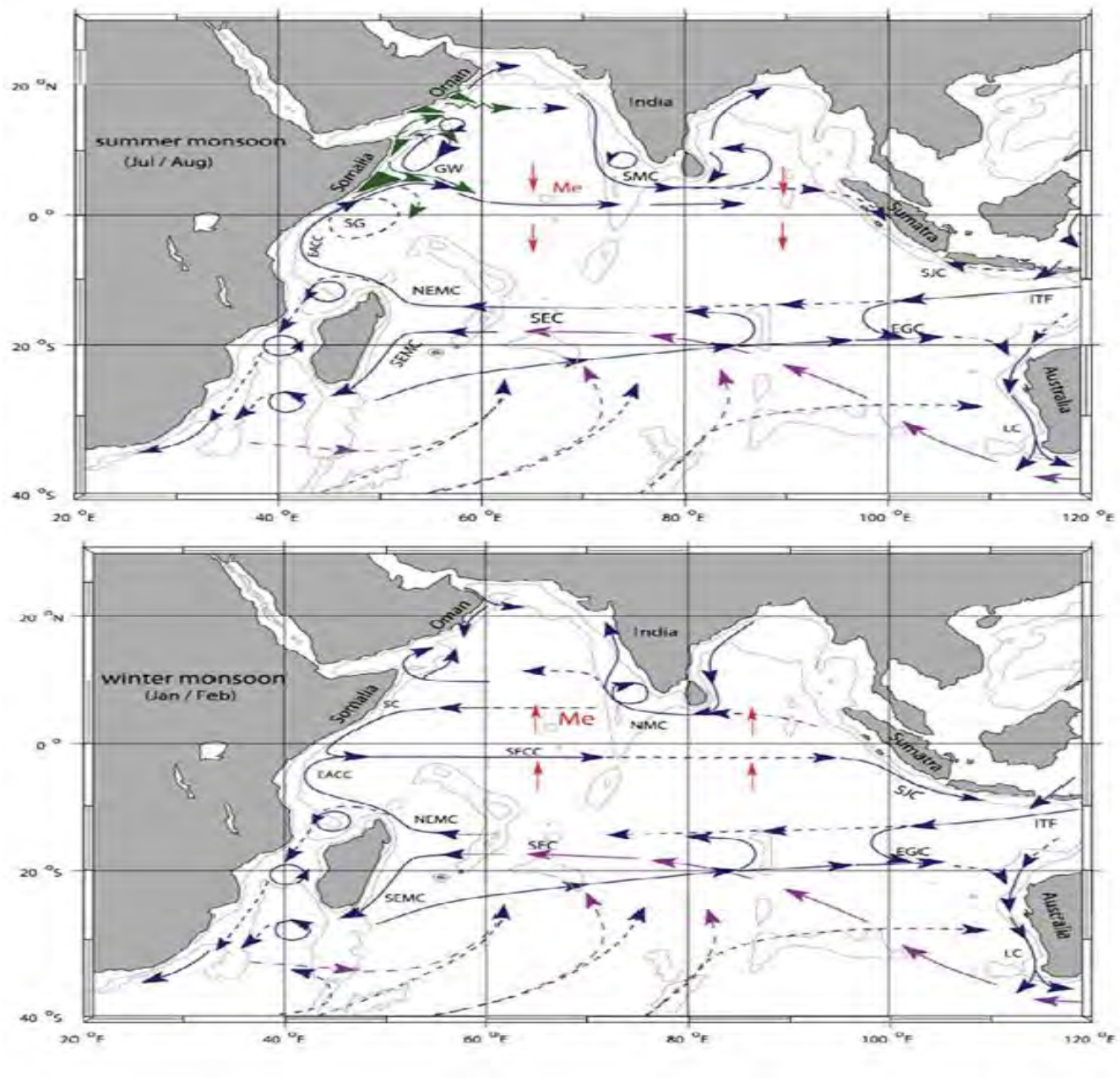

Fig. 1.2. The Schematic representation of identified current branches during the summer monsoon (southwest monsoon) and winter monsoon (northeast monsoon). Current branches shown are that of the South Equatorial Current (SEC), South Equatorial Countercurrent (SECC), Northeast and Southeast Madagascar Current (NEMC and SEMC), East African Coastal Current (EACC), Somali Current (SC), Southern Gyre (SG) and Great Whirl (GW) and associated upwelling wedges (green shades), Southwest and Northeast Monsoon Currents (SMC and NMC), South Java Current (SJC), East Gyral Current (EGC), and Leeuwin Current (LC). The subsurface return flow of the supergyre is shown in magenta. Depth contours shown are for 1000 m and 3000 m (grey); red vectors (Me) show directions of meridional Ekman transports. ITF indicates Indonesian Throughflow. (From Schott et al.2009).

McWilliams (2013) suggested that mesoscale eddies are the main suppliers of essential material and dynamical fluxes for the balanced stabilities of the overall circulation and climate since they generates heat and salt transports (Volkov et al. 2008) and the extent of zonal mass transport driven by eddies can be compared with that of large-scale circulation (Zhang et al. 2014). Crawford et al. (2005) also mentioned that the nutrient flux into the euphotic zone are regulated by mesoscale eddies, through vertical and horizontal mixing. Lévy and Klein (2004) added that the biogeochemical budgets are supplemented by strong upwelling of nutrients, when plankton is drawn down and by horizontal mixing caused by submesoscale eddies.

Morrow et al. (2004) used altimetry measurements to show that in the Southeast Indian Ocean, the anticyclonic eddies proliferate westward and equatorward, while the cyclonic eddies proliferate poleward. In austral spring the vertical velocity shear is intensified as there is an enhanced heat flux forcing that is combined with meridional Ekman geostrophic convergence which causes the upper ocean meridional temperature gradient to strengthen. This intensification of the vertical velocity shear alters the strength of the baroclinic instability linked with the surface-intensified South Indian Countercurrent (SICC) and the essential SEC system, causing the seasonal disparities of the eddy kinetic energy (EKE) which is at its maximum in austral summer and a minimum in austral winter (Jia et al. 2011). Using cruise data de Ruijter et al. (2004) showed that across the Southwest of Madagascar, the anticyclonic eddies promulgated principally westward, whereas cyclonic eddies deviated further between west and southwest (Fig. 1.3.(a)). Quartly et al. (2006) also showed that a number of westward-propagating eddies flow along the zonal band near 25^0S (Fig. 1.3) by using altimetry and sea surface temperature data.

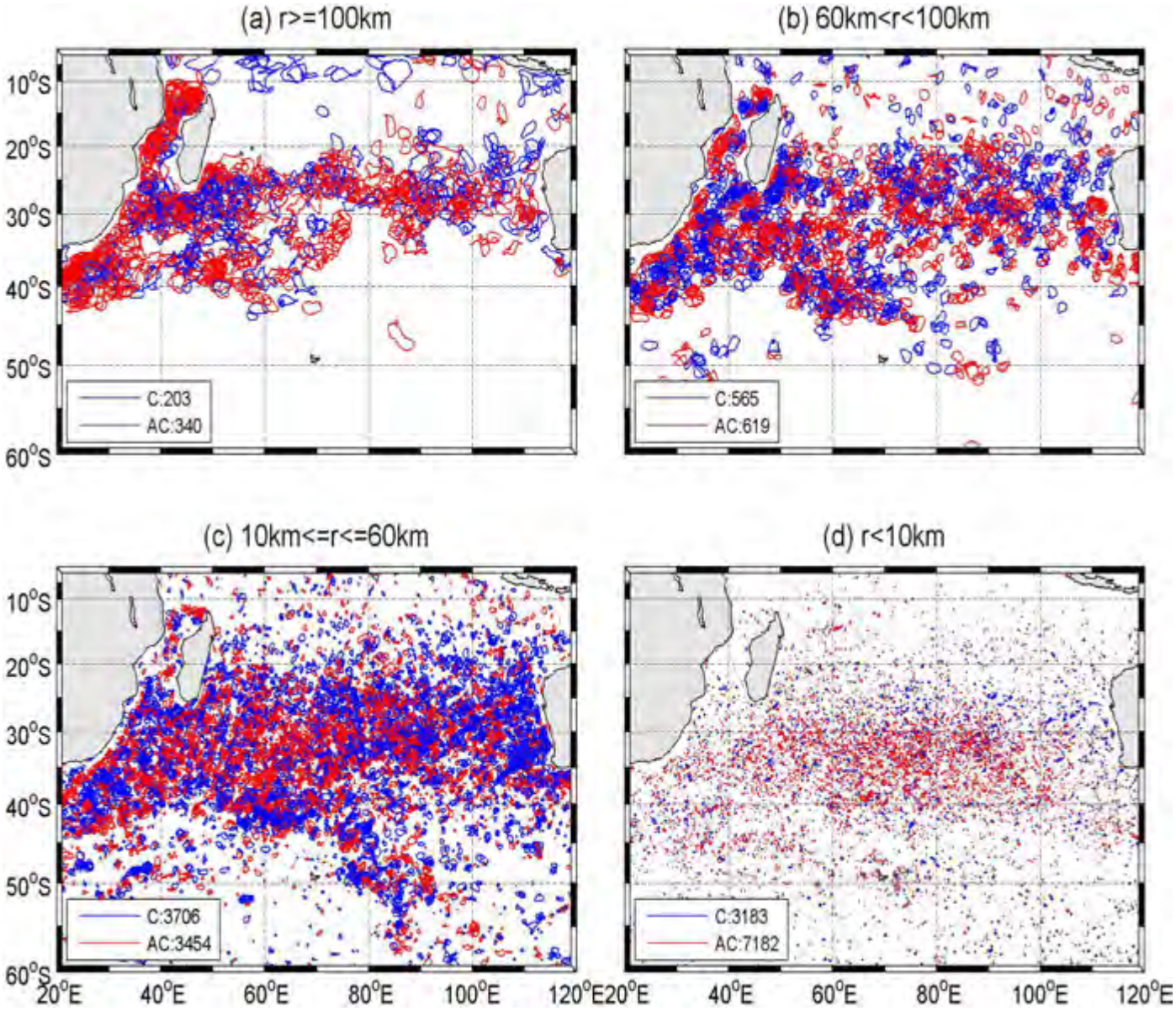

Fig. 1.3. The distribution of cyclonic (blue lines) and anticyclonic (red lines) eddies detected from drifters in the SIO (images from Zheng et al. 2015).

1.3 THE WIND REGIME IN THE INDIAN OCEAN: THE MONSOONAL CLIMATE

The Northern Indian Ocean is governed by the monsoonal climate which also affects the subtropics of the southern hemisphere. The Trade winds north of 10^0S reverse direction twice a year over the IO consequently determining the climate of that region (Shankar et al. 2002). During the summer monsoon (May–September), the Summer Monsoon Current

(SMC) flows eastward and during winter monsoon (November-february), the Winter Monsoon Current (WMC) flows westward. Also, according to Hermes and Reason (2008) the South-easterlies that are present south of about 10°S, throughout the year, happen to extend further north and are stronger exceptionally in austral winter. Additionally, the South easterlies only extends to around 13°S with monsoonal westerlies between 5°S and 11°S in austral summer. The winds blowing from the southwest during June-September (Boreal Summer/Austral Winter) are known as the Summer Monsoon and the winds blowing from the northeast during December-March (Boreal winter/Austral summer) are known as the Winter Monsoon. The winds are much stronger during the Summer Monsoon than during the Winter Monsoon and March-April and October are the transition months where the winds are weak (Shankar et al. 2002). A seasonally reversing circulation in the upper ocean over the north IO is forced by the seasonally reversing monsoon winds (Shankar et al. 2002).

1.4 THE STUDY AREAS

1.4.1 THE MASCARENE ISLANDS

The Mascarene Islands namely Reunion, Mauritius and Rodrigues Island lie between 19^0 and 22^0 S and between 55^0 and 64^0 E at the Southern end of the Mascarene Plateau (Fig. 1.4). Reunion Island which rises 7000m from the ocean floor is formed by two volcanoes, the inactive Piton des Neiges and the active Piton de la Fournaise. Mauritius Island found to the northeast of Reunion is an eroded volcanic island which is believed to have been built by three eruptive episodes. The third Island which is Rodrigues Island lies at the eastern end of the east west Rodrigues Ridge, about halfway between Mauritius and the Central Indian spreading ridges (McDougall 1971, Duncan et al. 1990).

The Mascarene Plateau which is an important feature in the Indian Ocean, affects the ocean dynamics across the Mascarene and adjacent islands. It is located in the South Western part of the Indian Ocean and is comprised of a series of shallow banks or ‘shoals’ separated by deeper ridges and channels (New et al. 2005). It lies east and northeast of Madagascar and the Crescent shape of the plateau starts from the Seychelles Bank southward through Saya de Malha, Nazareth, and Cargados Carajos Banks to Mauritius and it extends for 2300km (Fisher et al. 1967) oriented roughly north–south (New et al.2005). The prominent irregularity

of the topography of the Plateau southeast of the intersection of the Rodriguez Ridge with the Mascarene Plateau, is attributed to volcanism and block faulting. At this intersection, extending in the same direction to the Mauritius trench and to the southwest branch of the Mid-Indian Ocean Ridge lie the linear, marginally sedimented deeps and narrow ridges (Fisher et al. 1967).

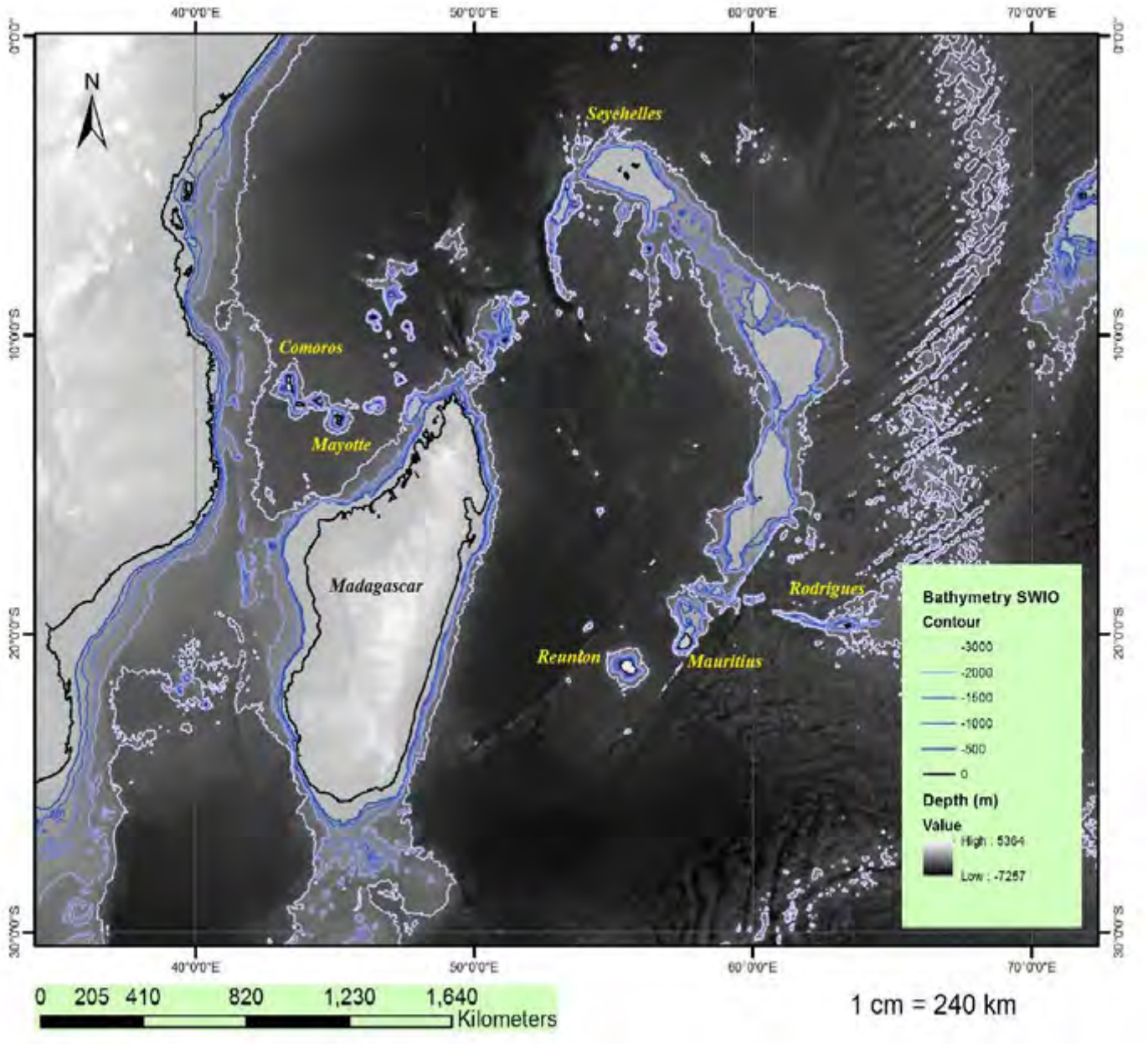

Fig. 1.4. The South West Indian Ocean including the Mascarene Plateau, the Mascarene Islands and Madagascar (Photo produced using the ETOPO 2 bathymetric grid dataset from the ETOPO2v2 (2006)).

1.4.2 MADAGASCAR

Madagascar is the fourth largest Island in the world with about 1580 km in length and 570 km wide (Conway 2005). It is located between the latitudes 12^{o}S and 26^{o}S and the longitudes 43^{o}E and 51^{o}E in the southwestern Indian Ocean (Figs.1.1 & 1.2). Its west coast faces eastern Africa and the Indian Ocean encircles the other 3 sides. It is separated from Africa by the Mozambique Channel. The East Madagascar Current (EMC) which originated from the South Equatorial Current is a western boundary current. It closely follows the continental shelf east of Madagascar from 17^{o}S till it reaches the southern tip of the island (Fig. 1.5) and it induces upwelling along the south coast of the Island when it deviates from the coast (Ho et al.2004).

An equatorial climate influences the northern part of Madagascar while the south experiences subtropical and temperate climates. Most of the precipitation is on the east and north given that the trade winds prevail from the east and monsoons from the northwest. The wet season is from November to March and in the wettest regions the annual precipitation can reach 360 cm which can lead to large river outflows, carrying extremely heavy sediment loads (Conway 2005).

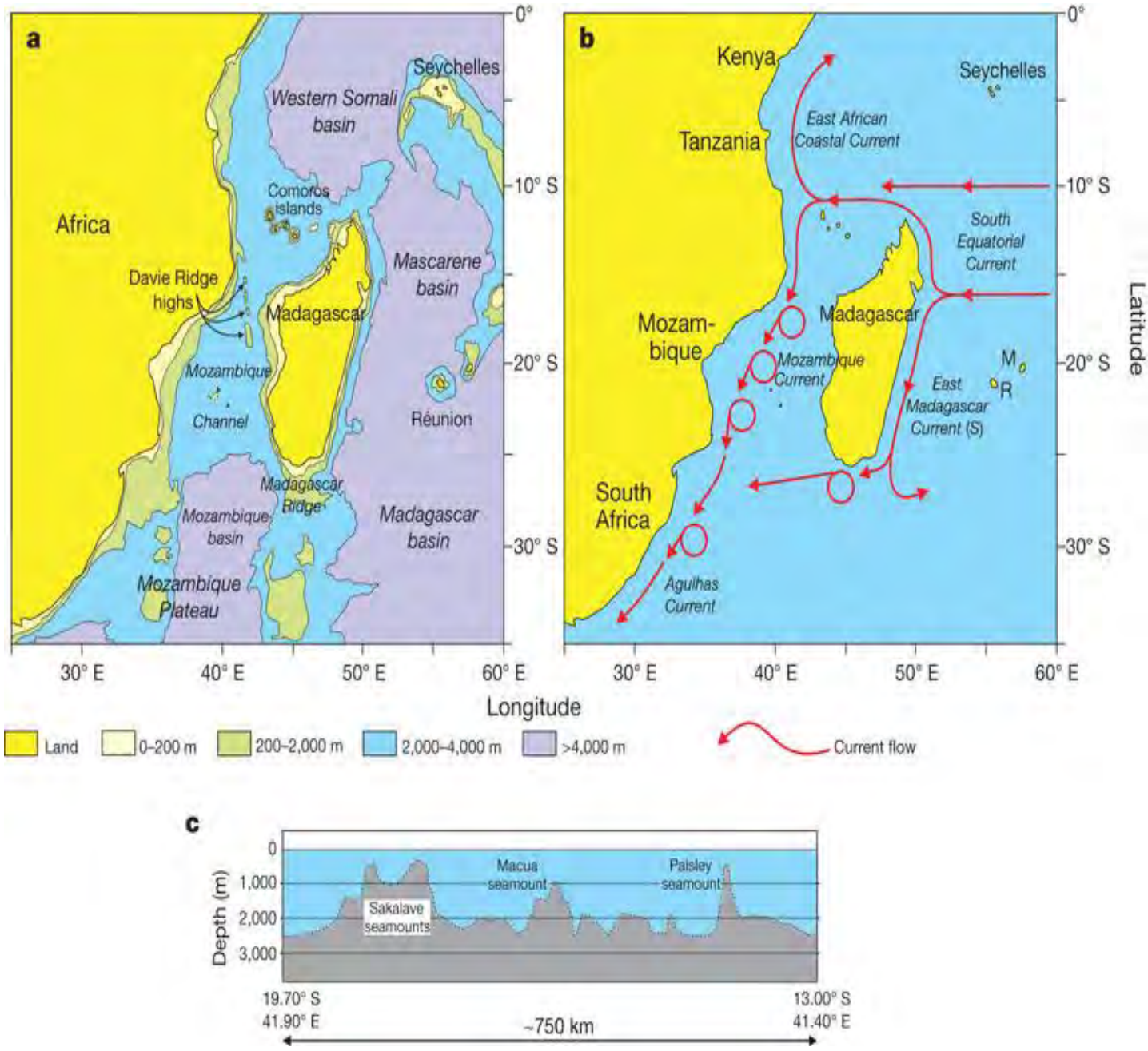

Fig.1.5. (a) Simplified bathymetric map. (b) Present-day surface-water circulation. (c) Bathymetric cross-section along the Davie Ridge (from Ali and Huber 2010).

1.5 Chl-a AS INDICATOR OF PHYTOPLANKTON CONCENTRATION

Phytoplankton such as diatoms (Order: Bacillariophyceae), dinoflagellates (Order: Dinophyceae), silicoflagellates and coccolithophorids are unicellular photosynthetic organisms that dominate the pelagic ecosystems that cover 70% of the world's surface area (Reynolds 2006). Furthermore, they are phototrophs as they use light energy from the sun to combine water and carbon dioxide into organic compounds such as carbohydrates through the process of photosynthesis which makes them the major primary producers of organic carbon in pelagic waters and they represent the base of the pyramid of productivity (Newell and Newell 1977).

During photosynthesis the conversion of light to chemical energy closely depends upon Chl-*a* and along with other pigments such as carotenes and xanthophylls, chlorophylls are also contained in the chloroplasts for most algae and the Chl-*a* occurs in all groups of algae including phytoplankton. Chlorophylls have their maximum absorption in the red (650-700 nm) and in the blue-violet (ca. 450 nm) ranges of the spectrum (Raymont 1980). Given that phytoplankton use the pigment chlorophyll to harness light energy for photosynthesis, a reliable predictor of phytoplankton density would be the measurement of Chl-*a* concentrations. This is why Chl-*a* measurements are used to estimate phytoplankton concentrations on local, regional and global scales (European Commission DG Environment News Alert Service October 2010).

The mapping of phytoplankton distribution in the ocean was made possible in the 1960s with the introduction of rapid spectrophotometric and fluorometric methods (Vaulot 2006). Vaulot (2006) also mentions that nowadays optical measurements of *in vivo* fluorescence are used instead as they allow real-time continuous monitoring of phytoplankton distribution. Such monitoring could be done by remote sensing from space and the optical properties of Chl-*a* are important for this purpose. In 1978 the first spaceborne ocean color sensor, the CZCS (Coastal Zone Color Scanner) was launched and provided data for 8 years (1978-1986). Since then other sensors has been launched such as SeaWiFS (Sea Wide Field-of-view Sensor) in 1997 and MODIS (Moderate Resolution Imaging Spectroradiometer) in 1999 and in 2002 (Alvain et al. 2005). These sensors provide Chlorophyll Ocean images globally or over a specific area in near real time that help scientists to monitor phytoplankton dynamics

more easily (Vaulot 2006). Additionally, the Chl-*a* used as a proxy for the phytoplankton (algae and photosynthetic cyanobacteria) biomass is actually the sum of the Chl-*a* and phaeophytin *a* concentrations. This so-called "Chl-*a* concentration" Chl-*a,* is estimated after the atmospheric correction is done for the blue-to-green ratio of water-leaving radiances (Alvain et al. 2005).

Most marine living organisms of higher trophic levels are directly or indirectly dependent on phytoplankton for energy supply, although there are some chemotrophic organisms inhabiting deep-sea vents (Sorokin et al. 2003). Marine phytoplankton are by far the most important producer of organic substances. Phytoplankton lie at the base of the pyramid of the marine food webs leading to fish and whales, through the mediation of largely crustacean herbivores (Vaulot 2006). The basic primary productivity of the ecosystem is determined by the rate at which phytoplankton store energy. They can at times produce their own weight of new organic materials within 24 hours, which is a rate much greater than can be reached by terrestrial plants (Chandy et al. 1991).

Additionally the distribution and abundance of diatoms in marine environments creates a favorable environment for active growth and survival of other organisms as they are the important group of phytoplankton. The population density of marine animals and their reproductive cycles are very often associated with the abundance of phytoplankton on which those animals themselves and/or their offspring are dependent for nutrition. Furthermore given that diatom cell abundance and Chl-*a* increase quickly and then drop back through grazing by zooplankton, diatom-based food webs often fluctuate and give rise to successional patterns in the phytoplankton. It is also important to understand the physical processes that are responsible for Chl-*a* distribution since economies of many coastal states depend on their biological productivity through fishery resources and marine industries (Schott et al. 2009). Also the distribution and variability of phytoplankton will control the population of fisheries through zooplankton availability and further affect the breeding of seabirds (Monticelli et al. 2007) as many feed on fish or zooplankton.

Marine phytoplankton play a significant part in the ocean carbon cycle and associated carbon fluxes as they use dissolved inorganic carbon (DIC) to produce organic matter such as particulate organic carbon (POC) and particulate inorganic carbon (PIC) which are recycled

in the water column itself or transported to sediments (Alvain et al. 2005, Stramski et al. 1999). Likewise according to Vaulot (2006) there is rapid distribution of photosynthetic carbon to the deep ocean since there are substantial losses at each step in the diatom-based food webs.

Primary productivity is not only affected by nutrient availability, but also by other factors such as light, mixed layer depth, climatic conditions etc.…Nutrient input can be affected by upwelling, and horizontal advection. Levy et al. (2007) used the general ocean circulation model (OGCM) to derive dynamical features such as the horizontal and vertical velocities and mixed-layer depth to compare the bloom patterns occurring in the Indian Ocean. He observed that the regional formation of the blooms is closely associated with these features driven by the monsoons (Fig. 1.6). Photosynthesis in the marine environment is driven by the visible light or photsynthetically active radiation (PAR) (400 to 700 nm) (Gao et al. 2012) which is absorbed by Chl-*a* and other pigments found in algae (Thomas 2013) .The quantity and quality of light transmission to the depths is influenced by factors such as the scattering of light by bubbles and suspended particles in the water as well as by the phytoplankton themselves (Thomas 2013), thus making photosynthesis in the marine environment more dynamic than in the terrestrial environment (Gao et al. 2012).

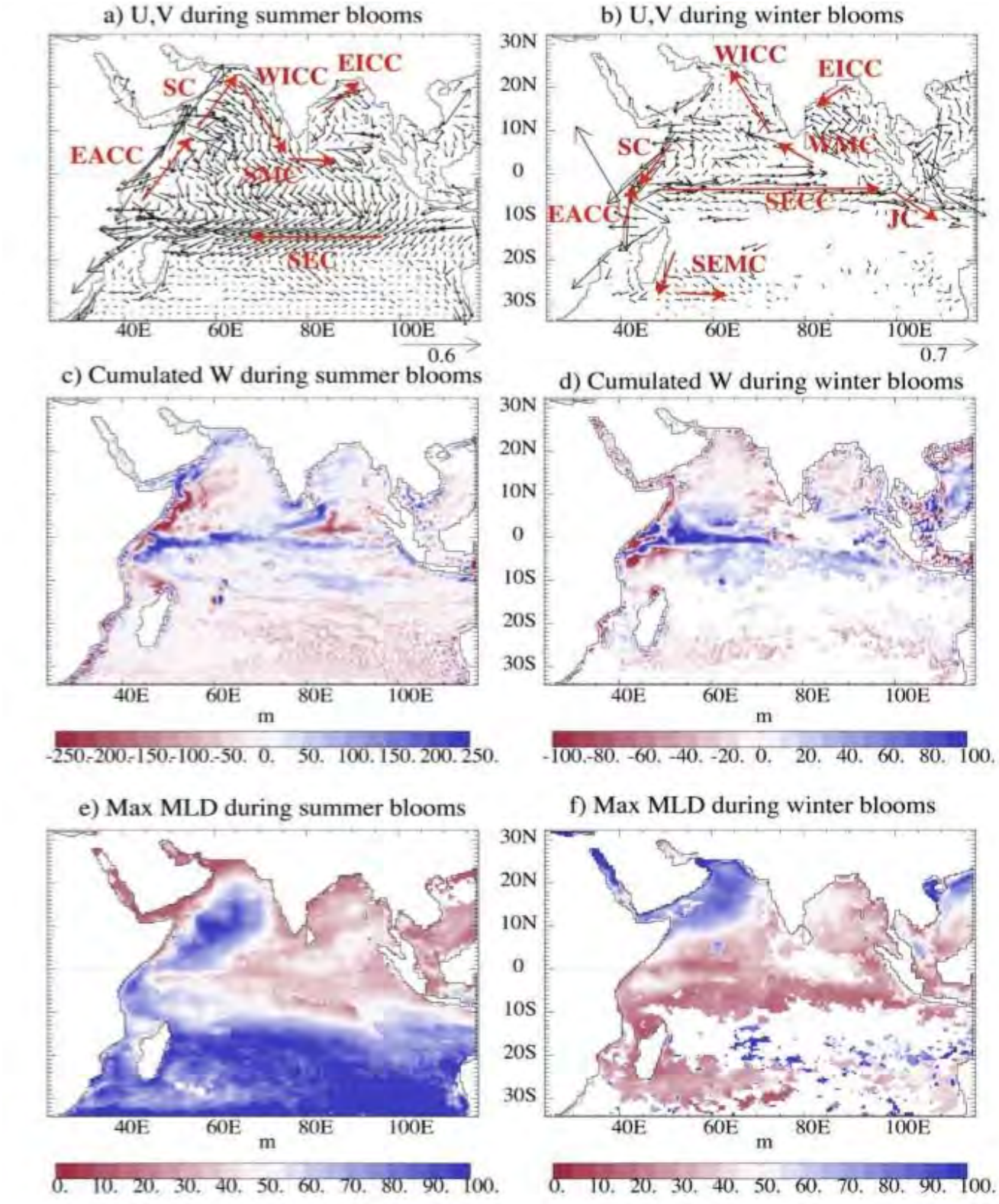

Fig. 1.6. North Indian Ocean and Northeast Madagascar. a) & b) are the mean horizontal currents averaged over 0-30m (U-V); c) & d) are the time-cumulative vertical velocity at 30m (positive values are upwelling and negative values are downwelling) and e) & f) are the maximum mixed-layer depth (MLD) during the summer and winter blooms (from Lévy et al.2007).

Furthermore, according to Saji et al. (1999) the interannual variability related with El Niño–Southern Oscillation (ENSO) and Indian Ocean Dipole (IOD) strongly contributes to the basin-wide surface Chl-*a* variability. Likewise, the study of the impact of climate modes on the variability of Chl-*a* can also contribute to the understanding of primary productivity within different regions of the world. Additionally, unlike the Pacific and Atlantic oceans, the Indian Ocean has a unique biogeochemical variability (Wiggert et al. 2006) which is affected by two distinct features. Firstly, in the north it is land-locked by Asia which prevents thermocline ventilation and contributes to iron dust deposition. Secondly, strong annual monsoon cycles influence the seasonality of ocean currents and the locations of upwelling (Hong et al. 2012). The local biodiversity and climate can be considerably influenced by small variability in the mean sea surface temperature in the Southern Tropical Indian Ocean (STIO) (Schott et al. 2009).

1.6 RESEARCH AIMS

This work aims to describe the variability of Chl-*a* concentrations using remotely-sensed data of sea surface temperature (SST) and surface Chl-*a* for three regions of the South-West Indian Ocean: 1) to the northeast of Madagascar, 2) to the southeast of Madagascar and 3) the Mascarene Islands (Rodrigues, Mauritius and Reunion). To further describe the variability of Chl-*a* concentrations by associating it with remotely-sensed data of Absolute Dynamic topography (ADT) and geostrophic velocities.

First, the seasonal variability of the SST and Chl-*a* concentrations will be estimated using 8-day composite data and afterwards the inter-annual variability will be calculated. These data will also be used to determine the monthly and weekly climatology of both the SST and Chl-*a* concentrations to have an idea of the patterns occurring across the different months and weeks of a year which will further give an idea on the seasonality and interannual patterns. Additionally, weekly (7-day composites) absolute dynamic topography and geostrophic current data will also be used to assess their effect on the patterns of the SST and the Chl-*a* concentrations within the study areas.

1.7 SPECIFIC OBJECTIVES

Interpretation of Moderate Resolution Imaging Spectroradiometer (MODIS) data and Satellite Altimetry data;

Assessment of the variability of the Sea Surface Temperature (SST) in the study regions on seasonal and interannual time scales.

Assessment of the variability of Chl-a in the study regions on seasonal and interannual time scales.

Assessment of the effects of absolute dynamic topography and geostrophic currents on the patterns of SST and Chl-a concentrations in the study regions.

CHAPTER 2 METHODOLOGY

2.1 DATA SOURCES

Below is a brief description of the data sets used for this study; more details on the data sources and how the data set are processed are available on the Ocean Color (http://oceancolor.gsfc.nasa.gov/cms/) and AVISO (http://www.aviso.altimetry.fr/en/my-aviso.html) websites. The observed data used in this study are the 8-day composite sea surface temperature (SST, °C) and Chl-*a* concentration (Chl-*a*, mg/m^3) obtained from the satellite based ocean color sensor Aqua MODIS, acquired from the Ocean Color Website and the weekly (7-day composite) Absolute Dynamic topography (ADT) and Geostrophic velocities obtained from the AVISO Website for the period January 2003 to December 2014.

The Aqua MODIS Chl-*a* and SST data sets:

The fundamental instrument MODIS (Moderate Resolution Imaging Spectroradiometer) is found on-board of the Terra (EOS AM-1) and Aqua (EOS PM-1) satellites and they eachcover the entire Earth's surface every 1 to 2 days, acquiring data in 36 spectral bands from a wavelength range of 0.4 μm to 14.4 μm. The Terra was launched on December 18, 1999 and it orbits around the Earth from north to south across the equator in the morning, while the Aqua launched on May 4, 2002 passes south to north over the equator in the afternoon (MODIS, NASA).

The data sets are collected and processed by The Ocean Biology Processing Group (OBPG) from Earth-viewing satellites. The SST and Chl-*a* data sets used for the study are Level 3 Standard Mapped Image (SMI) products which are image representations of binned data products with a resolution of 9km. The Level 3 SMI products are generated from the resultant Level 3 binned products and each SMI file contains a geographic projection of a single geophysical parameter. This projection consist of a cell-registered grid containing a value for each cell in that grid. A 'linear' or 'logarithmic' functional illustration of the data is used for the scaling and a scaling equation is needed to change the values back to the physical units. The level-3 bin files come in one of the three resolutions (111km, 9.28km and 4.64km) which

depend slightly on the mission and for the MODIS missions, the number of latitudinal rows is 4320 giving a resolution of 4.64-km bin size (OceanColor WEB, NASA).

Satellites data collected usually have “areas of missing data” due to factors such as cloud cover, sunlight, gaps in the inter-orbit and so on. In order to obtain the best results out of these data, the 8-day composites are regarded as a good agreement between the necessity to omit the ‘no data’ pixels as possible without losing a considerable amount of the “temporal variability” in the data (Ocean Color Forum, NASA). In addition, temporal composites of the satellite data are made to present global fields that are more completely filled in so that the composites have fewer ‘no data’ pixels. Besides, the data sets used are in Hierarchical Data Format (HDF) and are used to create images using MATLAB which will be used to assess their contributions to the variability of primary productivity.

1. ***The Chl-a data sets:***

The Chl-a concentration used for this study is calculated by the OBPG using an algorithm to generate the “near-surface concentration of Chl-a” in mg m^{-3}. Using in situ measurements of Chl-a and blue-to-green band ratios of remote sensing reflectances (Rrs), an empirical relationship is devised to calculate this concentration. Also, its implementation depends on the availability of remote sensing reflectances in the blue-green spectral region (e.g., 440 - 570 nm), which is supported by the MODIS-Aqua.

The **verbatim** extract from the OceanColor WEB of the Algorithm Description is as follows:

“**Inputs:** Rrs at 2-4 wavelengths between 440 and 570 nm

Outputs: chlor-a, concentration of Chl-a in mg m^{-3}

Approach: The algorithm is a fourth-order polynomial relationship between a ratio of Rrs and chlor-a.

i

$$log_{10}(chlor\_a) = a_0 + \sum_{i=1}^{4} a_i log_{10}\left(\frac{Rrs(\lambda blue)}{Rrs(\lambda green}\right)$$

Where the numerator, Rrs(blue), is the greatest of several input Rrs values and the coefficients, a_0-a_4, are sensor-specific".

2. <u>The sea surface temperature (SST) data sets:</u>

The SST products from the MODIS sensor undergo "standard processing" by the NASA using the Multi-Sensor Level-1 to Level-2 software (msl12) developed by the OBPG before being distributed. The MODIS bands 31 and 32 at 11 and 12 μm are used by the SST algorithm to generate the long-wave SST data and an inverse relationship (in linear space) of the observed radiances against blackbody temperature is used to devise the brightness temperatures. These relationships are computed to obtain the spectral response of each MODIS channel prior to operating the msl12 and the resultant tables are saved in HDF files to be loaded at run-time (OceanColor WEB, NASA). The SST measured from satellites is a skin measurement of the top layer of the ocean's temperature from about 10 μm below the surface (infrared bands) to 1mm (microwave bands) depth using radiometers (Physical Oceanography Distributed Active Archive Center (PODAAC), NASA). Thus one should bear in mind that satellite radiometers can only measure temperature in this skin layer, which may not represent the upper mixed layer of the ocean, especially during calm conditions when there is little mixing.

<u>The Absolute Dynamic topography and geostrophic velocities data sets:</u>

Weekly data of Ssalto/Duacs Gridded Absolute Dynamic Topography and absolute geostrophic velocities (1/4°x1/4° on a Cartesian grid) are used. AVISO no longer provides the weekly (7-day composites) data and old data could not be supplemented with the new ones given that they have been processed differently. Therefore, since all grid files are processed using 42 days (6 weeks) before and after the date they are dated from (AVISO+. Satellite Altimetry Data, 2015), thus, one file is taken every 7 days for weekly data from the daily data files for e.g. one for Jan. 3, 2012, then one for Jan. 10, 2012, one for Jan. 17, 2012

and so on for the whole period 2003-2014. The data used are in NetCDF (Network Common Data Form) format.

These data undergo a series of processing steps before they are made available for use. The processing sequences are broken into 7 main phases (Fig. 2.1) as listed below (AVISO+. Satellite Altimetry Data, 2015):

- Acquisition of data from various institutions such as NASA, CNES ESA etc.
- Homogenization of the data
- Input data quality control
- Mono and multi-mission cross-calibration
- Generation of products
- Merging to generate Merged, Gridded SLA (sea level anomaly) products
- Final quality control

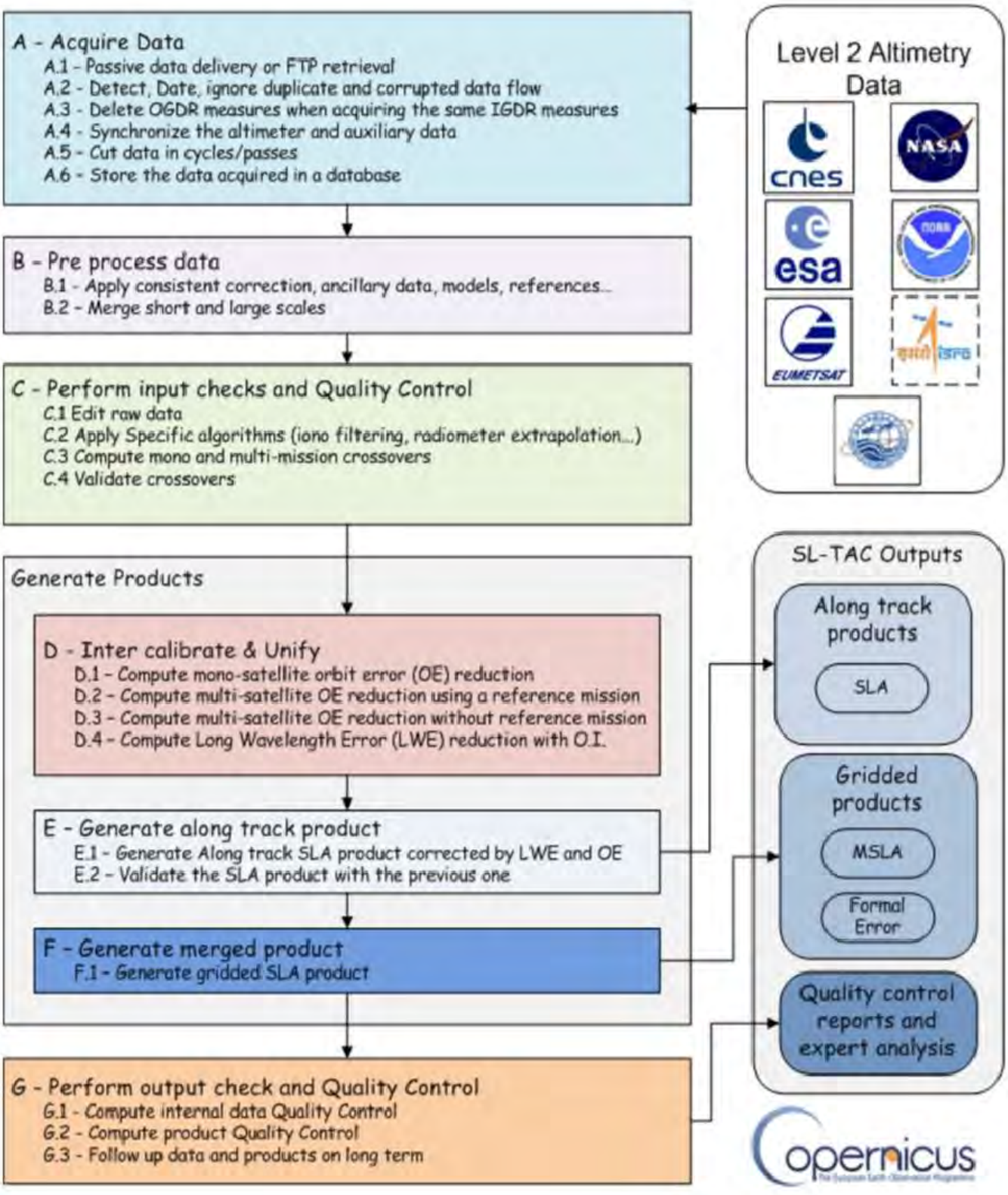

Fig. 2.1. Represents the SL-TAC (Sea Level-Thematic Assembly Centres) processing sequences used by the SSALTO/DUACS system (from AVISO+. Satellite Altimetry Data, 2015).

Computation of gridded Delayed time ADT Products according to AVISO+. Satellite Altimetry Data, 2015:

Gridded MADT and MSLA products are supplied in two types; the **two-sat-merged** and the **all-sat-merged** products. The **two-sat-merged** series takes into account a maximum of 2 satellites (Jason-2/AltiKa or Jason-2/Cryosat-2 or Jason-2 / Envisat or Jason-1 / Envisat or Topex/Poseidon / ERS) in the computation of the map while the **all-sat-merged** product takes into account all the satellites accessible which can be up to 4 satellites on one mission, therefore having the best probable sampling attainable. This fact makes the all-sat-merged series of better quality in that they are not homogenous for that stretch. On the other hand the two-sat-merged provides stable sampling and is homogeneous over the time but not of the best quality which is why all-sat-merged data was chosen.

It is the Delayed Time (DT) element of SL-TAC system which is in charge of the production of a “homogeneous, inter-calibrated and very accurate long time series of SLA and Map of Sea Level Anomaly (MSLA) altimeter data” from the data obtained from the HY-2A, Saral/AltiKa, Cryosat-2, Jason-1, Jason-2, T/P, Envisat, GFO, ERS1/2.

The DT products are more specific than NRT products for two reasons (AVISO+. Satellite Altimetry Data, 2015):

1. Greater fundamental quality of the Precise Orbit Ephemeris (POE) orbit is used in the Geophysical Data Record(s) (GDR) processing.

2. The products computed in the DT DUACS processing are most effective with a focused computation time window for Orbit Error Reduction (OER), LWE. They also have recording processes of 6 weeks before and after the date, which on the other hand cannot be done for the NRT products since "future" data are not available and therefore is not ideal.

The gridded DT products (e.g. merged global/regional – two-sat/all-sat) are all produced with a daily sequential resolution i.e. the maps are processed again for each day. In the past version where the "time decorrelation scale is close to 15 days", the weekly resolution employed for DT maps was inadequate. This was specifically a problem for the end-users wanting to implement a "simple linear time interpolation" between sequential maps, thus explaining the need for the daily reprocessing (AVISO+. Satellite Altimetry Data, 2015).

The ADT products are computed as follows:

ADT = SLA + MDT,

Where ADT is the absolute dynamic topography, SLA is the sea level anomaly and MDT is the Mean Dynamic Topography.

MDT corresponds to the Mean Sea Surface Height minus Geoid as it is part of Mean Sea Surface Height due to permanent currents. After the DUACS 2014 version, a new MDT has been used which takes into account the latest geoid mean field (GOCE DIR-R4) and in-situ dataset, on top of the upgraded processing method (AVISO+. Satellite Altimetry Data, 2015).

To be noted that the ADT products have been produced using consistent SLA and MDT fields:

$ADT = SLA_{20years} + MDT_{20years}$

2.2 SOFTWARE USED

1. **Matlab (Matrix Laboratory)** is software that has been designed for engineers and scientists to develop algorithms and create models by using a programming language that makes use of mathematical functions to acquire, assess and visualise data for their work in a shorter time than the traditional means such as excel (MathWorks, 2015). And for this study, Matlab is used to calculate the seasonal and interannual patterns of each variable as well as to compute image representations of these patterns.

2. **Windows Live Movie Maker** is a free video editing program from the Microsoft Website. It is used to make movies and slide shows using pictures which can later be played on a computer or television. These movies can also be saved on DVDs, CDs and uploaded to Web servers (Interactive Media Center, 2015). It is an easily accessible tool that can be used to determine any visual changes occurring in a given period of time as in this study.

3. **Microsoft Excel** is a spreadsheet with rows and columns representing the grid cells. The rows are numbered while the columns are letter-named. It was developed by Microsoft for Windows, Mac OS X, Android and iOS and is usually used for calculations and for the computation of graphical representations for statistical, engineering and financial purposes (Wikipedia, 2015).

2.3 DATA PROCESSING

The data sets are processed to assess any seasonal or inter-annual patterns in the Chl-*a* concentrations and SST and to assess if geostrophic currents have an effect on these patterns. When all the data sets are processed, the pixels containing missing values because of certain factors such as cloud cover and/or sun glint are replaced by **NaN** (Not-a-Number), so that when the means are calculated, the missing values are ignored to avoid any inconsistencies in the output.

- Near-surface Chl-*a*

- Matlab was used to process the near-surface Chl-*a*, 8-day composites data to produce weekly averaged images of the near-surface Chl-*a* concentration. The images are further compiled into a movie using the Microsoft Movie Maker to have an idea of the changes occurring in the study regions. Monthly climatology images were also produced to have an idea of the changes in Chl-*a* concentrations occurring in each

individual month. Weekly means were also computed using Matlab for each individual year of the period January 2003-December 2014 and Microsoft Excel was later used to plot time series for each individual years as well as for the whole period. The weekly climatology was also computed using Matlab and Microsoft Excel used to plot the time series of the weekly climatology. Hovmöller plots of the near-surface Chl-*a* concentrations were also produced to detect specific changes occurring in specific regions of each of the 3 study areas to see what changes occur in terms of seasonality and interannual variations in the Chl-*a* concentrations. The correlation coefficient, *r,* for the Chl-*a* and SST time series at 95 % confidence (=5% significance) level were also calculated using Matlab. The correlation values are then interpreted using the ranges below:

- **Exactly –1.** A perfect negative linear relationship
- **–0.70.** A strong negative linear relationship
- **–0.50.** A moderate negative relationship
- **–0.30.** A weak negative linear relationship
- **0.** No linear relationship
- **+0.30.** A weak positive linear relationship
- **+0.50.** A moderate positive relationship
- **+0.70.** A strong positive linear relationship
- **Exactly +1.** A perfect positive linear relationship

➢ Sea Surface Temperature (SST)

Similarly, for the SST, 8-day composites data were used to compute weekly averaged images of the SST using Matlab. The images were further compiled into a movie using the Microsoft Movie Maker to have a visual of any changes occurring in the study regions. Monthly climatology images were produced to give an idea of the changes in SST occurring in each individual month. Weekly means were also computed using Matlab for each individual year of the period January 2003-December 2014 and Microsoft Excel was later used to plot time series for each individual year as well as for the whole period. The weekly climatology was also computed using Matlab and Microsoft Excel used to plot the time series of the weekly climatology. The correlation coefficients for the SST time series at 95% confidence (=5% significance) level were also calculated using Matlab.

- Absolute Dynamic topography (ADT) and Geostrophic velocities

Similar to the SST and Chl-a concentration data sets, using Matlab, weekly averaged images of Absolute Dynamic topography (ADT) and Geostrophic velocities_were produced and compiled into a movie to visualise any changes occurring in the areas of interest.

CHAPTER 3 RESULTS

This chapter has been divided into 3 sections, one section for each study area as shown in Fig. 3.1 below. This will give an idea of how each study area is affected individually and will later allow comparison of the dynamics of the areas.

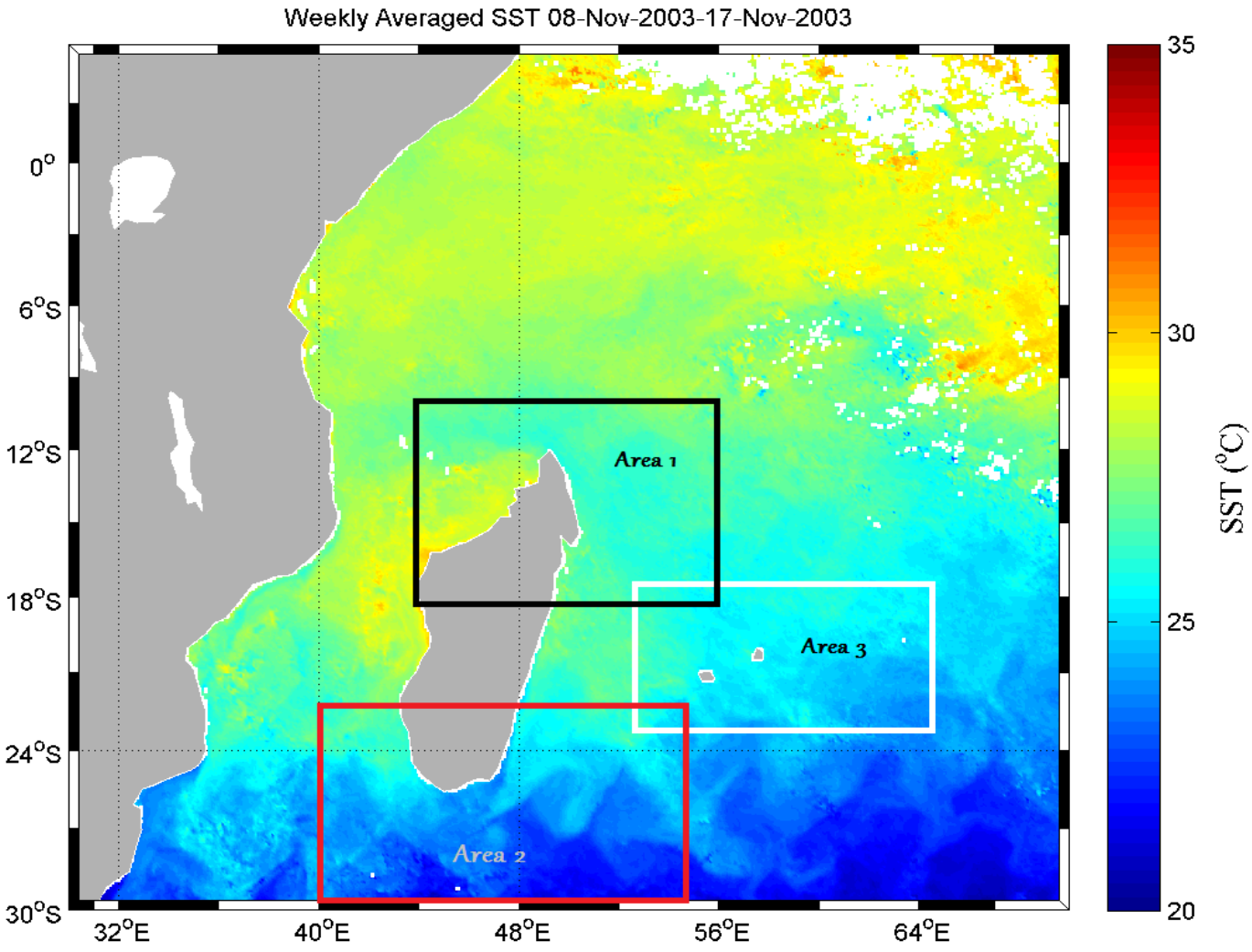

Fig. 3.1. The three study areas of the southwest Indian Ocean (inside boxes) and average weekly sea surface temperature MODIS composite (from the NASA Ocean Color website – 8th to 17th November 2003). Area 1 represents the North East Madagascar (NEM), Area 2 is the South East Madagascar (SEM) and Area 3 represents the Mascarene Islands (MI). The white areas in the ocean on the map are missing data due to cloud cover and those on the African continent are bodies of fresh water such as lakes.

SECTION 1. Northeast Madagascar, NEM (AREA 1)

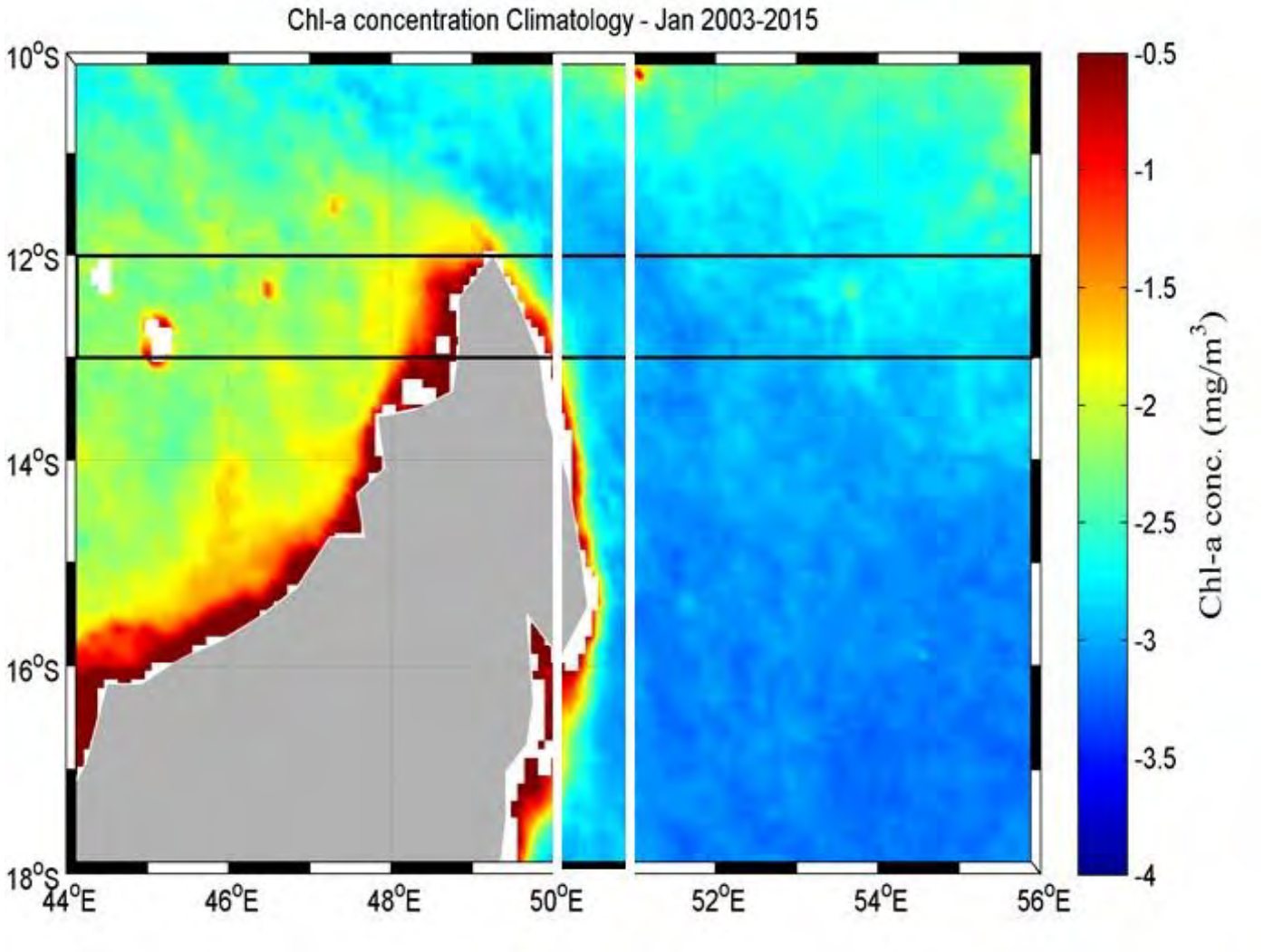

Fig. 3.2. Areas chosen for the Hovmöller plots of weekly Chl-*a* concentration averaged along the latitudes 12°S-13°S (black box) and along the longitudes 50°E-51°E (white box). The white areas at 12°S-13°S and 44°E-46°E represent land cover of the Mayotte Island and around the Madagascar Island it represents the shallow coatal areas of Madagascar.

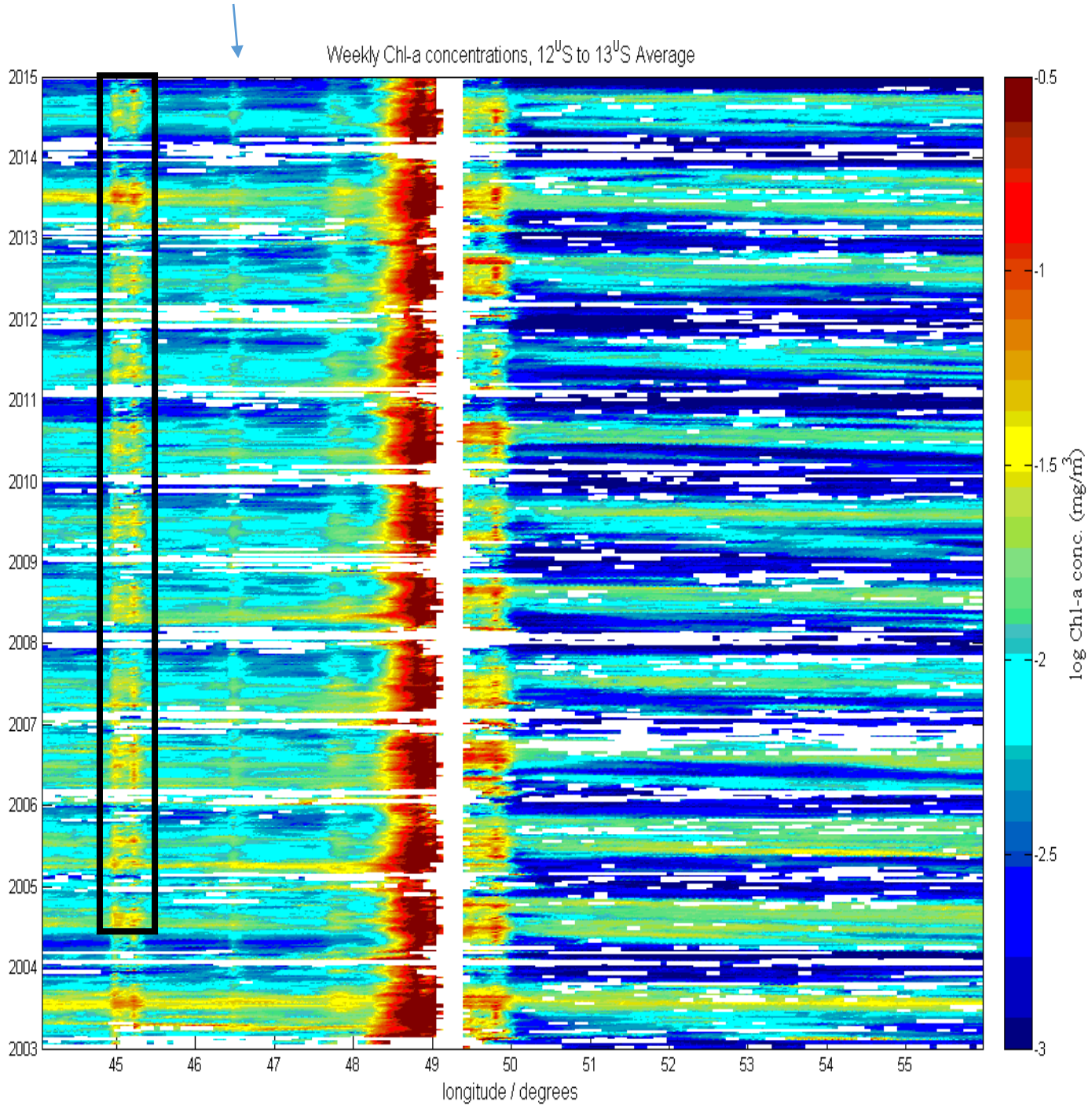

Fig. 3.3. NE Madagascar. Hovmöller plot of weekly Chl-a concentration averaged along the latitude 12^0S-13^0S for the period Jan 2003-Dec 2014. The black box shows the weekly Chl-a concentration across Mayotte Island. The white areas spread all over the picture represent missing data due to cloud cover and that along the 49^0E-49.5^0E represents a strip of land cover from Madagascar. The blue arrow between 46^0E-47^0 E shows the location of the Zelee Bank.

Fig. 3.2 shows that the Chl-*a* concentrations are stronger along the coasts, with the west coast (48^0 - 49^0 E) being higher than the east coast (49^0 - 50^0 E). Also, as we move away from the coasts the Chl-*a* concentration decreases on both the east and west side of the tip of Madagascar (the white strip on the Hovmöller plot along the 49^0E-49.5^0E, Fig. 3.3). However, along 45^0E (the black box), the Chl-*a* concentrations are quite high even though it is far from the west coast of Madagascar and this may be due to coastal runoffs from Mayotte Island which is situated along 12^0 S and 45^0 E. There is also, a faint but distinctive increased Chl-*a* concentration between 46^0-47^0 E (blue arrow on Fig.3.3) which might be due to the shallow Zelee Bank. The Chl-*a* concentrations are also higher on the west side compared to the east side because the Northeast Madagascar current (NEMC) displaces the water to the west side of the tip of Madagascar, thus carrying more nutrients to the west from the east. The blooms across the years also show that there is an annual variability in the Chl-*a* concentration along the latitude12^0S-13^0S.

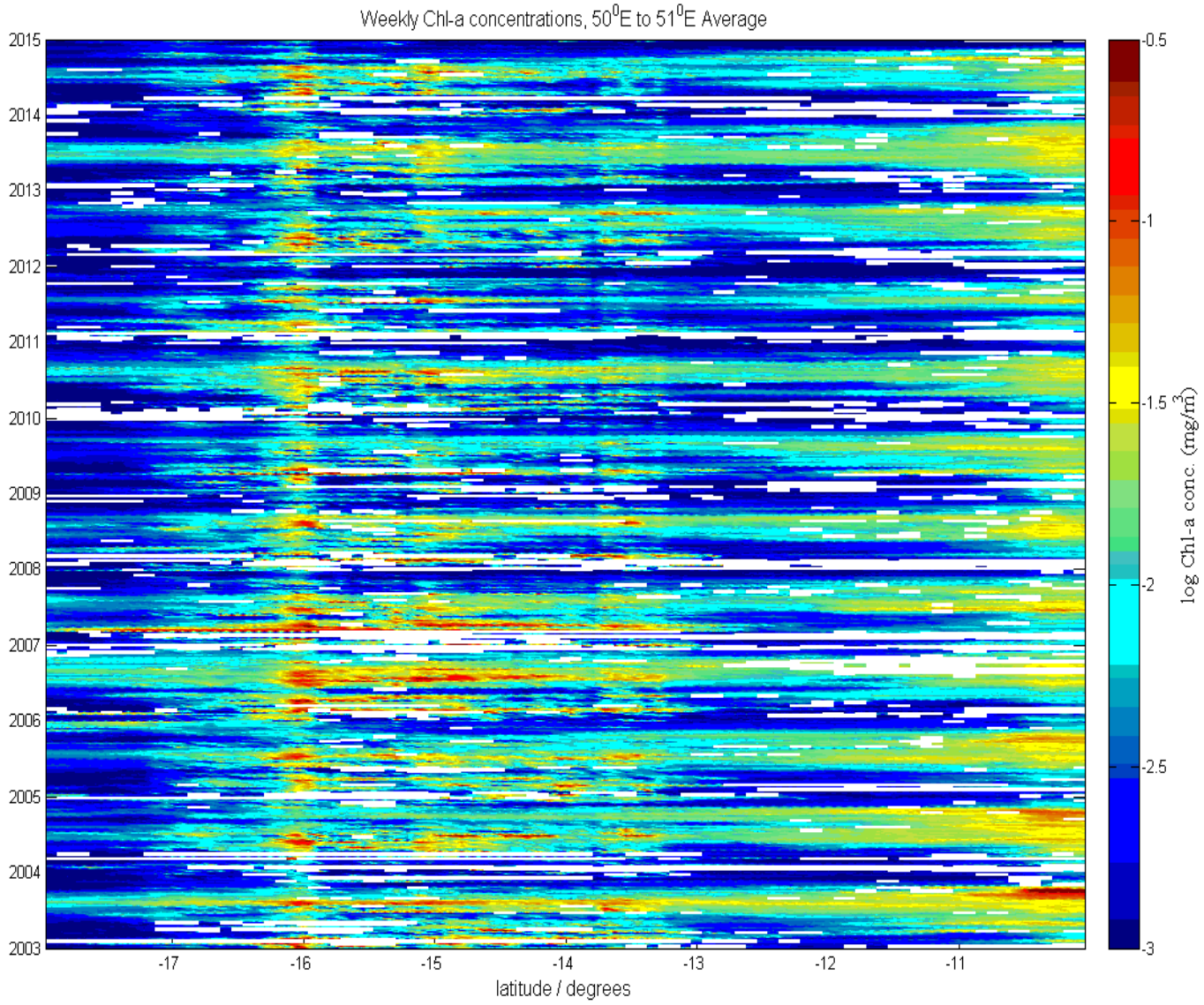

Fig. 3.4. NE Madagascar. Hovmöller plot of weekly Chl-a concentration averaged along the longitude 50^{0}E-51^{0}E* for the period Jan 2003-Dec 2014. *The white areas spread all over the picture represent missing data due to cloud cover.

Fig. 3.4 shows that across the years, there is inter-annual variability in the Chl-*a* concentration and a seasonal pattern which is more prominent in the north (10^0-11^{0}S) with high and low concentrations of Chl-*a*. The highest Chl-*a* concentration occurred along the coasts (13^0-16^{0}S) and some high concentrations also occurred along 10^{0}S, across the Farquhar group of Islands that belongs to the Seychelles (refer to the feature that appears on Fig. 3.2 at latitude 10^{0}S). The high concentration occurring along 10^{0}S, might be due to Island runoff that contributes to the nutrient budget thus causing high phytoplankton growth there.

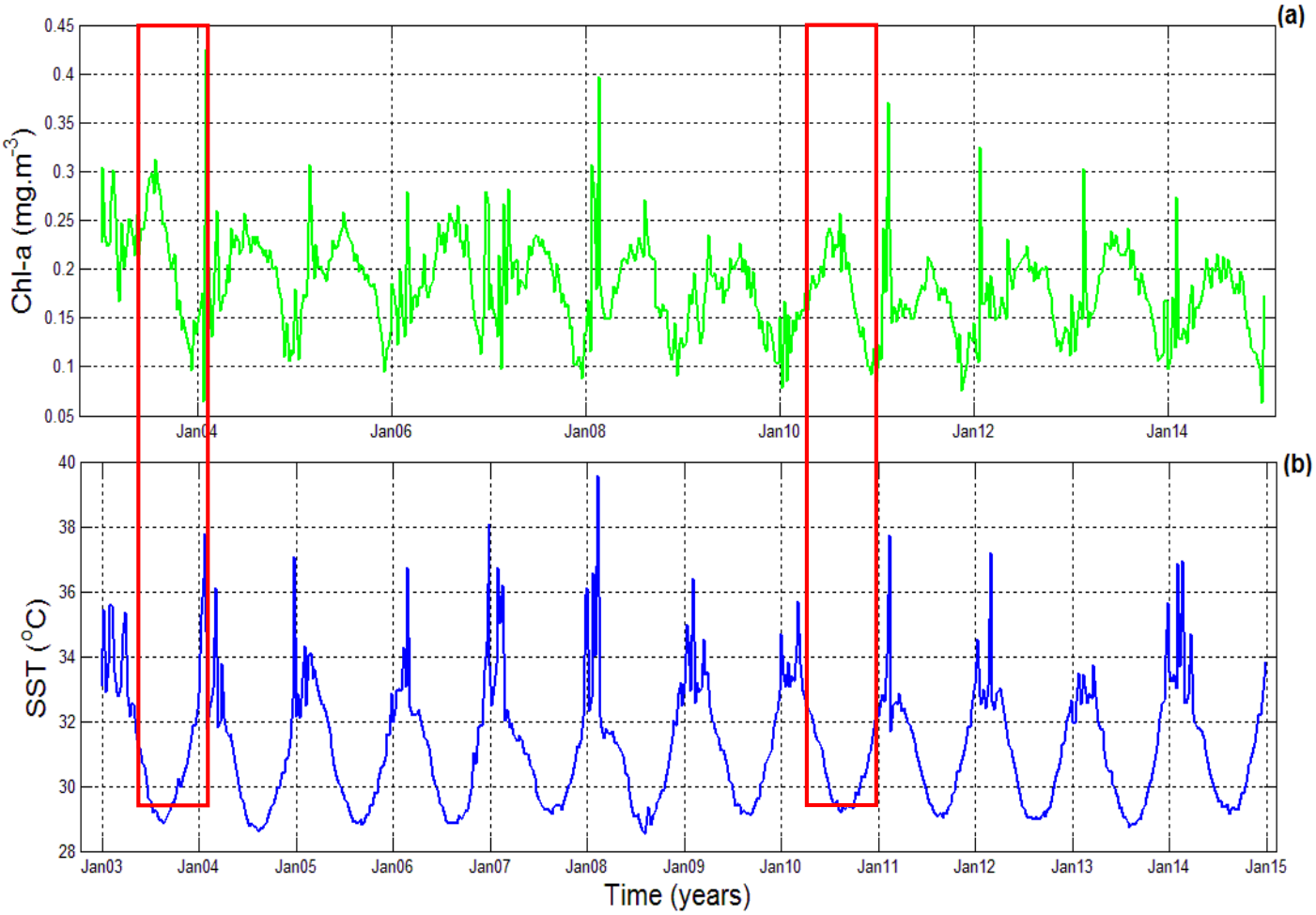

Fig. 3.5. Time series for (a) weekly mean* Chl-*a* *and (b) weekly mean SST for Jan 2003-Dec 2014 along the Northeast of Madagascar (Area between* 44^0-56^0E and 10^0-18^0S). *Red boxes highlight the highest Chl-* *a* *concentration occurring in 2003 and 2010 which are different compared to the other years.

Fig. 3.5 shows the time series for Chl-*a* indicating a fairly similar pattern in the Chl-a concentrations across the years with high concentrations occurring between June-October for the whole area and the low concentrations occurring between November-January or February. When comparing the SST and Chl-*a* time series, it appears that the Chl-*a* concentration is high when the SST is low and vice versa. However, the highest Chl-*a* peaks do not occur during the winter season i.e. during June-October (when the SST is lowest) but at the start of the years; during February 2004, March 2005, March 2006, March 2007, February 2008, April 2009, February 2011, February 2012, February 2013 and February 2014. Unlike all the other years, the highest Chl-*a* peak for 2003 is in July-August and for 2010 in August when the SST is low (refer to the red boxes in Fig. 3.5) but in January and

February, when the SST is highest, the Chl-*a* concentration is as high as that in July. It should be noted here that there are a few spikes in the time series at the start of the years when the SST is high. When comparing this value to the temperature images during those specific weeks, it can be seen that the temperature for the area does not go over 32°-33°C. Also the time series gives the average of SST over the whole area as a single value for the week while the image displays the average SST across the whole area. The video (not presented) of the SST for the 2003-2014 period shows that there is a high percentage of cloud cover occurring during that time and thus the cloud cover effect and the single value for the weekly average for that whole area might not reflect what really occurs at that time of the year. Weekly data are obtained by processing daily data and missing data (usually caused by cloud cover) are eliminated through the algorithms used and this might contribute to the spikes in the time series. However, it should be noted that the image displays do show that the SST is high (ca. 30°C) at the beginning of the years but not as high as the spikes (ca. 37°C).

Table 3.1. Time frame during which the highest Chl-a concentration occurs for each year across the Northeast Madagascar and the corresponding SST values. .

Year	Week	Month	Highest Chl-*a* concentration recorded in that year	SST corresponding to the Highest Chl-*a* concentration
2003	27	July-August	0.313	29.20
2004	5	February	0.425	31.78
2005	8	February-March	0.307	34.09
2006	45	December	0.279	34.44
2007	10	March	0.282	31.82
2008	7	February	0.396	32.15
2009	13	April	0.234	32.45
2010	29	August	0.257	29.19
2011	6	February	0.371	37.72
2012	4	January-February	0.324	32.54
2013	7	February	0.302	33.10
2014	5	February	0.273	36.86

Table 3.1 above shows that the highest Chl-*a* concentrations occur mostly during January-April, where the SST is quite high, with the exception of the years 2003 where it occurs during

July-August and 2010 during August, when the SST is lower (highlighted by red boxes in Fig. 3.5).

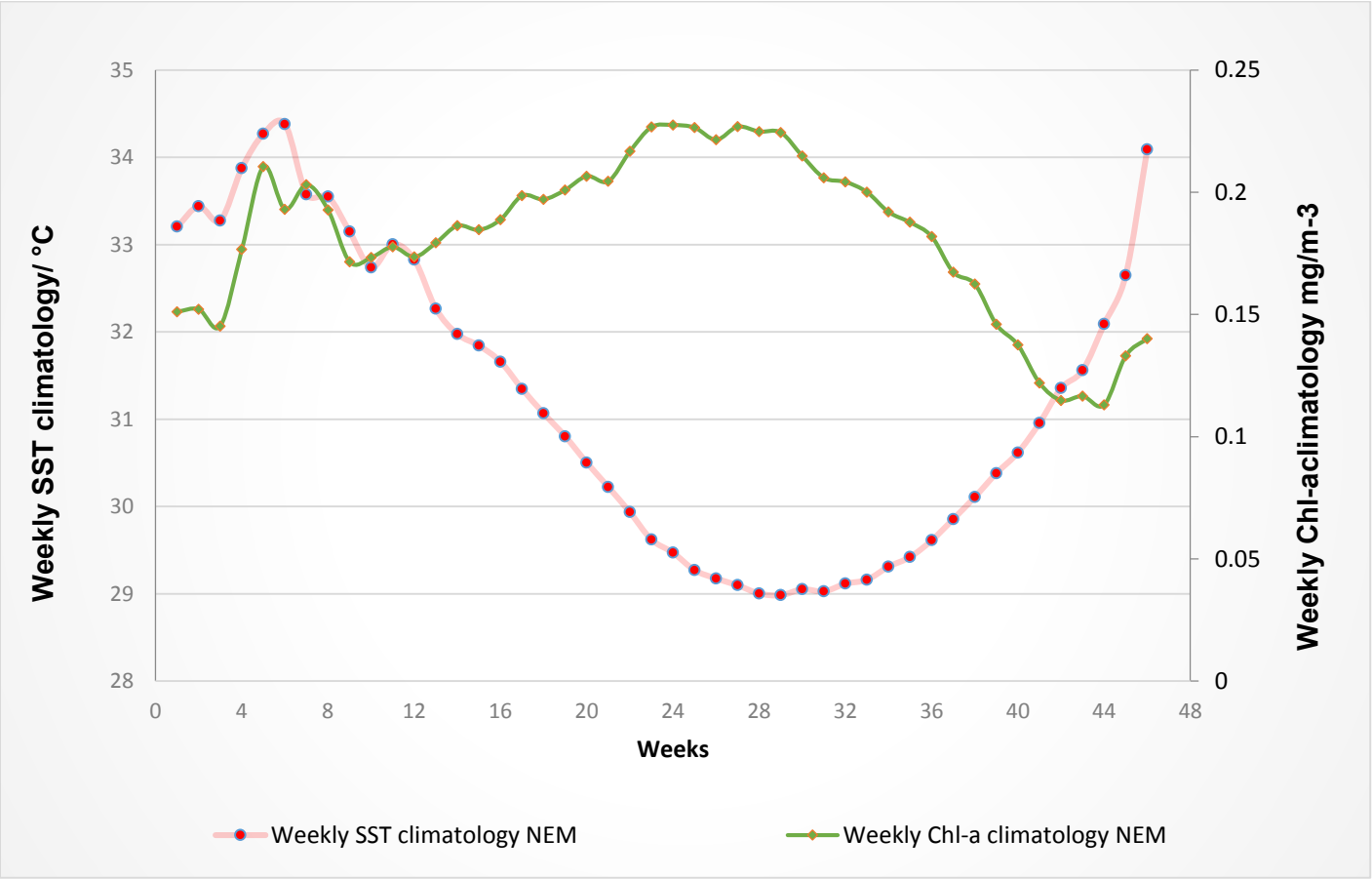

Fig. 3.6. Time series for the weekly Chl-a and weekly SST climatology for Jan 2003-Dec 2014 along the Northeast of Madagascar (Area between 44^0-56^{0}E and 10^0-18^{0}S).

Fig. 3.6 shows that at the beginning of the years, from weeks 1 to 12 and weeks 43 to 46, there is a positive relationship with SST and Chl-*a* concentration showing the same patterns during this period. From week 13 to 42 on the other hand there is an inverse relationship, where the Chl-*a* concentration is high when the SST is low. The weekly climatology shows that high Chl-*a* concentrations occur twice a year in this region, once at the beginning of the year when the SST is high and also during June-August when the SST is low. This shows a seasonal pattern in Chl-*a* concentrations across the years.

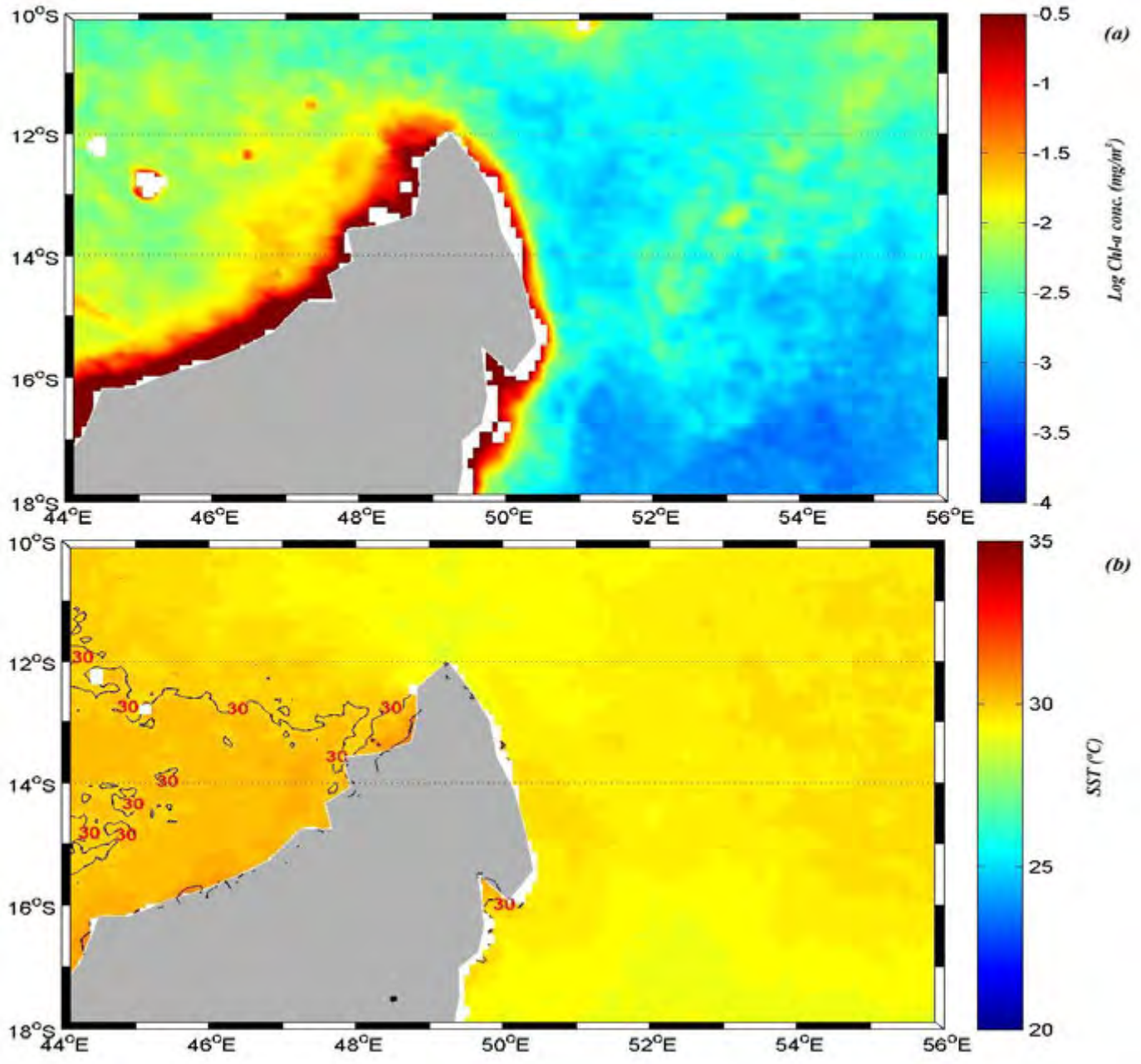

Fig. 3.7. NE Madagascar. Monthly climatology for February over the period 2003-2015 (a) for Chl-a concentration, and (b) for SST. The white areas at 12^0S-13^0S and 44^0E-46^0E represent land cover of the Mayotte Island and around the Madagascar Island they represent the shallow coatal areas of Madagascar.

Fig. 3.7 shows that the SST is also slightly higher on the west side of the Island and along the coasts which seems to correspond to the high Chl-*a* concentration occurring in these areas. The Chl-*a* concentration is high across the whole study area but the highest concentration is still along both coasts. However, the intensity of the coastal Chl-*a*

concentration is less than that in February. The SST over the whole study area is lower than in February.

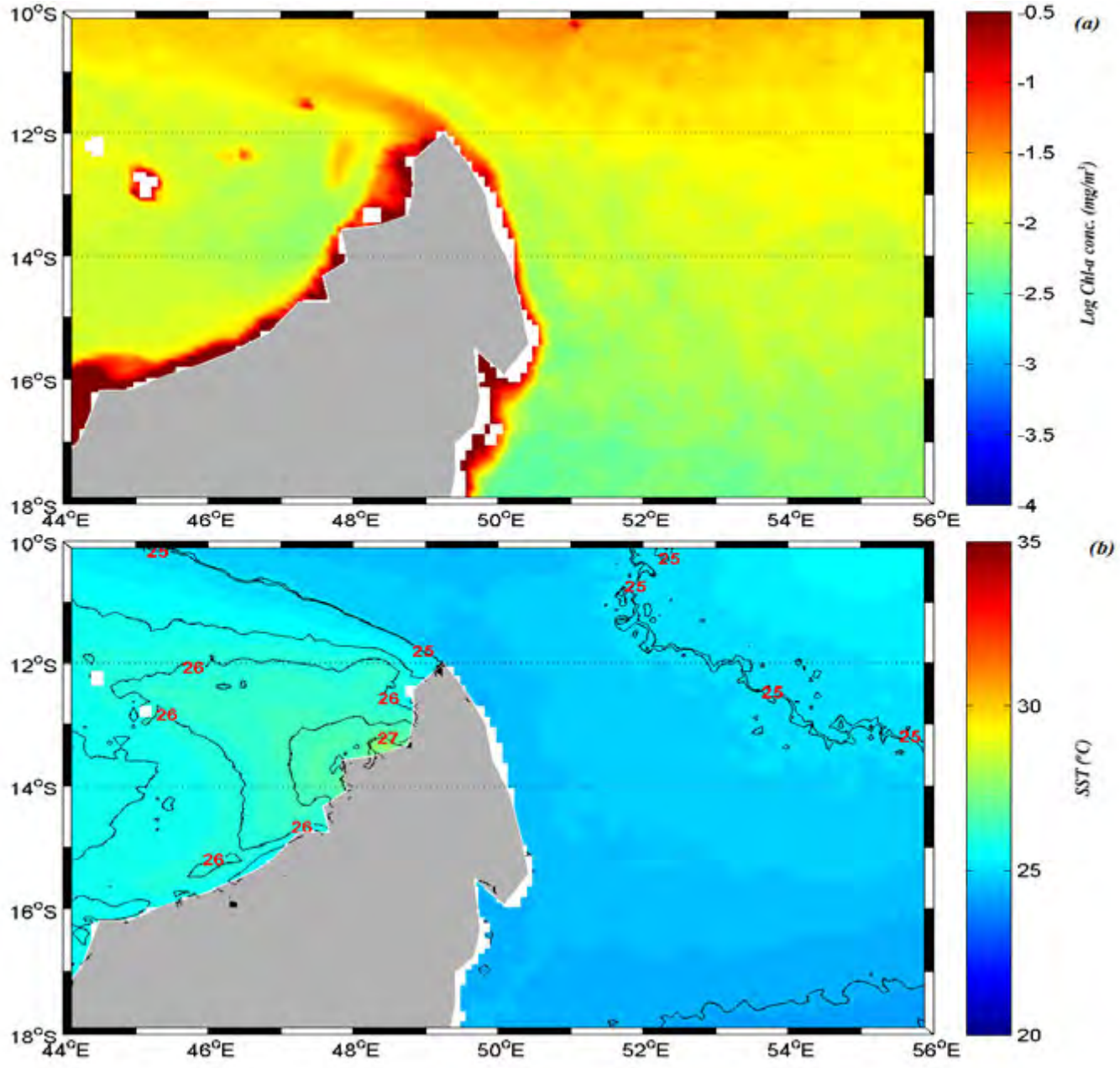

Fig. 3.8. NE Madagascar. Monthly Climatology for August over the period 2002-2014 (a) for Chl-a concentration and (b) for SST. The white areas at 12^{0}S-13^{0}S and 44^{0}E-46^{0}E represent land cover of the Mayotte Island and around the Madagascar Island they represent the shallow coatal areas of Madagascar

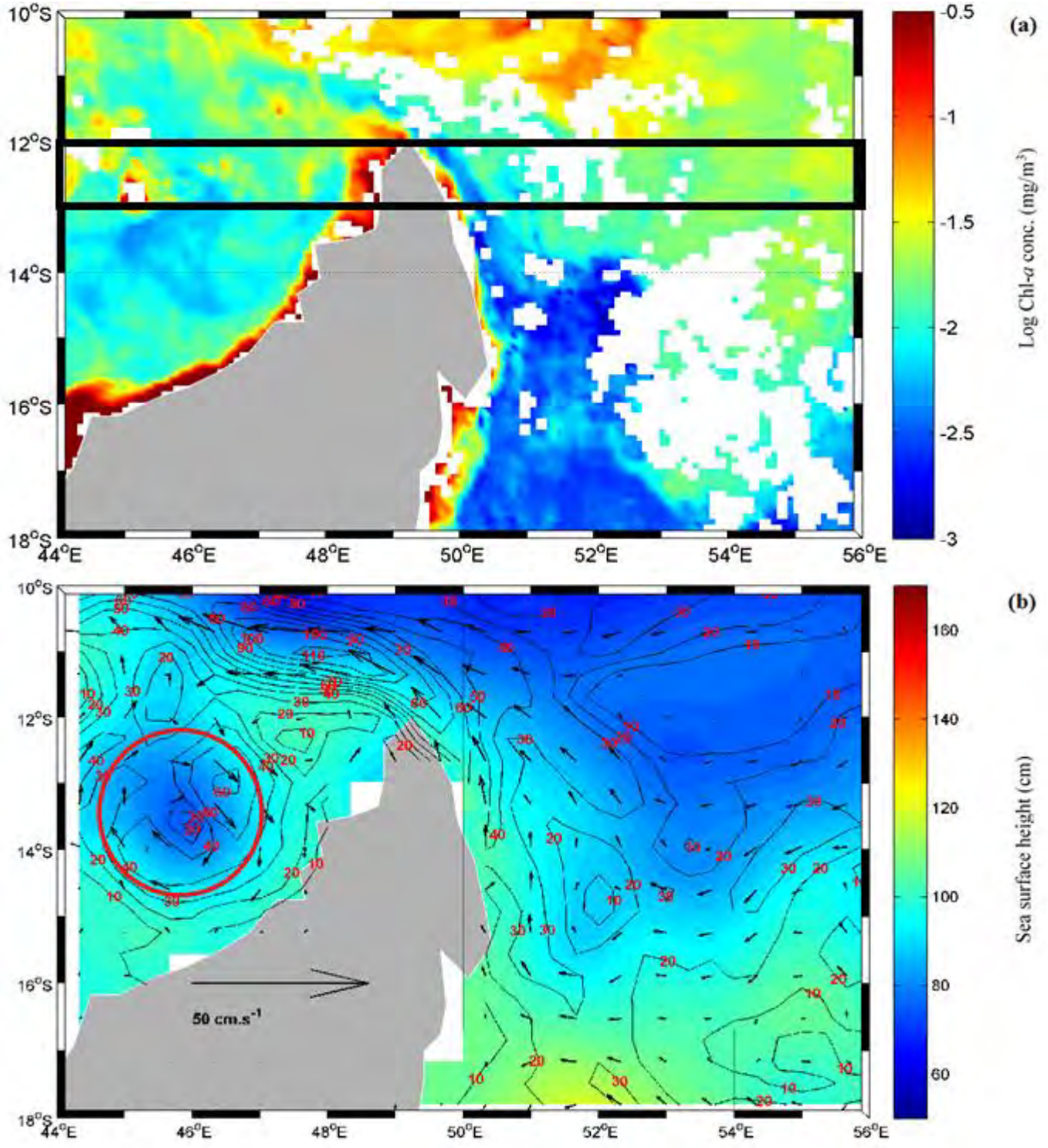

Fig. 3.9. (a) Weekly averaged Chl-a concentration (12-20 August 2004) and (b) weekly averaged ADT and geostrophic velocities (12-18 August 2004). The black box is the area chosen for the Hovmöller plot (Fig. 3.3) and the red circle show the presence of a cyclonic ring occurring in the region. The white areas at 12^0S-13^0S and 44^0E-46^0E represent land cover of the Mayotte Island and around the Madagascar Island they represent the shallow coatal areas of Madagascar, while the white areas that is spread all over the ocean in Fig. 3.9 (a) represent missing data due to cloud cover.

Fig. 3.9 (a) shows that the Chl-*a* concentration during August is high and well spread over the whole area. The concentrations along the coasts are higher and might be due to land runoff. The Chl-*a* concentrations are higher on the west side of the Northern tip given that there is a cyclonic ring (red circle) in that part which is causing the upwelling of nutrient rich cold water around that ring. The SSH in the cyclonic ring is lower (70-80 cm) compared to the rest of the west side (90-110 cm) since the surface water is being diverged. The geostrophic velocity within the cyclonic ring varies from 20-60 cms^{-1} and the NEMC have geostrophic velocities reaching upto 110 cms^{-1}. When comparing the Fig. 3.9 (a) to that of Fig. 3.9 (b), it can be seen that the higher Chl-*a* concentration is occurring around the cyclonic ring, along the coasts and along the northern tip along the 10^0S-12^0S strip, where the water is being displaced. The year 2004 was chosen as example as it displays the highest Chl-*a* concentration among all the years. Fig. 3.6 shows that the Chl-*a* concentration is also high during spring (July-August), thus an image from the month of August for the year 2004 is chosen to show the Chl-*a* concentration occurring during that month. Also, the SST (Fig. 3.8) seems to be following the same patterns as the currents (Fig. 3.9), thus suggesting that cool water is being brought to the surface as the Northeast Madagascar Current (NEMC) displaces water towards the west. This explains how the whole area has a high Chl-*a* concentration unlike February.

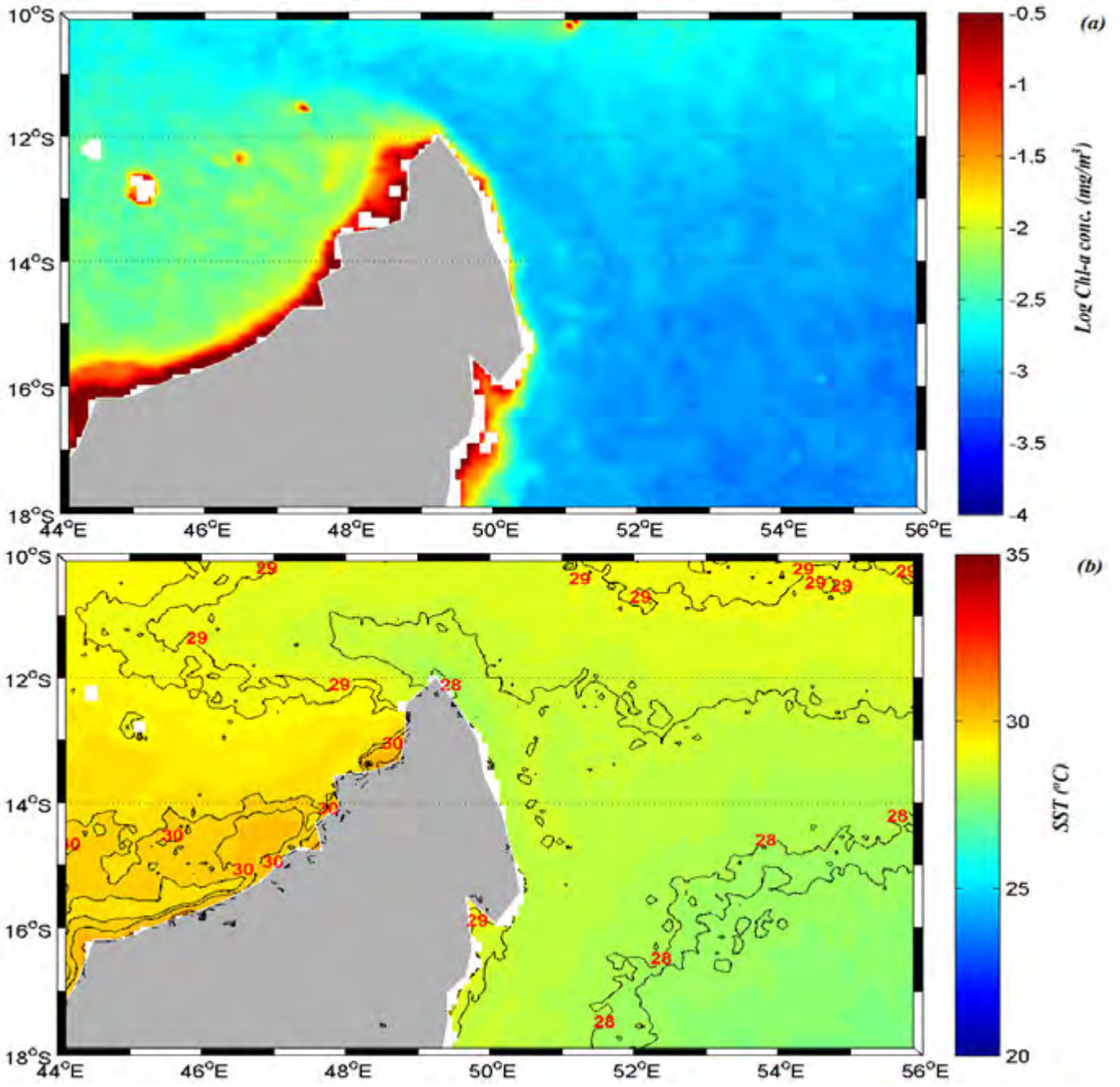

Fig. 3.10. NE Madagascar. Monthly Climatology for December over the period 2002-2014 (a) for* Chl-*a* *concentration and (b) for SST. The white areas at 12^0S-13^0S and 44^0E-46^0E represent land cover of the Mayotte Island and around the Madagascar Island they represent the shallow coatal areas of Madagascar.

Fig 3.10 shows that the Chl-*a* concentration in December is at its lowest, but along the coasts it is still high compared to the rest of the area. The SST is high and it gets warmer on the west side of the Island. However, it is cooler than in February when the coastal bloom occurs.

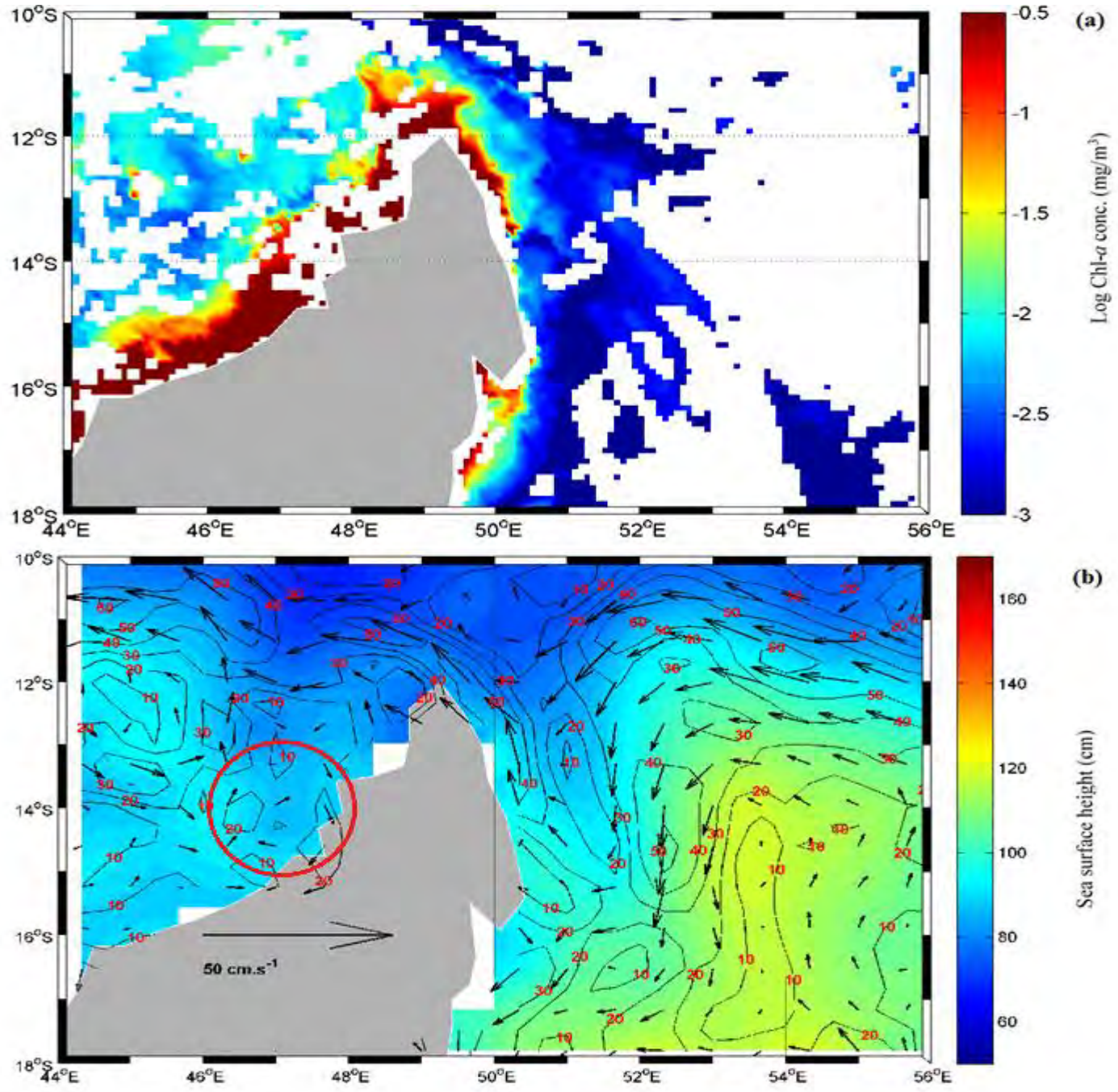

Fig. 3.11. NE Madagascar. Weekly averaged (a) Chl-a concentration (02-10 February 2004) and (b) ADT and geostrophic velocities (05-11 February 2004). The red circle depicts a cyclonic ring. The white areas that are spread all over the Fig. 3.11 (a) represent missing data due to cloud cover and in Fig. 3.11 (b), around the Madagascar Island they represent the shallow coastal areas.

Fig. 3.11 (a) shows that there is high Chl-*a* along the coasts of Madagascar. Also, on the east side of Northeast Madagascar (NEM), at about 16^{0}S, the water is displaced to the south

and the north while on the west there are small cyclonic eddies along the coasts. The sea surface heights (SSH) along the coasts of NEM and Mayotte Island are around 80-100 cm high and further on the east side the SSH is around 120-130 cm high. The geostrophic velocity inside the small coastal cyclonic ring varies between 10 cms^{-1} and 20 cms^{-1}, while the waters being displaced by the NEMC have geostrophic velocities of upto 50 cms^{-1}. And on the east side the geostrophic velocity is mostly between 10 cms^{-1} and 20 cms^{-1}. When Fig. 3.11 (a) and (b) are analysed, it can be seen that the Chl-*a* concentrations are higher along the west coasts where the small cyclonic ring is present and where the SSH is low. The NEMC is also displacing water from the east side to the west further explaining the high concentration of Chl-*a* in the west compared to the east, since more nutrients are being carried to the west. The eddy close to the coast also explains why the Chl-*a* concentrations are higher close to the coast compared to the rest of the west side of the Island, given that the cyclonic rings are causing coastal upwelling. On the east side there are no cyclonic rings and the SSH is also higher, thus the Chl-*a* concentration on that side is low probably due to lack of nutrient supply. In contrast to August (Fig. 3.8), in February (Fig. 3.7), the Chl-*a* concentrations are higher along the coasts, while in August they are quite well spread over the whole area. The week 02-10 February 2004 is chosen as the Chl-*a* concentration is highest then and the ADT and geostrophic velocities corresponding to that same week are used to display any relationship between these variables.

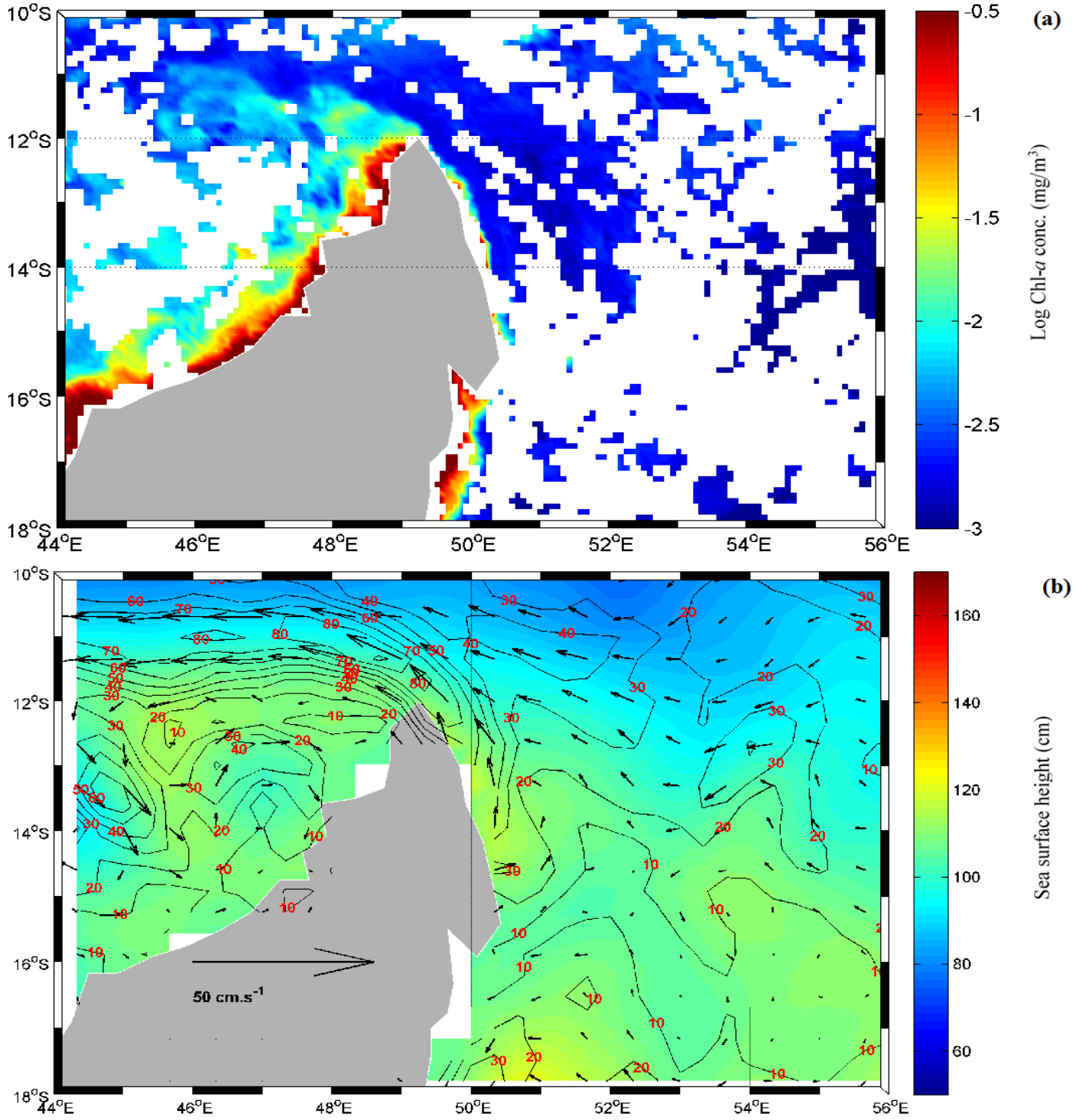

Fig. 3.12. NE Madagascar. Weekly averaged (a) Chl-a concentration (02-10 December) and (b) ADT and geostrophic velocities (02-08 December 2004). Note that the white pixels in the Chl-a image are due to cloud cover and those in the image (b) probably represent shallow coastal areas where SSH cannot be calculated.

Fig. 3.12 (a) shows that in December the Chl-*a* concentrations are lower compared to February (Fig. 3.11) and August (Fig. 3.9). The SSH along the coasts is between 120-130 cm high and the NEMC seems to be weaker compared to the other months (Fig. 3.11(b) and Fig. 3.9(b)). No cyclonic eddies are present during this time and the geostrophic velocity of the NEMC reaches upto 80 cms^{-1} and on the east side it reaches upto 30 cms^{-1}. Even though the geostrophic velocity of the NEMC is higher in December compared to February, the SSH is still higher than in August and February, thus explaining why the Chl-*a* concentration during December is lower. Also the enhanced Chl-*a* occurs mostly along the west side of the Island and not over other parts of the study area. The monthly climatology shows that the lowest Chl-*a* concentration occurs around December, thus the week 02-10 December is used as an example to show the difference between the Chl-*a* concentration between February (Fig. 3.11), August (Fig. 3.9) and December (Fig. 3.12), where February and August have high concentrations and December has the lowest concentration.

Table 3.2 showing the correlation between the time series of Chl-a and SST for each individual years and the whole time period of 2003-2014.

Time Period	Correlation coefficient for the Chl-*a* and SST time series at 95 % confidence level for Northeast Madagascar
Jan-Dec 2003	-0.0411
Jan-Dec 2004	-0.4882
Jan-Dec 2005	-0.1718
Jan-Dec 2006	-0.2205
Jan-Dec 2007	-0.3703
Jan-Dec 2008	-0.1284
Jan-Dec 2009	-0.4396
Jan-Dec 2010	-0.5587
Jan-Dec 2011	-0.2138
Jan-Dec 2012	-0.4202
Jan-Dec 2013	-0.5280
Jan-Dec 2014	-0.5768
Jan 2003- Dec 2014	-0.2646

From Table 3.2 above it can be noted that as in Fig. 3.6, there is an inverse relationship between SST and Chl-*a*.

SECTION 2. Southeast Madagascar, SEM (AREA 2)

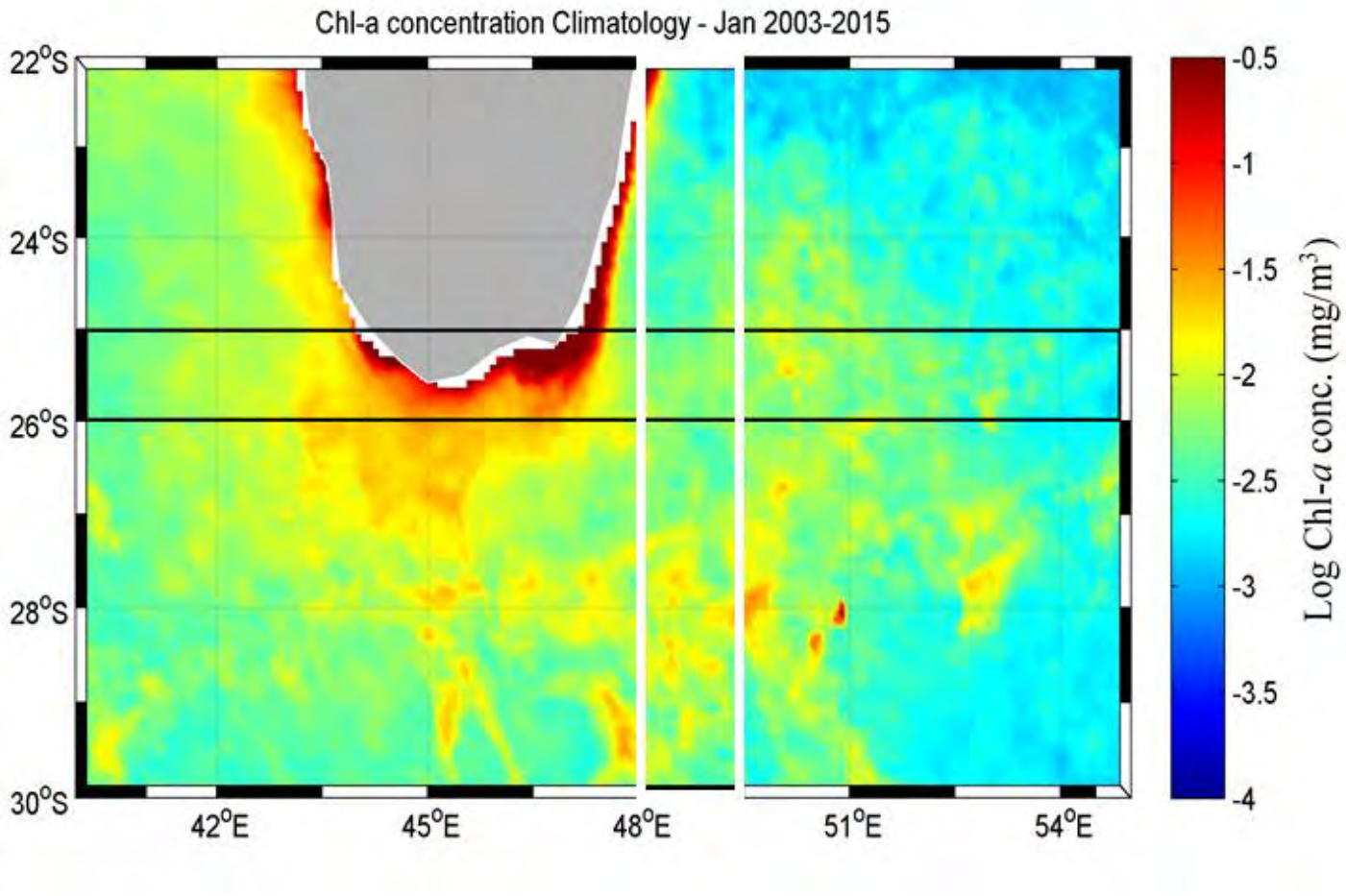

Fig. 3.13. SE Madagascar. Areas chosen for the Hovmöller plots of weekly* Chl-*a* *concentration averaged along the latitudes 25^0S-26^0S (black box) and along the longitudes 48^0E-49^0E (white box). The white areas along the coasts of SEM represent shallow coastal areas.

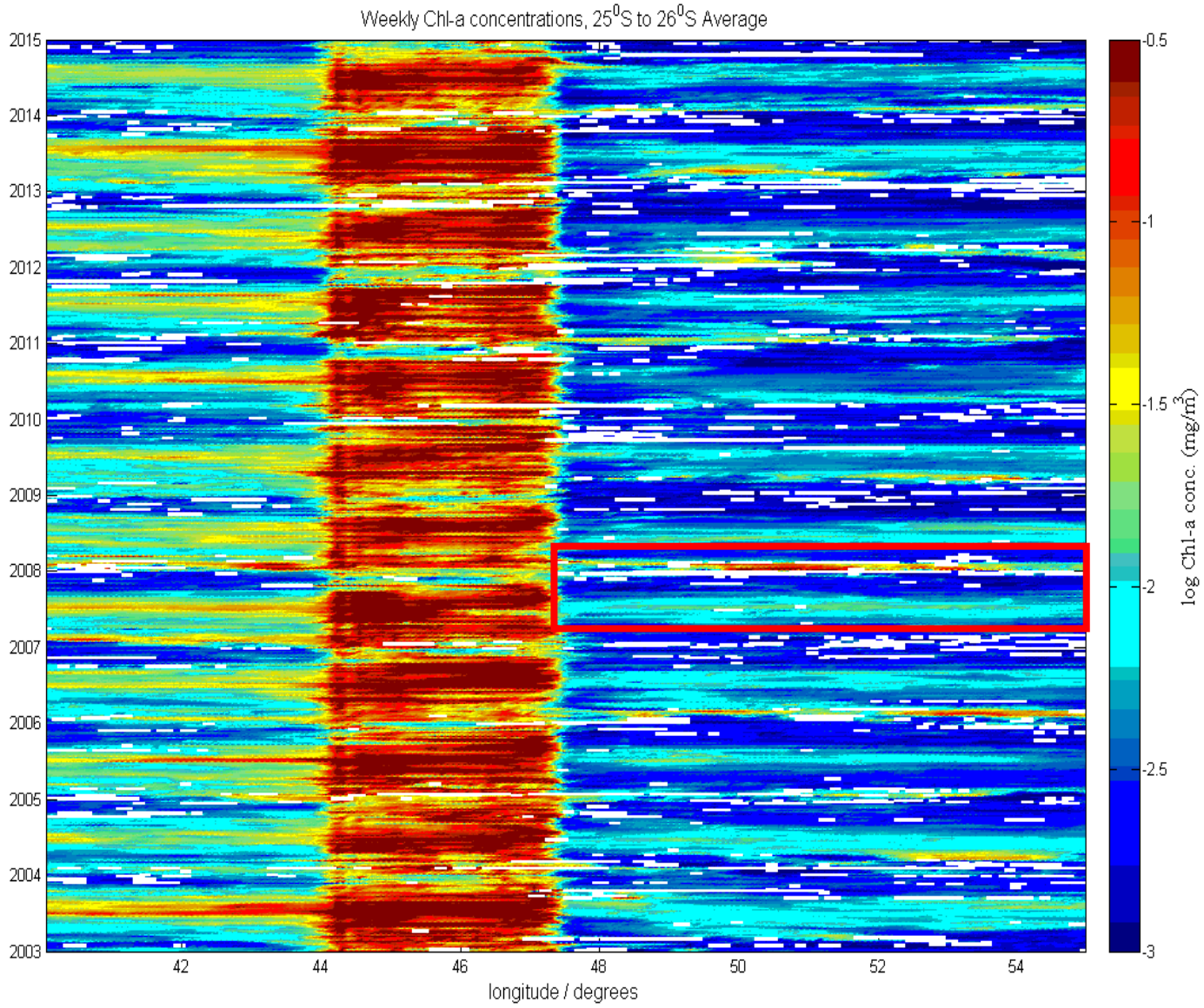

***Fig. 3.14. SE Madagascar. Hovmöller plot of weekly Chl-a concentration averaged along the latitude 25^{0}S-26^{0}S* for the period Jan 2003-Dec 2014. *The white areas spread all over the picture represent missing data due to cloud cover.* The red box highlights the strongest bloom on the east side of SEM.**

Fig. 3.14 shows that the highest Chl-*a* concentration occurred along the coast (44^0-48^0 E) and that the Chl-*a* concentration is higher on the west side of the plot (40^0-44^0 E) compared to the east (48^0-55^0 E) which suggests that the southwest of Madagascar might be more dynamic than the southeast side. On the other hand, in the east there are 2 blooms, one at the start of the year and the other during the middle of the year. The bloom occurring at the

start of the year is found only on the east side and is strongest in 2008 (highlighted by the red box). There are also annual and seasonal patterns over the years depicting seasons of high and low Chl-*a* concentrations.

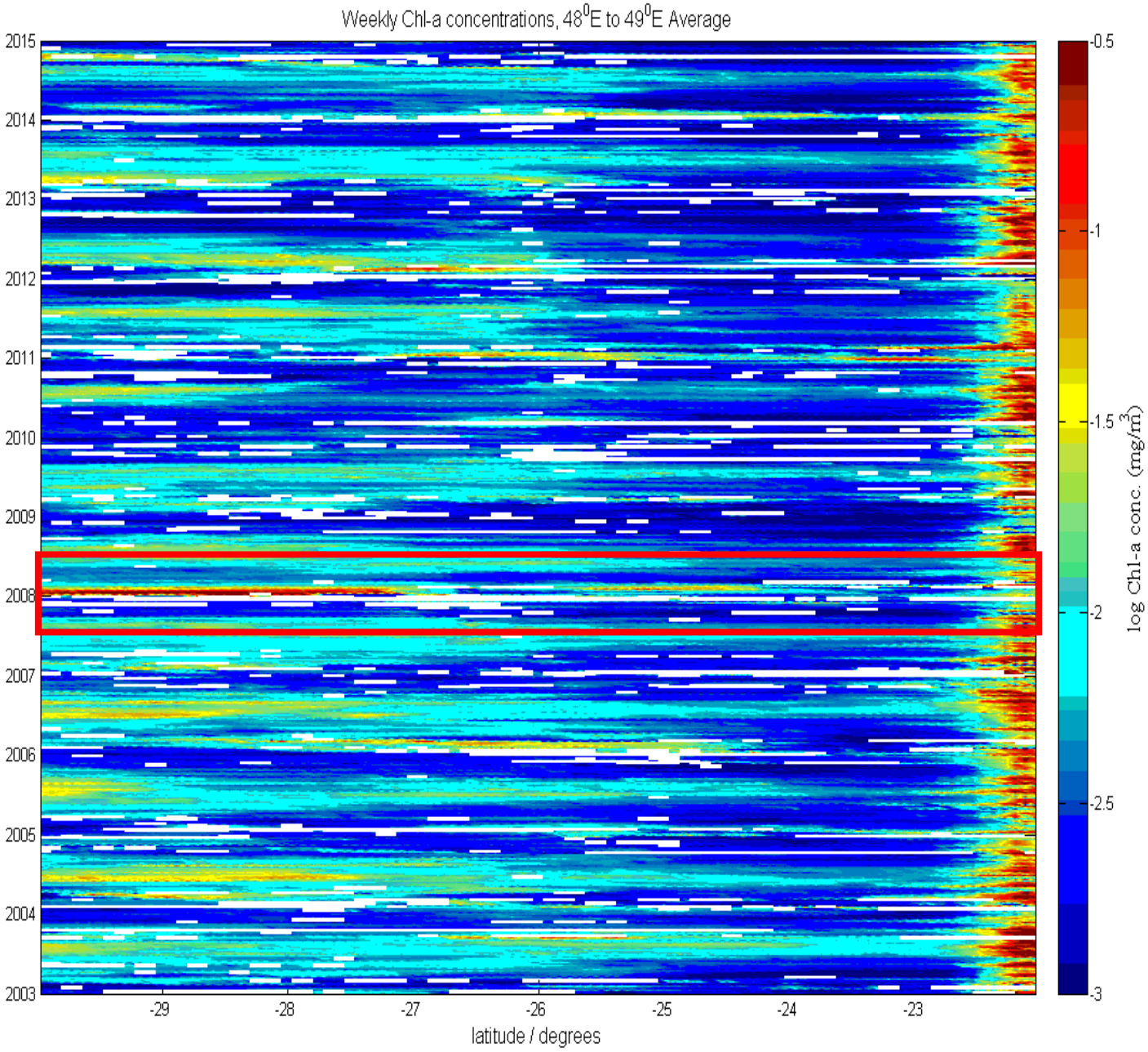

***Fig. 3.15. SE Madagascar. Hovmöller plot of weekly Chl-a concentration averaged along the longitude 48^{0}E-49^{0}E* for the period Jan 2003-Dec 2014. *The white areas spread all over the picture represent missing data due to cloud cover.* The red box highlights the strongest bloom across SEM.**

Fig. 3.15 shows that there is a seasonal pattern across the years, with two blooms, one at the beginning of the year and the second during the middle of the year. In the year 2008 the bloom at the beginning of the year has higher concentrations than other years (highlighted by the red box). The seasonal signal shows that there are high (during June-September) and low (during October-January) levels of Chl-*a* concentration across the years (refer to time series, Fig A.7 and Fig A.8 in the appendix). It can also be seen that the highest Chl-*a* concentration occurred across the 22^0S-23^0S, which is along the coast of south east Madagascar.

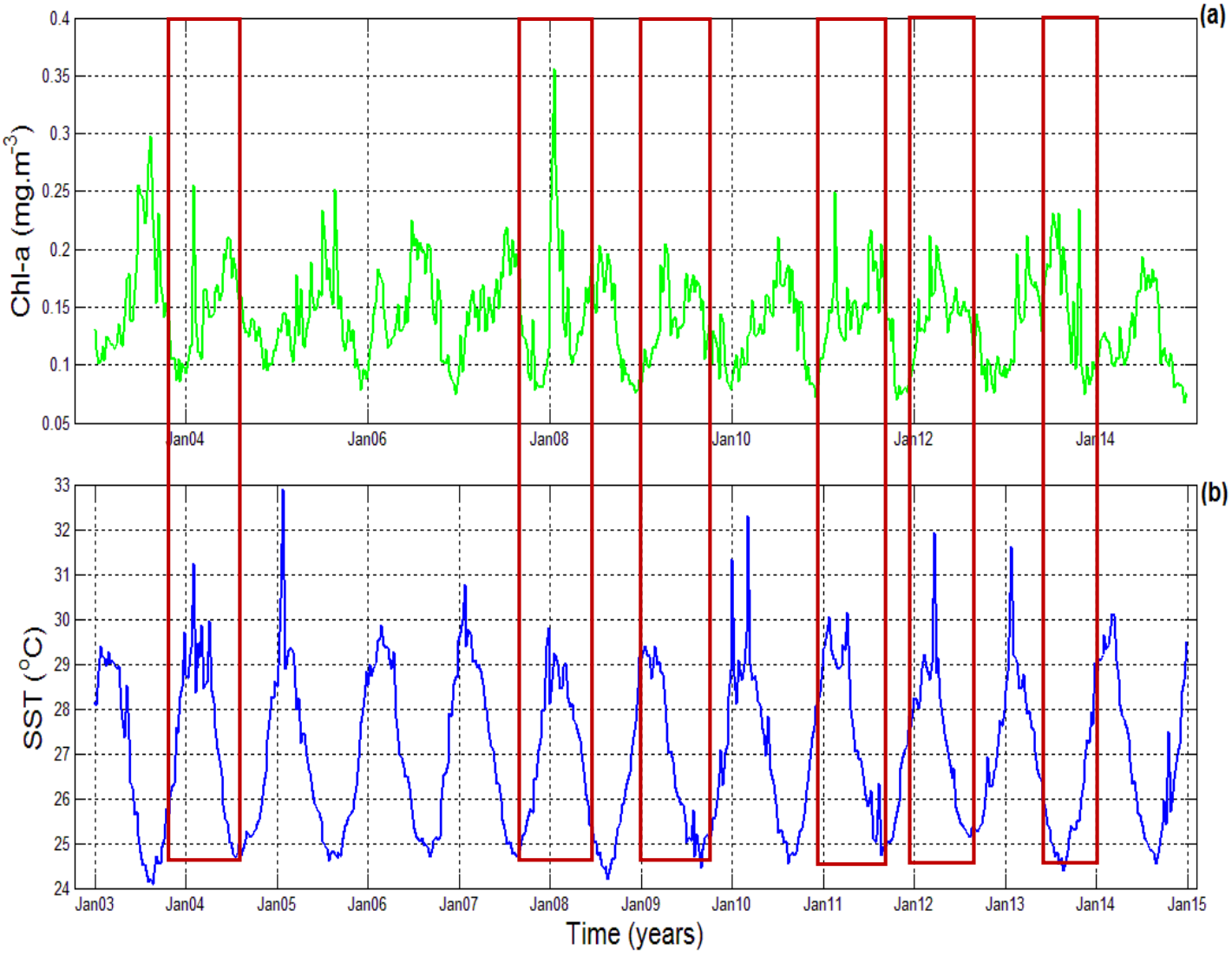

Fig. 3.16 SE Madagascar. Time series of (a) weekly mean Chl-a and (b) weekly mean SST for Jan 2003-Dec 2014 (Area between 40^0-55^0E and 22^0-30^0S). Red boxes depict the years when the highest Chl-a concentration did not occur during the spring bloom (June-August).

The time series for the Chl-*a* (Fig. 3.16) shows that there is a similar pattern in the Chl-*a* concentration across the years 2003, 2005, 2006, 2007, 2010 and 2014 with the highest concentration occurring between June-September for the whole area and the lowest concentration occurring between October-January. The highest peaks conversely do not occur during June-September for the years 2004, 2008, 2009, 2011, 2012 and 2013, they occur at the beginning of the year for example during February 2004, January 2008, April 2009, February-March 2011, March-April 2012. In October-November 2013 the peak occurs near the end of the year (See Table 3.3 below and the red boxes of Fig. 3.16). From Figs 3.14 and 3.15, it can be seen that the highest peaks for this period (2003-2014) occur in August 2003 (about half-way through the year) and January 2008.

The SST is high between December-April and low between June-November. SST starts to decrease as from June and is lowest during August-September, then starts to rise slowly after November, where the pattern is quite a smooth curve. The high SST period also follows a smooth pattern, with the exception of 2004, 2005, 2010, 2011, 2012 and 2013 where there are more spikes.

In general the Chl-*a* concentrations are high when the SST is low and Low when the SST is high. However, it can be seen from the individual time series that the Chl-*a* concentration is high when the temperature is high for the years 2004 (Feb), 2008 (Jan-Feb), 2009 (Apr-May), 2011 (Feb-Mar) and 2012 (Mar-Apr) (see Table 3.3 and the time series, Fig A.7 and Fig A.8 in the appendix).

It should also be noted here that there are a few spikes in the time series at the start of the years 2004, 2005, 2010, 2012 and 2013. When comparing this value to the temperature images during those specific weeks, it can be seen that the temperature for the area seems to peak when there is a high percentage of cloud cover. Weekly data are obtained by processing daily data and missing data are eliminated by the algorithm and this might result in very few data points on calm days forming the spikes in the time series. It should be noted that the image displays show that the SST is high (ca. 28 °C) at the beginning of the year whereas the spikes reach ca. 32 °C.

Table 3.3 SE Madagascar. Time frame during which the highest Chl-a concentration is found each year and the SST values corresponding to these Chl-a concentrations.

Year	Week	Month	Highest Chl-a concentration recorded in that year	SST corresponding to the Highest Chl-a concentrations
2003	29	August	0.298	24.20
2004	5	February	0.256	31.23
2005	30	August	0.252	2478
2006	23	June-July	0.225	25.75
2007	25	July	0.219	24.97
2008	3	January	0.356	29.22
2009	13	April	0.204	28.10
2010	24	June	0.210	25.23
2011	7	February	0.249	29.11
2012	9	March	0.212	28.64
2013	38	October-November	0.235	25.48
2014	24	June	0.194	25.38

Table 3.3 above shows that in 2003, 2005, 2006, 2007, 2010 and 2014, the highest Chl-a concentration occurred between June-August, when the SST is lower and in 2004, 2008, 2009, 2011 and 2012 it occurs between January-April and in 2013 during October-November, when the SST is higher. Also, the highest Chl-a concentration is found in January 2008 (Fig. 3.18) and the second highest Chl-a concentration occurs in August 2003 (Fig. 3.19).

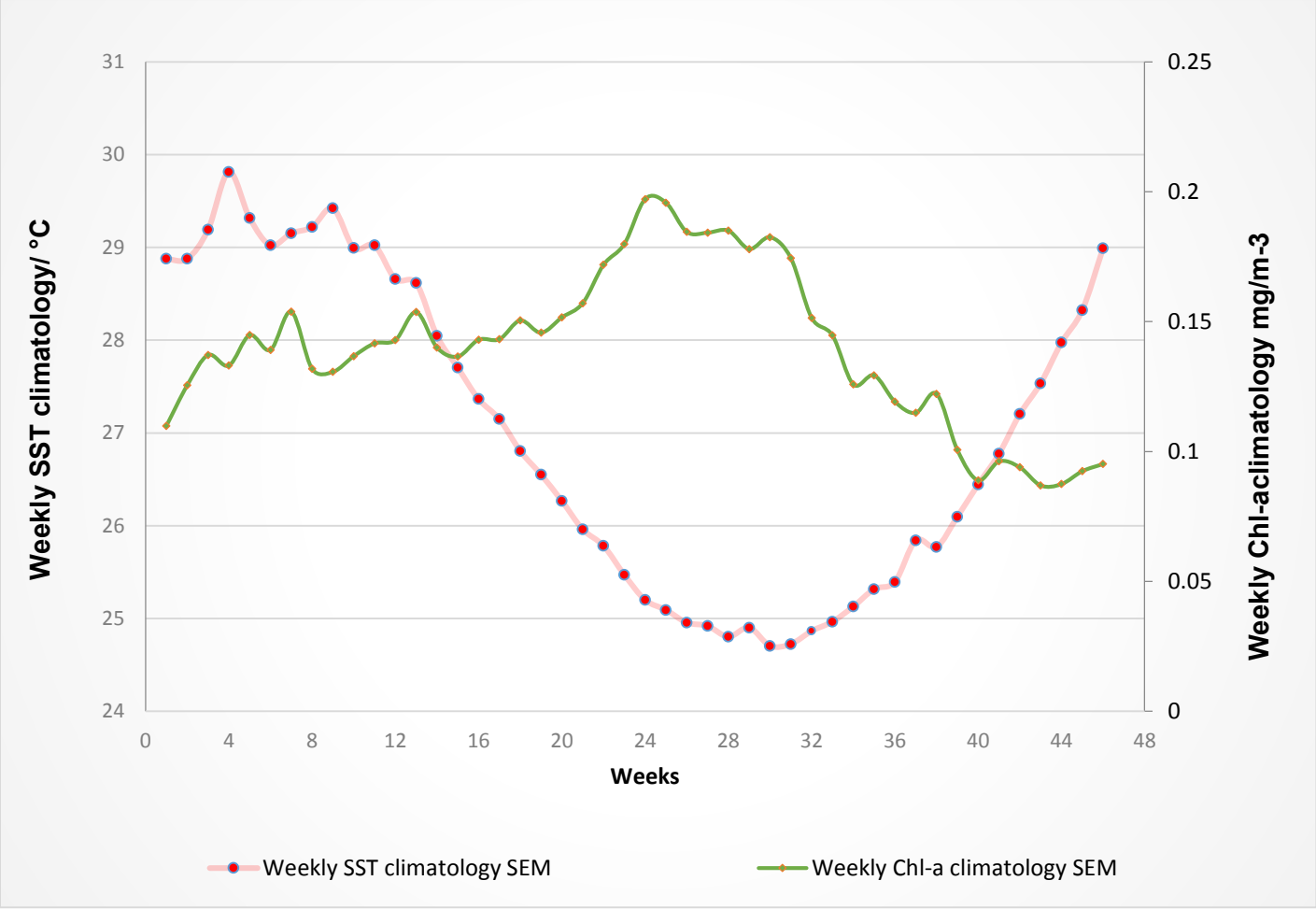

Fig. 3.17. SE Madagascar. Time series of weekly* Chl-*a* *and weekly SST climatology for Jan 2003-Dec 2014 (Area between 40^0-55^0E and 22^0-30^0S).

Fig. 3.17 shows an inverse relationship between the weekly SST and the weekly Chl-*a* concentration occurring during the years 2003-2014. The weekly Chl-*a* concentration starts to increase slightly from week 15 when the SST starts to decline. The Chl-*a* concentration peaks during the weeks 23-31 and starts to decrease as the SST slowly increases. During the weeks 39-46 the Chl-*a* concentration is lowest and during the weeks 1-14 the SST is higher than that during the weeks 39-46, yet the Chl-*a* concentration is quite high which is also shown in the Table 3.3 above. This suggests that there are two seasons in that area, one occurring during July/August and one during January/February when the Chl-*a* concentration is higher than the rest of the year.

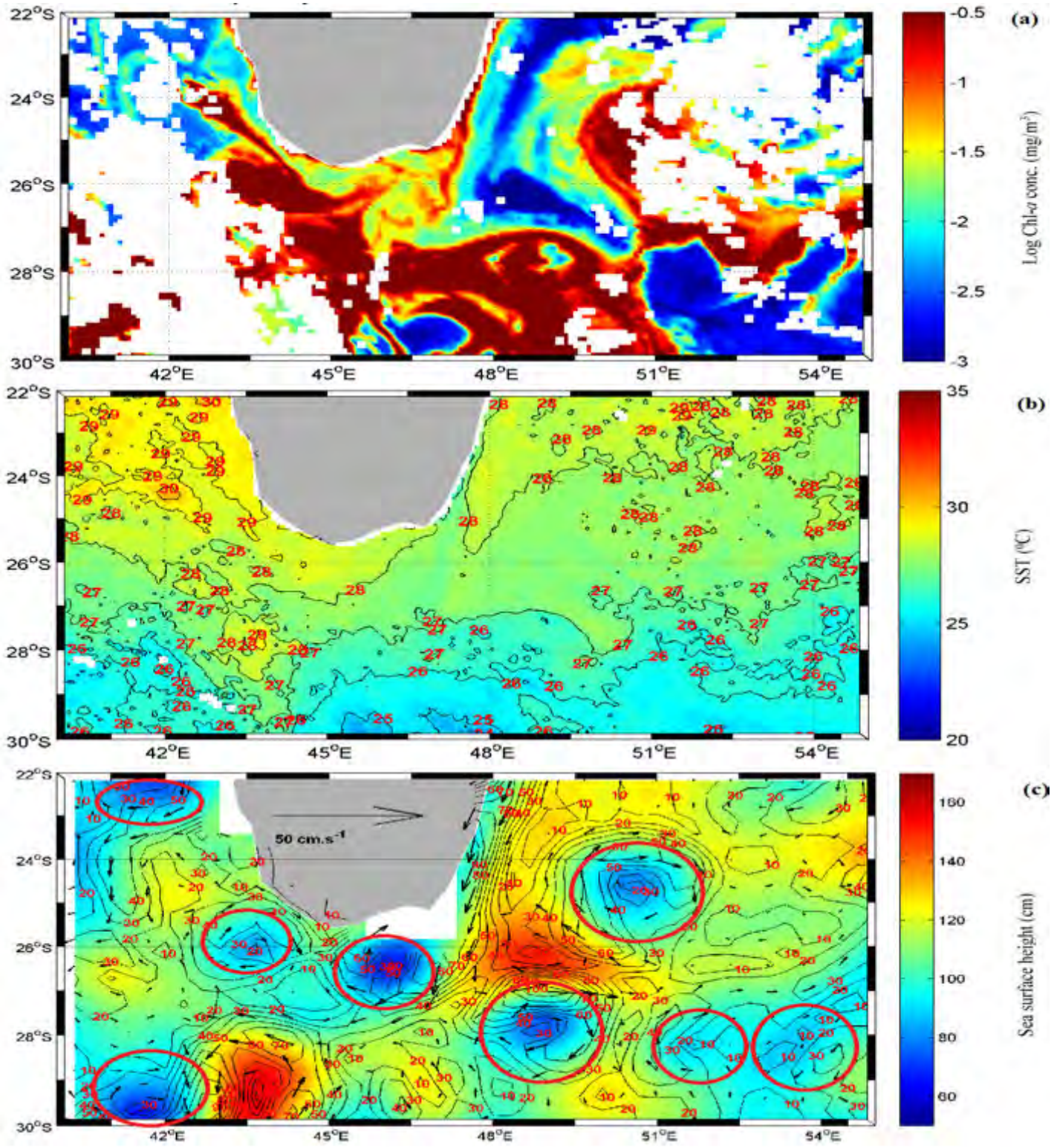

Fig. 3.18. SE Madagascar. (a) and (b) are the weekly averaged (17-25 January 2008) Chl-a concentrations and SST respectively; and (c) is the weekly averaged ADT and geostrophic velocities (16-23 January 2008). Red circles depict cool core cyclonic eddies. The white areas spread over the Fig. 3.18 (a) & (b) represent missing data due to cloud cover, while the white areas along the coasts represent shallow coastal areas.

Fig. 3.18 shows that in 2008, the SST in January is higher compared to that in July (Fig. 3.19) and December (Fig. 3.20) and yet the Chl-*a* concentration is higher in January. The week 17-25 January 2008 was chosen as an example as it displayed the highest Chl-*a* concentration of all the years and is also one of the years where the secondary bloom (January-February) (Longhurst 2001) is higher than the spring bloom (June-August) (Srokosz et al. 2004). The corresponding week for the ADT and geostrophic velocities is chosen to explain how the current dynamics and the Chl-*a* concentrations are related. The very high Chl-*a* concentration during January 2008 seems to correspond to the patterns of the cyclonic cold cores in that area (the red circles in Fig. 3.18 (c)). The cyclonic eddies have geostrophic velocities varying between 20-60 cms^{-1} and also have shallower SSH (60-100 cm, blue centres), thus suggesting the displacement of warm water and the upwelling of cool and nutrient rich water to the surface, which explains the high productivity of that area. The eddies along 26^0-30^0S seem to be moving towards the southeast which also corresponds to the displacement of the Chl-*a*.

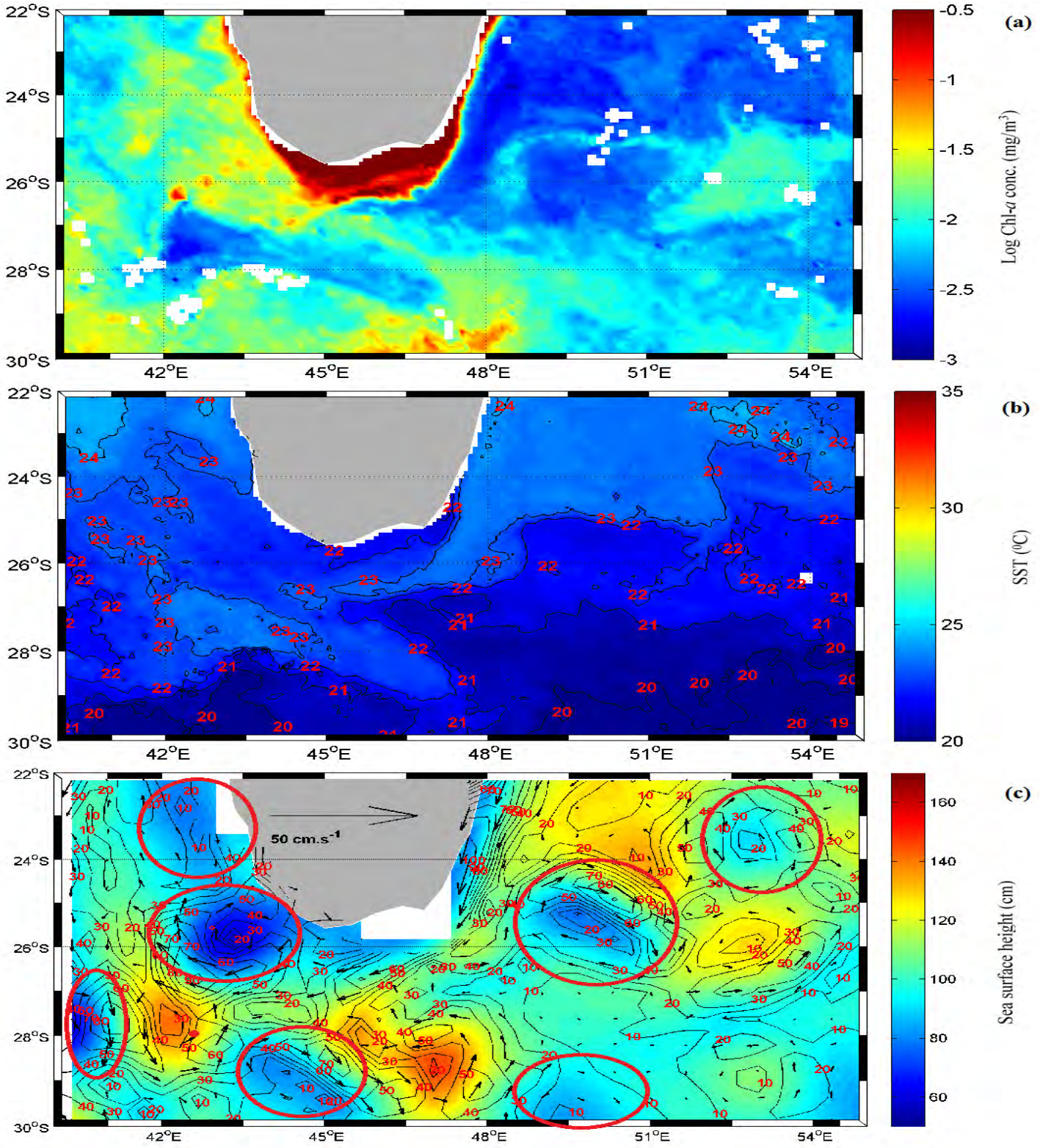

Fig. 3.19. SE Madagascar. (a) and (b) are the weekly averaged (12-20 August 2008) Chl-a concentrations and SST respectively; and (c) is the weekly averaged ADT and geostrophic velocities (13-20 August 2008). Red circles depict cool core cyclonic eddies. The white areas spread over the Fig. 3.19 (a) & (b) represent missing data due to cloud cover, while the white areas along the coasts represent shallow coastal areas.

Fig. 3.19 shows that in August, the SST is low and the Chl-*a* concentration is quite high but not as high as in January. There are still a number of the cold core rings during August explaining the high Chl-*a* concentrations. The SSH inside the eddies that are closer to the coast and along the west side seems to be lower, thus explaining the higher Chl-*a* concentrations around that area compared to the east side. There are more eddies in January than in August which also explains the higher Chl-*a* concentrations in January. The geostrophic velocities of the eddies for this period vary between 10-70 cms^{-1} with the ones along the southwest coast being stronger than those on the east. The week 12-20 August 2008 was chosen so that the Chl-*a* concentration occurring then could be compared to that of the same week in 2003 when the highest Chl-*a* concentration occurred (Fig. 3.21).

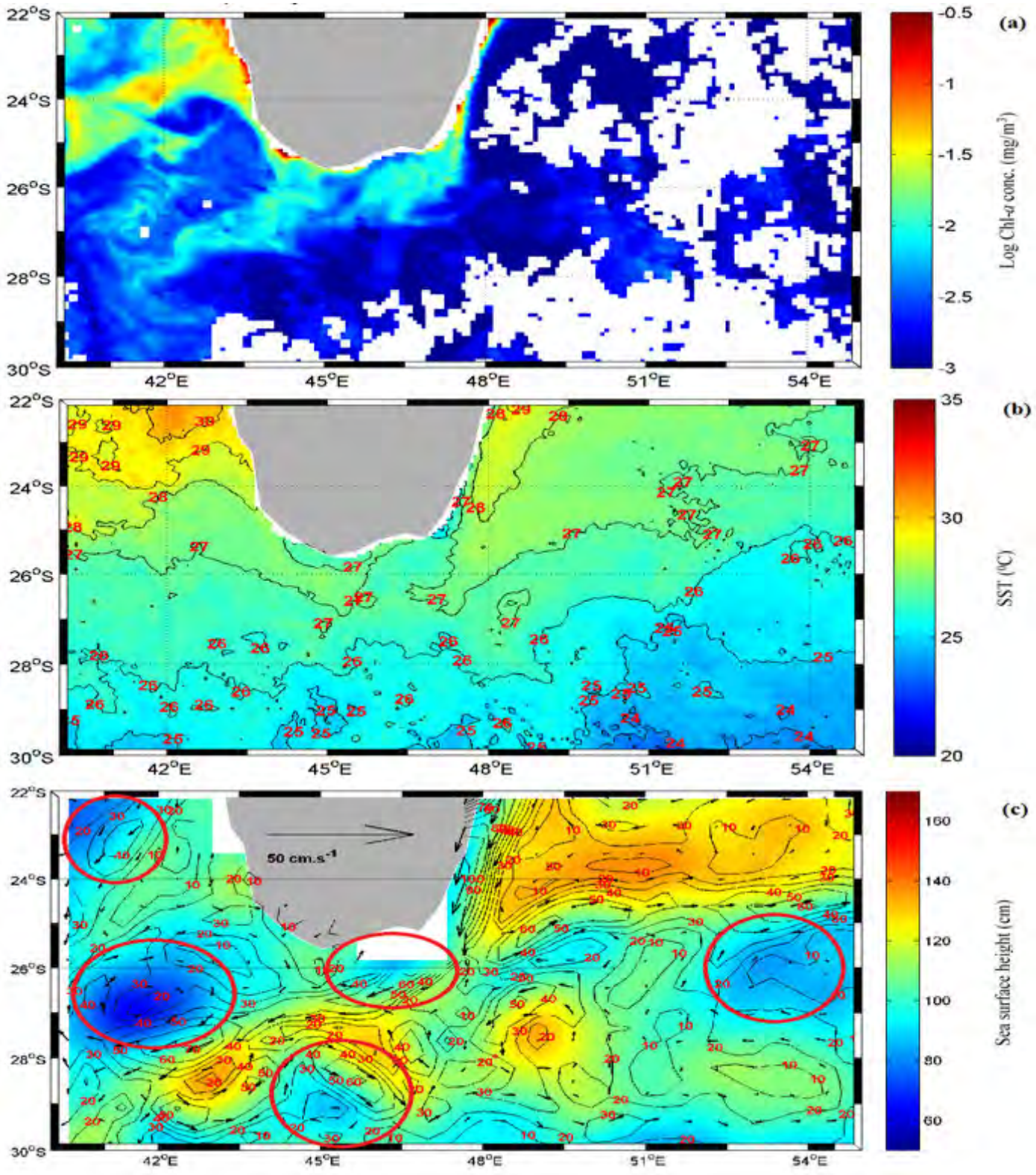

Fig. 3.20. SE Madagascar. (a) and (b) are the weekly averaged (18-26 December 2008) Chl-a concentrations and SST respectively; and (c) depicts the weekly averaged ADT and geostrophic velocities (17-24 December 2008). Red circles show cool core cyclonic eddies. The white areas spread over the Fig. 3.20 (a) represent missing data due to cloud cover, while the white areas along the coasts represent shallow coastal areas.

Fig. 3.20 shows that the SST and the Chl-*a* concentration are both low during December 2008. The geostrophic velocities of the eddies for this period vary between 10-60 cms^{-1} on the southwest coast and between 10-20 cms^{-1} in the east, explaining the occurrence of enhanced Chl-*a* concentrations mostly along the coasts and in the west. Also, there are only a few cold core rings during this month, thus there is less upwelling and less nutrient-rich cool water being brought to the surface, resulting in low Chl-*a* concentrations across the area. The week 18-26 December 2008 was chosen as the lowest Chl-*a* concentration of 2008 occurred during that week.

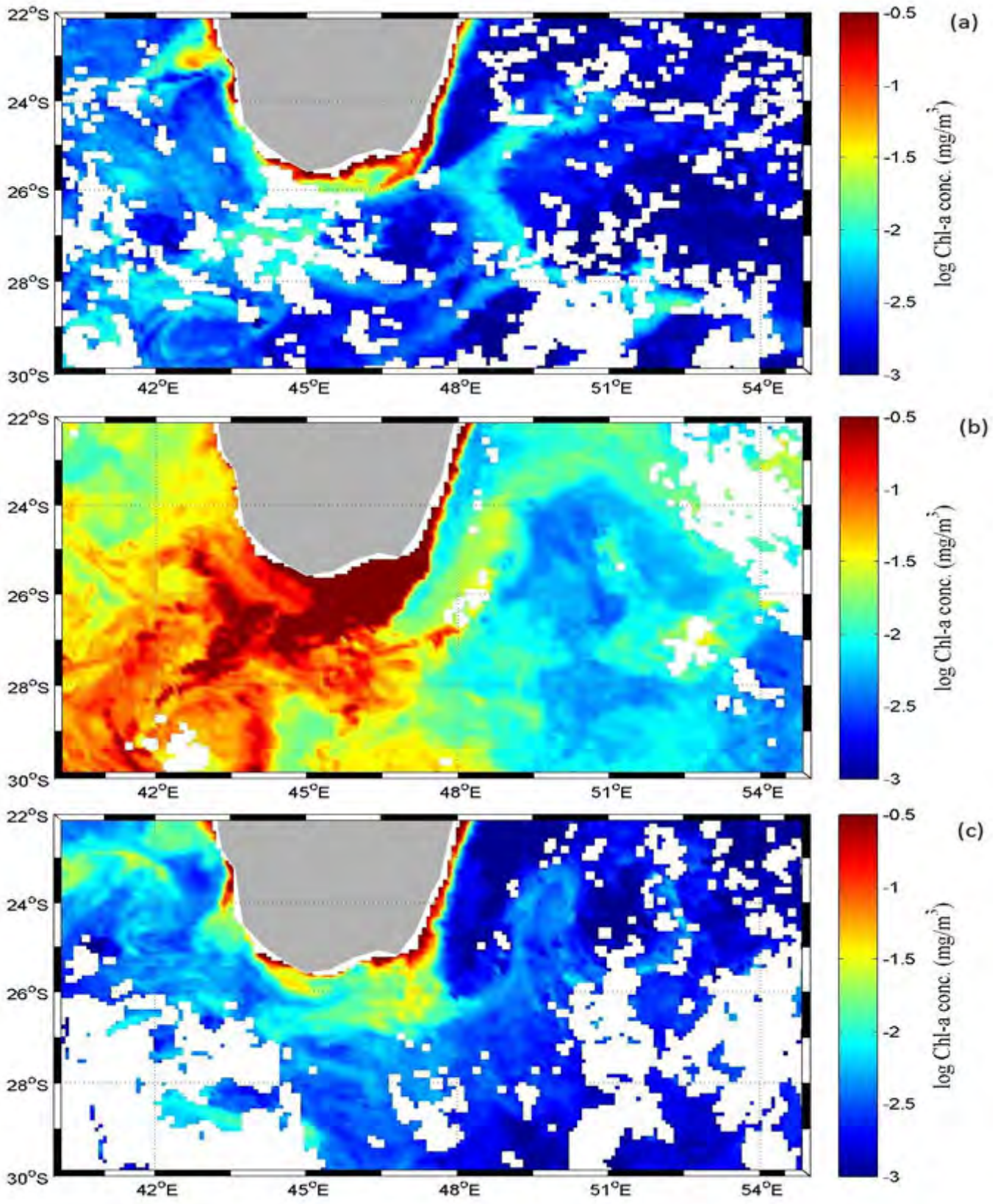

Fig. 3.21. SE Madagascar. Weekly averaged Chl-a concentrations for the weeks (a) 17-25 January 2003 (b) 13-21 August 2003, and (c) 19-27 December 2003. The white areas spread over the Fig. 3.21 (a), (b) & (c) represent missing data due to cloud cover, while the white areas along the coasts might be representing shallow coastal areas.

Fig. 3.21 shows that the highest Chl-*a* concentrations for the year 2003 occurred in August and the lowest in December. The highest concentrations are found towards the southwest of Madagascar. In January, even though the SST is high as in December, the Chl-*a* concentration is slightly higher than in December and is higher along the coasts. When comparing Figs 3.21 and 3.22, the Chl-*a* concentration coincides with the cold core ring patterns and the SSH. If we look at the Chl-*a* concentrations in January 2003, they are slightly higher than in December and the eddies in January seem to be stronger than in December. Furthermore, the SSH is also slightly higher in December than in January. Also, there are more eddies occurring in August than in January or December thus explaining the higher Chl-*a* concentration in August compared to that in January and December. The Chl-*a* concentration is stronger along the coasts in all cases. The water that is displaced from the coasts by the SEMC is replaced by nutrient rich waters and there is also land run-off contributing to the high Chl-*a* concentrations along the coast. The images for the same weeks as in 2008 were chosen for Chl-*a* concentration to show how the Chl-*a* concentrations occurring during the same week vary for these years (comparing Fig 3.18 - 3.21). There is a very strong secondary bloom in January 2008 compared to 2003 when the January bloom is very weak or absent. In 2003, the highest bloom occurred in August which is considered to be the spring bloom whereas in 2008 this bloom is very weak; the lowest Chl-*a* concentration occurs in December of both years.

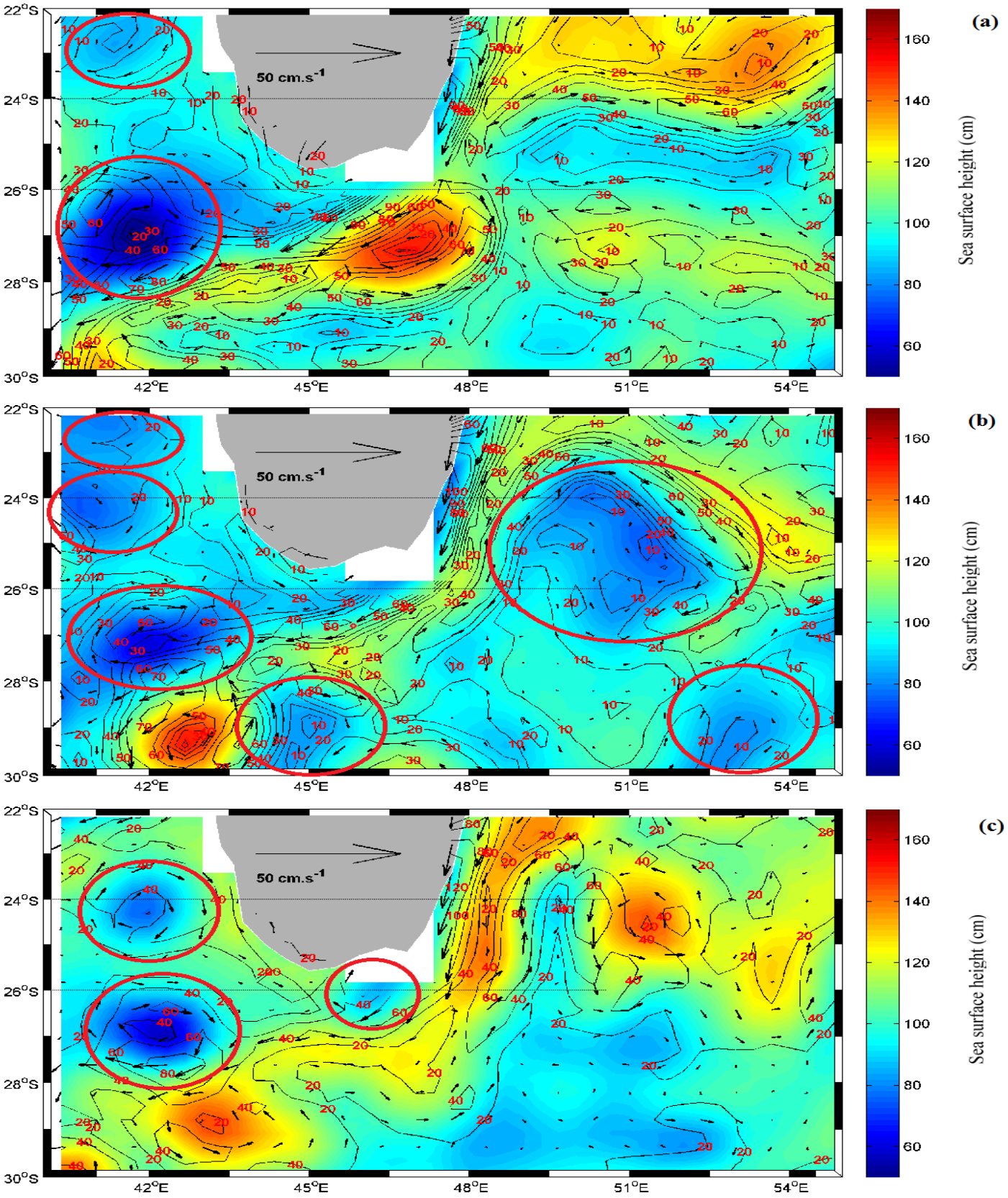

Fig. 3.22. SE Madagascar. Weekly averaged ADT and geostrophic velocities for the weeks (a) 15-22 January 2003, (b) 13-20 August 2003 and (c) 17-24 December 2003. Red rings highlight cyclonic eddies. The white areas along the coasts represent shallow coastal areas.

Fig. 3.22 shows that in August 2003, the cold core rings in this area are more abundant than in January or December. In January, there is a weak cyclonic ring with geostrophic velocities of 10-20 cms^{-1} and a strong cyclonic ring with geostrophic velocities of 20-80 cms^{-1}, both on the west side of the area. In August, there are more strong eddies than in January with geostrophic velocities of 20-70 cms^{-1} and most are found on the south and west side than on the east side. In December, the eddies are only along the south and the west side with geostrophic velocities of 20-60 cms^{-1}. Also, the SSH in August is lower compared to that of January or December and that of January is slightly lower than that of December. The corresponding weeks for ADT and geostrophic velocities were chosen to display the relationship between the current dynamics and the Chl-*a* concentration for the year 2003 (Fig. 3.21).

Table 3.4. Correlation between the time series of Chl-a and SST for each individual years and the whole time period of 2003-2014.

Time Period	Correlation coefficient for the Chl-*a* and SST time series at 95 % significance level for Southeast Madagascar
Jan-Dec 2003	-0.7629
Jan-Dec 2004	-0.2145
Jan-Dec 2005	-0.4358
Jan-Dec 2006	-0.5216
Jan-Dec 2007	-0.3846
Jan-Dec 2008	0.0905
Jan-Dec 2009	-0.3666
Jan-Dec 2010	-0.6517
Jan-Dec 2011	-0.1781
Jan-Dec 2012	0.2905
Jan-Dec 2013	-0.4433
Jan-Dec 2014	-0.5554
Jan 2003-Dec 2014	-0.3468

From Table 3.4 it can be noted that, similar to Fig. 3.16, there is an inverse relationship between SST and Chl-*a* concentration, except in 2008 and 2012 where the correlation is slightly positive. This is because during these years, the Chl-*a* concentration was high when the SST was also high. Similarly, in 2004, 2009, 2011 and 2013, the correlation is less negative than in the other years and this may be because the highest Chl-*a* concentrations

during these years occur at the beginning of the years when the SST is high. However, when compared over the whole year, there is an inverse relationship between the SST and the Chl-*a* concentration in that area.

SECTION 3. Mascarene Islands, MI (AREA 3)

Fig. 3.23 shows the January climatology of the MI area in terms of Chl-*a* concentration and also the longitude band used in the Hovmöller plot in Fig. 3.2. Note the generally low phytoplankton levels found in this region, as indicated by Chl-*a* concentrations.

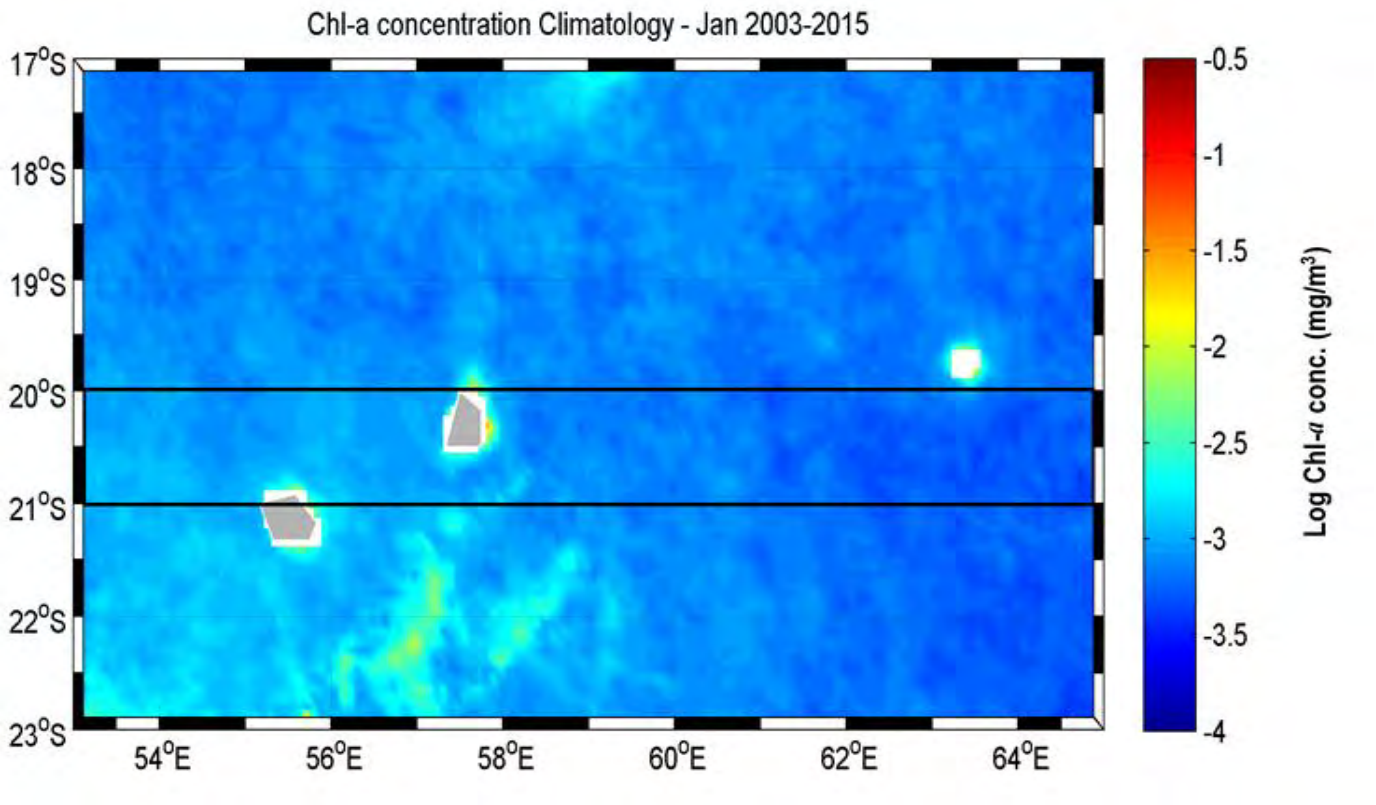

Fig. 3.23. Mascarene Islands (MI). Area chosen (the black box) for the Hovmöller plot of weekly Chl-a concentration averaged along the latitude 20^0S-21^0S. The white areas along the coasts represent shallow coastal areas.

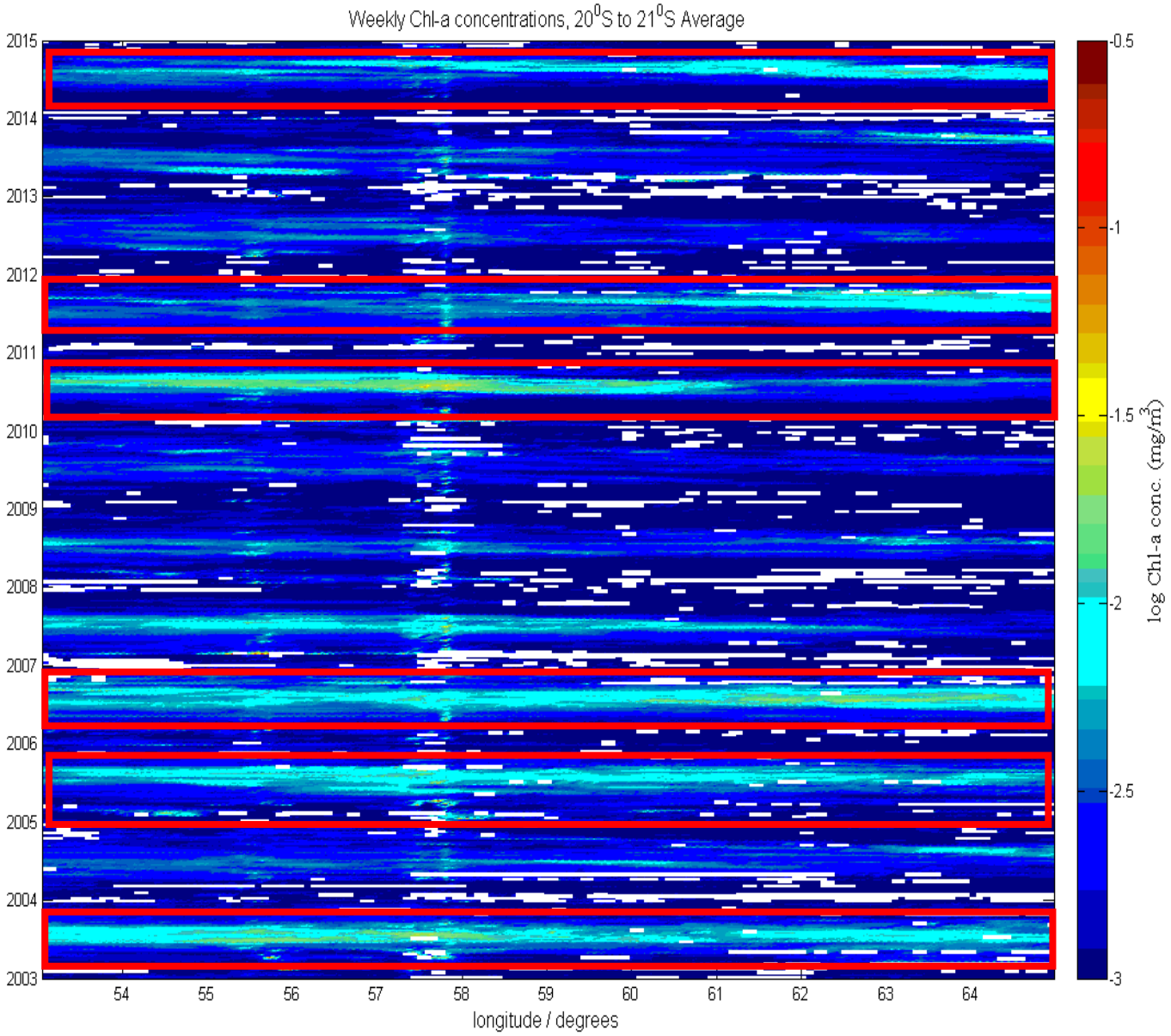

Fig. 3.24. Mascarene Islands (MI). Hovmöller plot of weekly Chl-a concentration averaged along the latitude 20^{0}S-21^{0}S. The white areas spread all over the pictures represent missing data due to cloud cover. **The red boxes highlight the highest Chl-a concentrations around the MI.**

Fig. 3.24 shows the slight annual variability in the Chl-a concentration as it moves from low concentration (in January) to high concentration (in July) across the years. There appears to be a seasonal signal in Chl-a concentrations across the years with slight variability along the longitude as in some years it is further east and in others more in the west. The Chl-a

concentration is higher in 2003, 2005, 2006, 2010, 2011 and 2014 (highlighted by the red boxes) with the highest concentrations in 2003 and 2006.

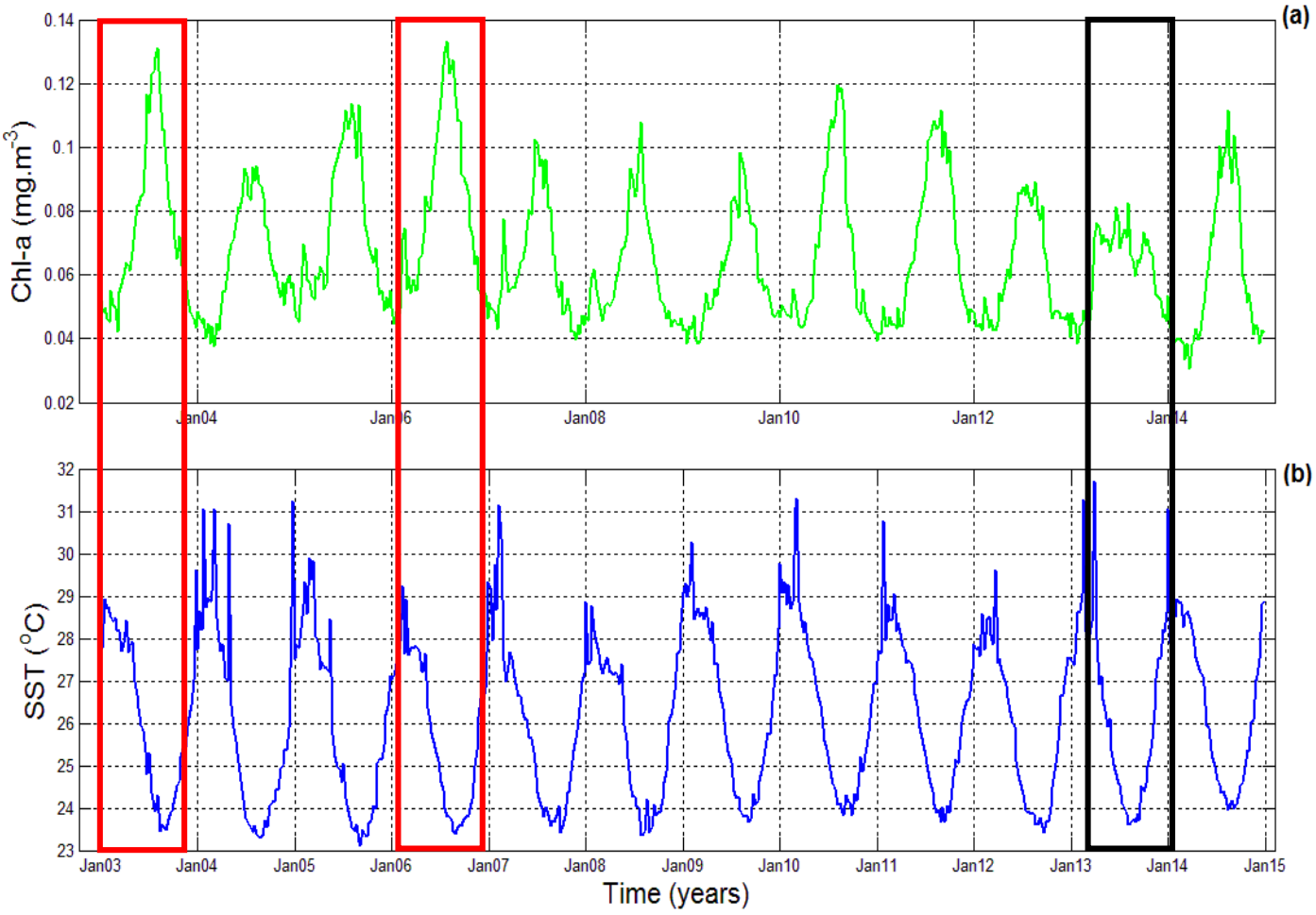

Fig. 3.25. Time series for the weekly mean Chl-a (a) and weekly mean SST (b) for Jan 2003-Dec 2014 along the Mascarene Islands (Area between 53^0-65^0E and 17^0-23^0S). Red boxes show years of highest Chl-a concentration and black box shows the year of lowest Chl-a concentration.

The highest Chl-*a* concentration occurs between June-September across all the years with the exception of the year 2013, where it is between April-September and the lowest Chl-*a* concentration occurs between December-April (Fig. 3.25). There is a similar pattern across the years, with the SST following a reverse pattern compared to that of the Chl-*a* concentration. When the SST is high, the Chl-*a* concentration is low and vice versa. The Chl-*a* concentration is highest in the years 2003 and 2006 and lowest in 2013.

It should also be noted here that there are a few spikes in the time series. When comparing these spikes to the temperature images during those specific weeks (not presented), it can be seen that the temperature for the area seems to peak when there is a high percentage of cloud cover. Thus a few images may give very high temperature readings, especially if those weeks are characterised by calm periods allowing a warm thin skin to develop at the ocean surface (see Section 2.1).

Table 3.5 Shows the time frame during which the highest Chl-a concentration is occurring for each years across the Mascarene Islands and the SST values corresponding to these Chl-a concentrations.

Year	Week	Month	Highest Chl-a concentration recorded in that year	SST corresponding to the Highest Chl-a concentrations
2003	28	July	0.131	24.29
2004	29	August	0.094	23.40
2005	28	July	0.113	23.56
2006	27	July-August	0.133	23.79
2007	23	June-July	0.102	25.06
2008	27	July-August	0.108	23.36
2009	28	July	0.098	23.94
2010	28	July	0.119	24.08
2011	31	August-September	0.112	23.68
2012	30	August	0.089	23.61
2013	28	July	0.082	23.60
2014	29	August	0.112	23.96

Table 3.5 also confirms the similar patterns displayed in the Fig. 3.25, showing that the highest Chl-a concentration across the Mascarene Islands occurs between June-September, the years 2003 and 2006 had the highest concentrations among all the years and 2013 had the lowest Chl-a concentration.

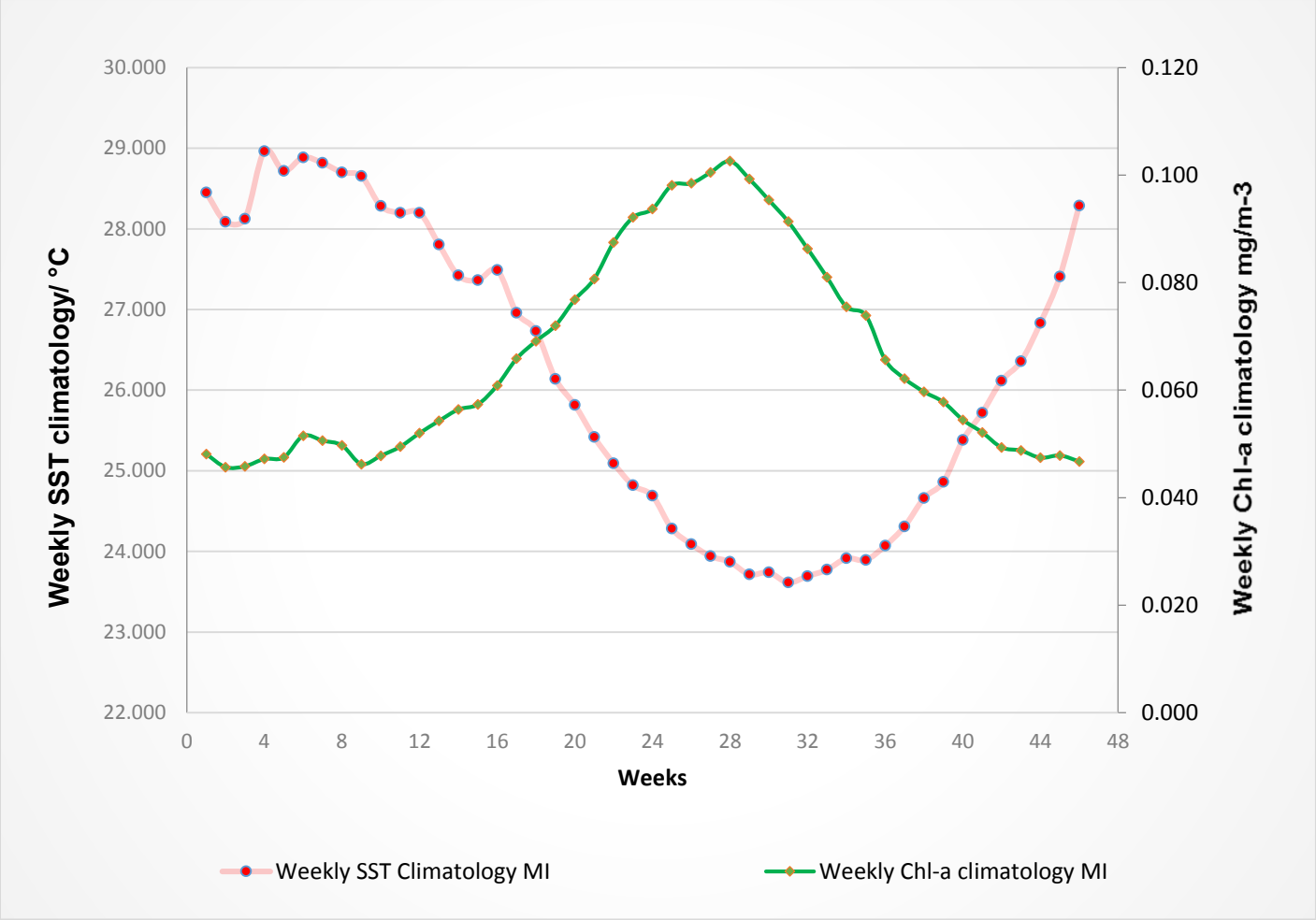

Fig. 3.26. Time series for the weekly Chl-a and weekly SST climatology for Jan 2003-Dec 2014 along the Mascarene Islands (Area between 53^0-65^0E and 17^0-23^0S).

Fig. 3.26 shows that the weekly Chl-*a* concentration and the weekly SST follow an inverse pattern as the Chl-*a* concentration is low when the SST is high and vice versa. The Chl-*a* concentration is high between the weeks 20-34 and low between the weeks 1-15 and 41-46. This suggests that there are two seasons, one with high Chl-*a* concentrations and one with low Chl-*a* concentrations. Note that the Chlorophyll peak is in week 28 wheras SST is at its minimum later, in week 31.

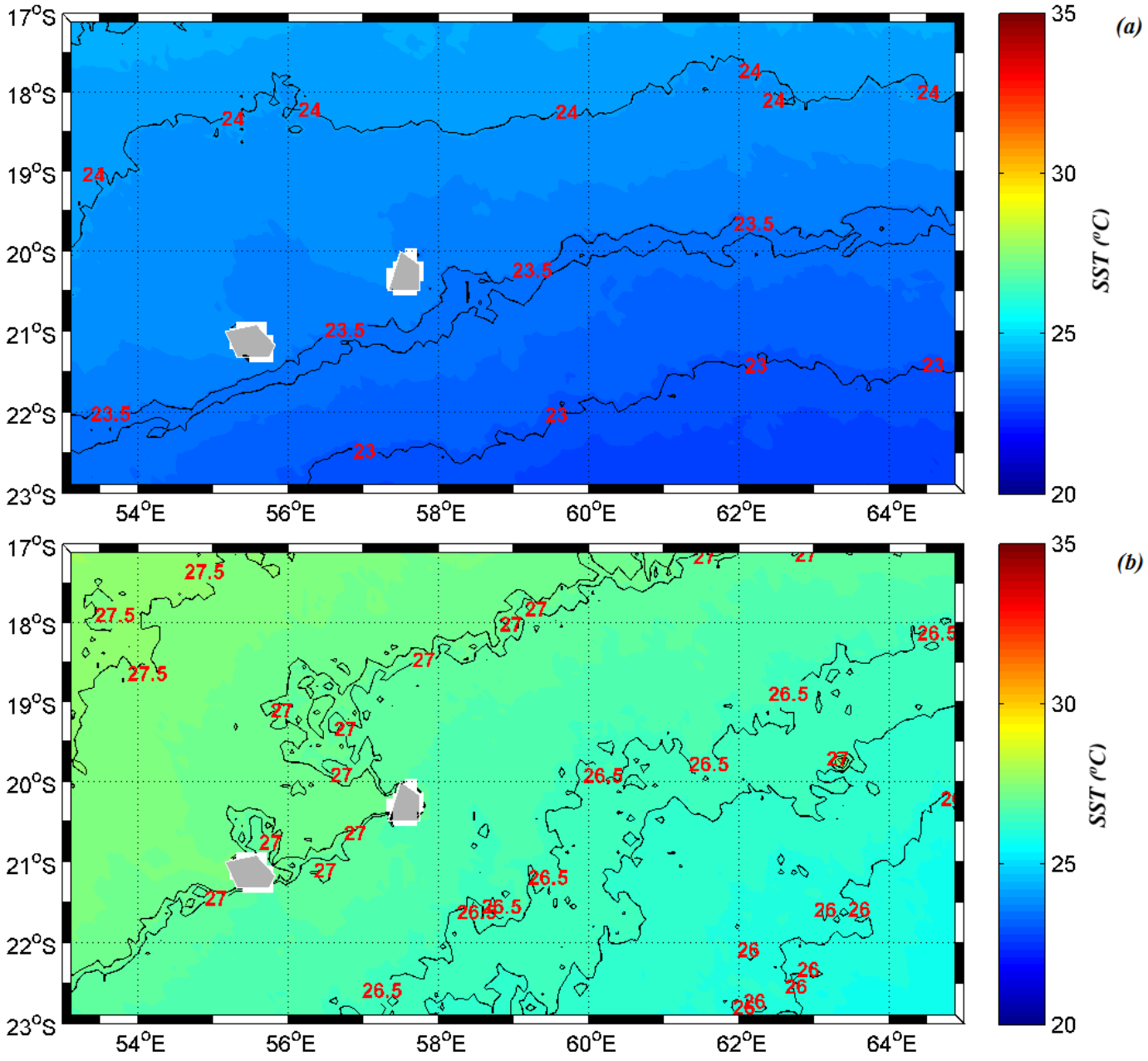

Fig. 3.27. Mascarene Islands. Monthly SST Climatology over the period 2002-2014 for (a) August and (b) December. The white areas along the coasts represent shallow coastal areas.

The monthly SST climatology shows that around the Mascarene Islands region, it is cooler in August (Fig. 3.27 (a)) than in December (Fig. 3.27 (b)). There is little difference between these two seasons; there is a gentle gradient in SST from warmer in the northwest to cooler in the southeast; in both seasons the highest climatological SST is about 27.5 ^{0}C in December, and in August about 24 ^{0}C.

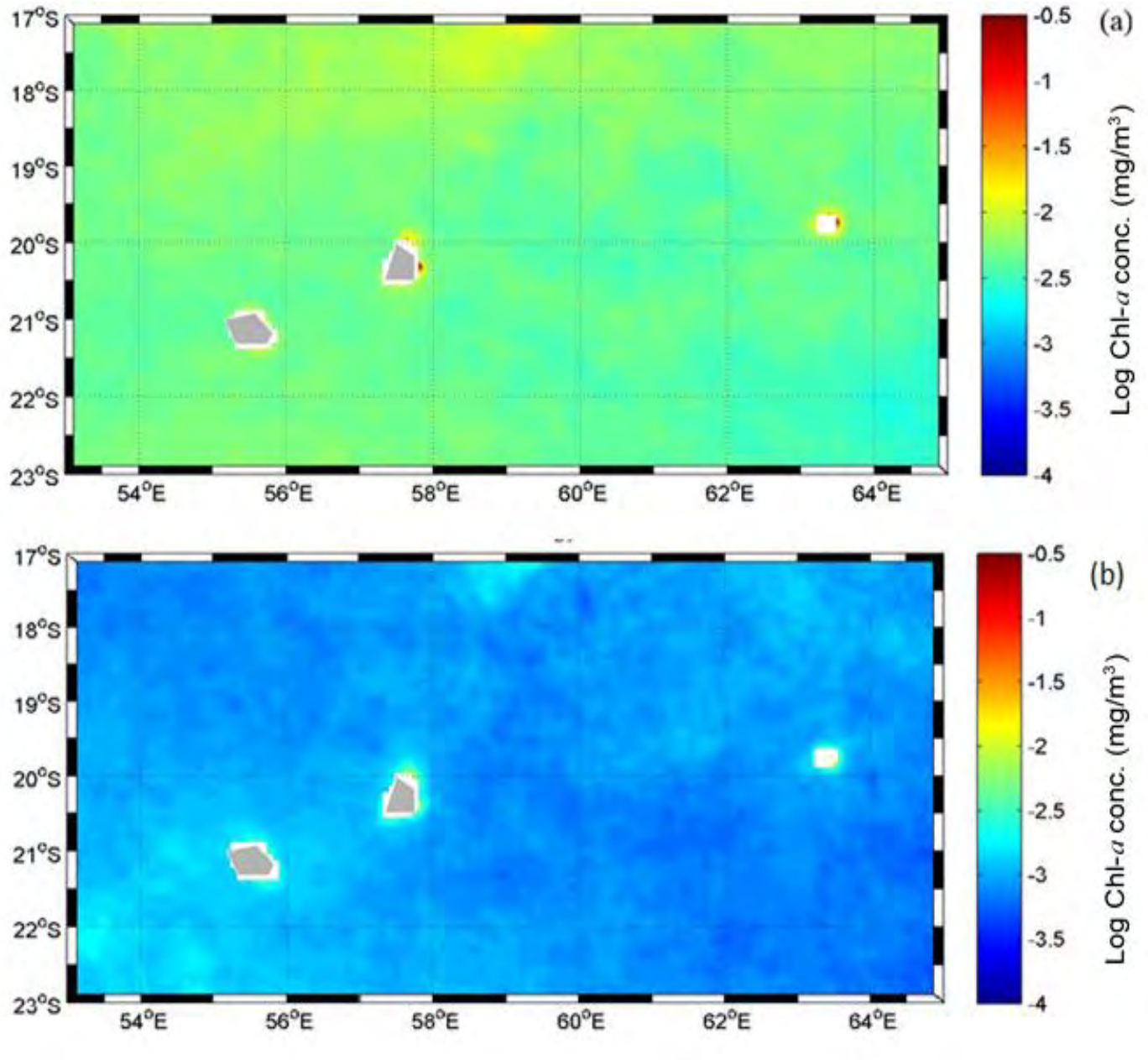

Fig. 3.28. Mascarene Islands. Monthly Chl-a concentration Climatology over the period 2002-2014 for (a) August and (b) December. The white areas along the coasts represent shallow coastal areas.

Fig. 3.28 shows that the Chl-*a* concentration in December is lower than in August. Also, the Chl-*a* concentration is higher around the Islands. When comparing Fig. 3.27 and Fig. 3.28, it can be seen that the Chl-*a* concentration is high when the SST is low and vice versa. During August, the Chl-*a* concentration is high and spread out over the whole area and in December it is generally low and higher along the coasts of the Islands.

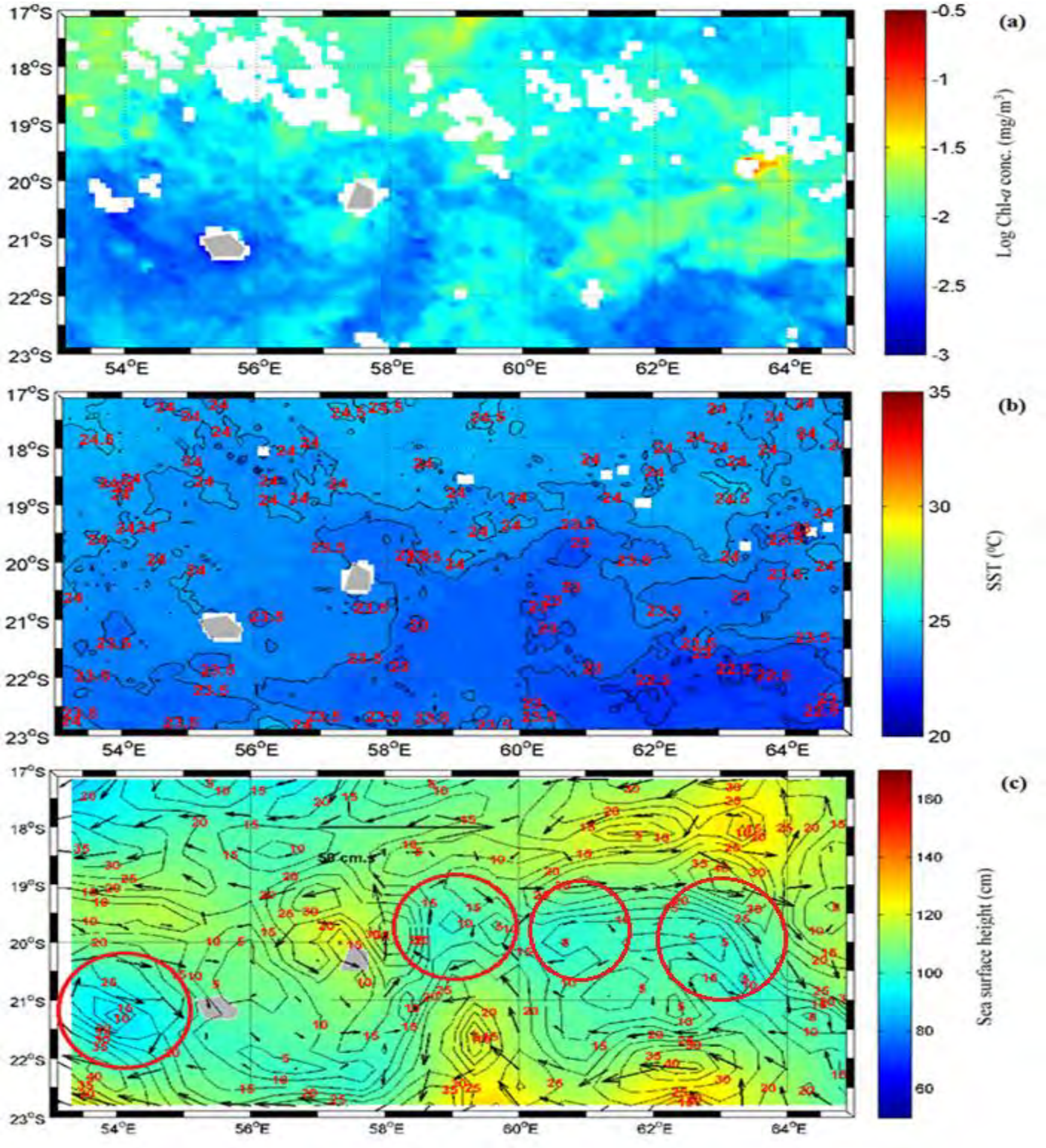

Fig. 3.29. Mascarene Islands. (a) and (b) are the weekly averaged (05-13 August 2006) Chl-a concentrations and SST respectively; and (c) is the weekly averaged ADT and geostrophic velocities (2-9 August 2006). The red circles depict cool core cyclonic eddies. The white areas spread all over the panels (a) & (b) represent missing data due to cloud cover, while the white areas along the coasts represent shallow coastal areas.

The Chl-*a* concentrations for this area are highest in 2006 compared to the other years and from the Table 3.5, it can be seen that the highest Chl-*a* concentration usually occurs during the months July-August, which is why the week 05-13 August 2006 was chosen to show how the Chl-*a* concentration varies in that area. The geostrophic velocities of the eddies in August varies between 5-35 cms^{-1}. Also, in August the SSH is lower and there are more cold core rings across the Mascarene Islands' area (Fig. 3.29) than in December (Fig. 3.30). The southeasterlies are stronger during June-September (Hermes and Reason 2008); these strong southeasterlies drive the currents that bring cold nutrient rich water to the surface. This might explain why the SST in that area is lower in August than in December when cool water is being brought to the surface. Also, this cool water, being rich in nutrients, also causes the higher Chl-*a* concentrations in August compared than in December. The year 2006 was chosen as an example as the Chl-*a* is highest during that year compared to the other years. The week 5-13 August was chosen to display the difference in Chl-*a* concentration between the phytoplankton "bloom" period (July-August) and the low concentrations found in December (Fig. 3.30).

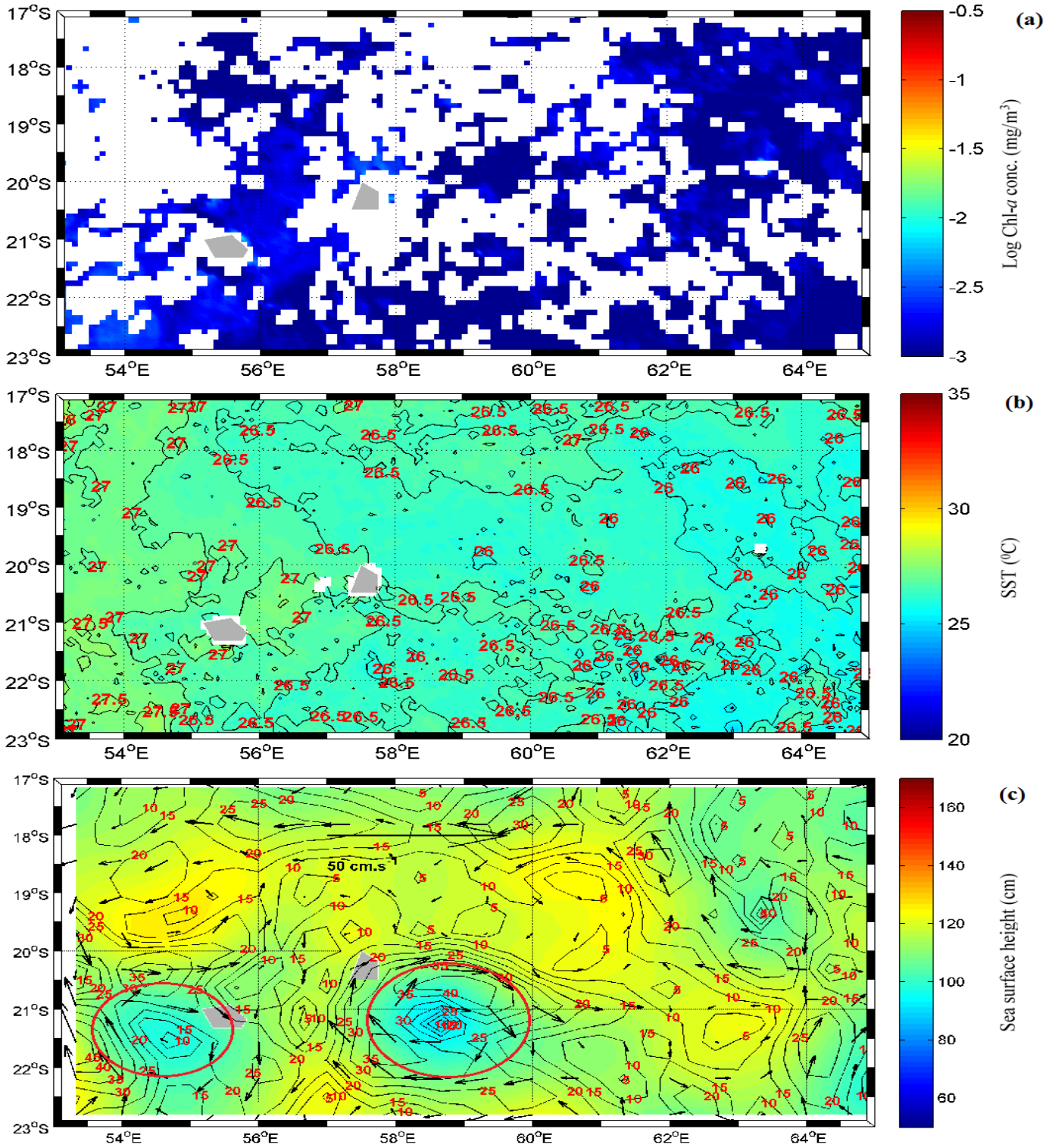

Fig. 3.30. Mascarene Islands. (a) and (b) are the weekly averaged (03-11 December 2006) Chl-a concentration and SST respectively; and (c) is the weekly averaged ADT and geostrophic velocities (6-13 December 2006). Red circles depict cool core cyclonic eddies. The white areas spread all over the panels (a) & (b) represent missing data due to cloud cover, while the white areas along the coasts represent shallow coastal areas.

The Fig. 3.26 shows that the lowest Chl-*a* concentration occurs during December-February, thus the week 03-11 December is used to illustrate the low Chl-*a* concentration of that area. The geostrophic velocities are slightly higher (10-40 cms^{-1}) in December (Fig. 3.30) than in August, while, the SSH is lower in August than in December. Therefore, less nutrient rich cold water is reaching the surface which explains the high SST and lower Chl-*a* concentration during December. Also, as shown in Fig. 3.28, the Chl-*a* concentration is higher around the Islands as the only eddies occurring in that area (Fig. 3.30) are close to the Islands. Fig. 3.30(a) also shows a large amount of cloud cover in the area in the southern summer, with less light reaching the euphotic zone for photosynthesis, thus leading to low Chl-*a* concentrations.

Table 3.6. Correlation between the time series of Chl-a and SST for each individual years and the whole time period of 2003-2014.

Time Period	Correlation coefficient for the Chl-*a* and SST time series at 95 % significance level for the Mascarene Islands
Jan-Dec 2003	-0.7555
Jan-Dec 2004	-0.7656
Jan-Dec 2005	-0.6357
Jan-Dec 2006	-0.7789
Jan-Dec 2007	-0.4028
Jan-Dec 2008	-0.6418
Jan-Dec 2009	-0.8631
Jan-Dec 2010	-0.6636
Jan-Dec 2011	-0.9131
Jan-Dec 2012	-0.7814
Jan-Dec 2013	-0.7234
Jan-Dec 2014	-0.9016
Jan 2003-Dec 2014	-0.6733

From Table 3.6 above it can be noted that, as in Fig. 3.25, there is quite a strong inverse relationship between SST and Chl-*a* concentration.

CHAPTER 4 DISCUSSION

Chl-*a* concentration is very often considered as a major indicator of the productivity of an area and the higher the Chl-*a* concentration, the more productive the area (GlobalChange.gov. U.S. Global Change Research Program). Productivity depends on several factors such as Chl-*a* concentration, sea surface temperature, speed and direction of currents and wind, amongst others. In this study, the variability in the patterns of Chl-*a* concentration, sea surface temperature (SST) and absolute dynamic topography (ADT) and geostrophic velocities of the three study areas: Northeast Madagascar (NEM), Southeast Madagascar (SEM) and the Mascarene Islands (MI) are assessed separately.

Northeast Madagascar, NEM (AREA 1)

This study revealed that the Northeast Madagascar area has two phytoplankton blooms. The first bloom occurs during January-April and the second one during July-August and this seems to follow an annual pattern. Lévy et al. (2007) made similar findings, suggesting that the seasonal cycle of phytoplankton occurs during the summer (July-August) and winter monsoons (January-February). According to Wiggert et al. (2006), these two growth periods are the results of the semi-annual wind reversals associated with the monsoon system. There is a seasonally reversing circulation in the upper ocean across the North Indian Ocean (north of 10^0S) that is forced by the seasonally reversing winds blowing from the southwest during the summer monsoon and from the northeast during the winter monsoon, which results in vertical mixing that generates coastal and open ocean upwelling and downwelling (Schott and McCreary 2001).

Study area 1 which lies between 10^0-18^0S, displays the same patterns as the North Indian Ocean with two blooms occurring during the same two periods mentioned by Wiggert et al. (2006). From Figs 3.9 and 3.11, it can be seen that the bloom occurring during the summer monsoon is widespread over the whole area, while the one occurring during the winter monsoon is mostly concentrated along the northwest and along the coasts. This is because during the winter monsoon, there is a small cyclonic ring (low SSH) present along the west

coasts and the Northeast Madagascar Current displaces the coastal water to the northwest, explaining why the bloom occurs mostly along the northwest and along the coasts. When the water is displaced along the coasts by the cyclonic ring and the NEMC, nutrient rich water is brought to the surface, giving rise to strong coastal blooms. During the summer monsoon on the other hand, It can be seen that along with the cold core ring present on the west side of the Island, SSH is low on the east side indicating that there is upwelling of cooler water on both sides of NEM, explaining the bloom that occurs over the whole area during that period. Additionally, from Table 3.1, it can be seen that the winter monsoon bloom is of higher Chl-*a* concentration compared to that in summer, suggesting that even though the winter bloom is mostly coastal, it is of greater intensity than the summer bloom.

These blooms do not depend only on the dynamic topography and geostrophic velocities or the SST patterns but also on other physical environmental factors such as the mixed layer depth. Mixed layer depth gives an indication of the depth to which phytoplankton cells are carried by vertical mixing (usually wind-induced); if the MLD is greater than the critical depth (depth at which the phytoplankton growth and the loss of phytoplankton biomass are equal (Sverdrup 1953)) then primary production is inhibited because cells are carried out of the euphotic zone for some of the daylit period, reducing productivity. There is an optimum MLD for primary production, too shallow and it is diminished and if too deep production is also reduced (Sverdrup 1947). Lévy et al. (2007), also showed that horizontal currents, vertical velocity and MLD are dynamical features affecting the occurrence of these blooms during the summer and winter monsoons (Fig. 1.6). The monsoons further affect the horizontal and vertical circulations which closely affect these blooms.

On the other hand Hermes and Reason (2008) mentioned that the southeasterlies south of 10^0S occur throughout the year and happen to extend further north and are stronger during austral winter. During austral summer, the southeasterlies only extend to around 13^0S with monsoonal westerlies between 5^0S and 11^0S. The fact that the Southeasterlies are present all year round might explain the coastal bloom that is always present along the coasts. During the austral summer, the combination of the southeasterlies in the south and the monsoonal westerlies in the north of the region might explain the occurrence of the summer bloom which is stronger along the west coast because of the effect of those winds. This suggests that the

south westerly monsoon and the trade wind easterlies both affect the phytoplankton blooms in the region.

Lévy et al. (2007) state that the thickness of the upwelled volume of water is shown by the time-cumulative vertical velocity and it can be seen that the upwelling is well spread over the whole northern part of Madagascar during the summer monsoon and mostly to the northwest of Madagascar during the winter monsoon (Figs 3.9 and 3.11). Similarly the MLD during the summer monsoon is deeper across the whole northern part of Madagascar than during the winter monsoon when it is shallower along the west coast than the east coast of northern Madagascar. It can further be seen that during the summer monsoon, there is more forcing by the SEC along 10^0-20^0 S (Fig. 1.6 (a)) than during the winter monsoon which is why only the northwest part of Madagascar is affected during the winter monsoon while during the summer monsoon the whole northern area is affected. The wind/current system during the summer monsoon deepens the mixed layer across the whole northern part of Madagascar, which produces a well spread bloom in that area. However, during the winter monsoon the northwest is most affected by these factors, thus producing a bloom that is restricted to the coasts and the northwest side of Madagascar. This shows that the blooms occurring in the summer and winter monsoons follow the same patterns as the horizontal currents, vertical velocity and mixed-layer depth patterns in the area.

The Fig. 3.6 shows that the SST and the Chl-*a* concentrations follow an inverse relationship from weeks 12-40, with Chl-*a* concentration increasing when the SST decreases. This relationship is confirmed by Table 3.2 which shows that the relationship between these variables varies between a weak and moderate negative relationship at a 95% confidence level. However, during weeks 4-12 SST and Chl-*a* do not have an inverse relationship, both Chl-*a* and SST are high: this is also the period of the winter monsoon bloom. The same pattern is followed across the years, forming an annual pattern in the relationship between SST and Chl-*a* concentration.

Southeast Madagascar, SEM (AREA 2)

The analysis of the Chl-*a* movie (not presented in this dissertation) made from the compilation of the weekly averaged Chl-*a* display images shows that two phytoplankton blooms occur in the Southeast Madagascar (SEM) region as mentioned by previous studies (e.g Ho et al. 2004); a bloom occurring annually between June-August and a second bloom occurring during January-April. The study of Srokosz et al. (2004), revealed the occurrence of a spring bloom in July-August in the southern Indian Ocean and a second bloom occurring during January-April along the southeast of Madagascar (22^0-30^0S). A bloom that spreads east into the Indian Ocean has been reported as a secondary phytoplankton bloom by Longhurst (2001) who suggested that it was caused by changes in the MLD that are controlled by the presence of eddies. Also, the southeasterlies being stronger during June-September (Hermes and Reason 2008) further explain this bloom since the strong southeasterlies drive the East Madagascar Current (EMC), bringing more nutrient rich water to the surface. Fig. 3.14 also shows that there is a seasonality in the occurrence of this bloom along the east coast (48^0-55^0E) where the bloom seems to occur at the beginning of the year; in some years the concentration is higher than in other years. Srokosz et al. (2004) suggest that this bloom which they call the "plankton wave" occurs in the opposite direction, moving towards the east while the other features such as eddies move towards the west. This bloom spreads rapidly due to the combination of the phytoplankton bloom growth and the effective diffusion caused by eddies. Apparently, the retroflection of the EMC south of Madagascar triggers this eastward spread of the bloom (de Ruijter et al. 2004, DiMarco et al. 2000). Srokosz et al. (2004) proposed that this eastward proliferation occurs firstly by coastal processes near Madagascar leading to faster phytoplankton growth. Secondly, the westward propagation of the bloom is prevented by the Madagascar Island and thirdly, given that the variability of eddies is greater in the east (~22^0-28^0S), the spread is restricted to the east and limited in the north-south directions.

The present study shows that the Chl-*a* concentration is strongest along the coast of SEM. According to DiMarco et al. (2000) the combination of anomalously strong wind-stress and frictional interaction between the western boundary EMC flowing southward and the continental shelf and slope might cause the upwelling along the southern part of Madagascar.

The EMC, being oriented along the bathymetry, explains why the Chl-*a* concentration is always strongest along the coast, which is because the wind-stress causes the transport of bottom water to be directed towards the left of the current (southern hemisphere) offshore thus causing upwelling on the shelf and the upwelling gets weaker when it moves offshore (DiMarco et al. 2000). Ho et al. (2004) also found that the upwelling that occurs during the austral summer and winter each year are caused by current and wind stress along the edges of the EMC in the east and the south.

Huhn et al. (2012) suggested that the presence of zonal jets in the South Indian Ocean Countercurrent (SICC), starting at ~25^{0}S and extending further east (~2500km) at the Southern tip of Madagascar, restricts the secondary bloom within a narrow zonal band and causes it to propagate to the east. The horizontal advection of these jets leads to a fast and persistent eastward transport of the bloom and the zonal jet-like Langrangian Coherent Structures (LCS) represent a transport barrier in the meridional direction that shapes the boundary of this bloom. It is also found that the Chl-*a* concentration and the SST across the SEM, display a negative relationship from weeks 15-40 since the Chl-*a* concentration is high when the SST is low. This relationship is further confirmed by the Table 3.4 which shows that the relationship between these variables varies between weak to moderate negative relationship at a 95% confidence level. However, during the weeks 1-14 the SST and the Chl-*a* do not follow an inverse relationship, the Chl-*a* concentration is high when the SST is high (Fig. 3.17). . Also, the same pattern is followed across the years, showing an annual pattern in the occurrence of the SST and Chl-*a* concentration. The Fig. 3.18 and 3.19 further show that the Chl-*a* concentration is high in regions of low SST that correspond to the presence of the cold core rings.

Mascarene Islands, MI (AREA 3)

The study of the SST and Chl-*a* concentration patterns along the Mascarene Islands area shows that there is only one phytoplankton bloom in the MI region during the summer monsoon and low Chl-*a* concentrations during the winter monsoon (Fig. 3.25). Also, Fig. 3.29 shows that there are more eddies during the summer monsoon, therefore more nutrients are brought to the surface which explains why the area is more productive then. According

to Wilson and Adamec (2001), there is a negative correlation between the SSH and chlorophyll; a higher SSH leads to the deepening of the thermocline which causes a reduction in the supply of nutrients to the euphotic zone. This supports our results, where the Chl-*a* concentration is higher when the SSH is lower (comparing Figs 3.29 and 3.30), indicating that the thermocline is pulled to the surface by the eddies present in that area during winter. This leads to an input of nutrients to the surface which in turn causes an increase in chlorophyll production.

Figs 3.29 and 3.30 further show that the SSH across the Mascarene Islands during the summer monsoon is lower than during the winter monsoon, explaining the occurrence of the bloom during summer. It is perceived that across the years, there is an annual pattern of alternating high and low Chl-*a* concentrations. The SST also displays a seasonal pattern, with high SST corresponding to the low Chl-*a* concentration period and vice versa. From Fig. 3.26 it can be seen that there is an inverse relationship between SST and Chl-*a* concentration. Weeks 20-34 display high Chl-*a* concentrations when the SST is low and weeks 1-15 and 41-46 show low Chl-*a* concentrations when SST is high. Figs 3.27 and 3.28 show that the Chl-*a* concentration is high in regions of low SST corresponding to the presence of the cold core rings. Table 3.6 demonstrates that there is a strong inverse relationship between these variables.

The Chl-*a* concentration in this area seems to be reduced compared to the other two study areas (NEM & SEM). Sarma et al. (1990) proposed that there are several small scale gyres that are entrenched in the extensive South Equatorial Current (SEC) system around the Mascarene Islands and these gyres exhibit a predominantly westward flow when the geostrophic circulation crosses the Seychelles-Mauritius ridge. Upwelling in that region occurs when a strong divergence on the leeward side is caused by the confrontation of this westward flowing current with the ridge. This shows that the MI area is only affected by the SEC current while the NEM and SEM areas are affected by the SEC splitting into the respective NEMC and SEMC at the east coast of Madagascar near 17^0S thus causing much more water to be displaced in those areas. Reduced production might also occur because the SSH in the region is higher than the other areas (Figs 3.11(b), 3.18 (b) and 3.29 (b)), suggesting that larger volumes of water need to be displaced in this region to bring nutrients

to the surface. From Fig. 1.5, it can be seen that the ocean is shallower around Madagascar (2000-4000m depth) compared to the Mascarene Islands area (depth >4000m), suggesting that nutrients might be available at shallower depths across the NEM and SEM areas compared to the MI area. Fig. 1.3 shows that across the Mascarene Islands there are more anti-cyclonic eddies than cyclonic eddies which also explains why that area is less productive compared to the 2 other areas (NEM & SEM) given that these anti-cyclonic eddies are warm core eddy rings with high SSH, implying less upwelling and thus less chlorophyll production.

CHAPTER 5 CONCLUSION

According to Woodberry et al. (1989) the basin-wide clockwise southern hemisphere (cyclonic) gyre which consists of the South Equatorial Current in the south, the South Equatorial Countercurrent in the north, and the East African Coastal Current in the west is the main distinctive property of the tropical Indian Ocean. The SST and Chl-*a* patterns are affected by these currents and from this study, it can be seen that the SEC is affecting the Chl-*a* and SST patterns across the three study areas namely Northeast Madagascar, Southeast Madagascar, and the Mascarene islands.

Previous studies have shown that there are two plankton blooms along the Tropical Band more precisely along 10^0-17^0S (e.g. Lévy et al. 2007). Study area 1 (10^0-18^0S) coincides with this band and also shows the occurrence of two blooms. Lévy et al. (2007) also mention that the summer and winter monsoons only affect the Indian Ocean north of 10^0S. However, we can see that this area (10^0-18^0S), is also affected by the summer and winter monsoons, and the two blooms occur at the same time as these events, showing that the summer and winter monsoons might also affect the Indian Ocean south of 10^0S. The occurrence of the blooms across the southeast of Madagascar (22^0-30^0S), appears to be caused by the tradewind southeasterlies. However, these blooms coincide with the monsoons; one during the summer monsoon and one during the winter monsoon. This suggests a remote or indirect effect of the monsoon on the blooms.

New et al. (2005) and Gallienne and Smythe-Wright (2005) indicated that the SEC creates a sharp boundary between the subtropical water masses from further south and further north when it passes through the Mascarene plateau, caused by its complex structure. Also, compared to the southern regions of the plateau, the SEC brings high levels of nutrients to the surface waters of the plateau's central and northern regions. Smythe-Wright et al. (2005) propose that the westward flowing current is restrained by the plateau, and the flow is forced through constricted gaps in the bottom topography to converge principally between the Nazareth and Saya de Malha Banks at 12–14^0S. This demonstrates that less water is displaced in the south, thus there is less mixing of nutrients into the uper layers and less Chl-

a production which explains why the Mascarene Islands' area, which encompasses the southern part of the Mascarene plateau is not as productive as the other two study areas.

According to Gallienne and Smythe-Wright (2005) the higher levels of nutrients and Chl-*a* at the northern end of the plateau are associated with the elevation of the thermocline and that the mixed-layer depth in the northern side is shallower (30m) than the southern side (100m). This shows that the southern side, which is part of the study area 3 (MI), is less productive than the northern side of the plateau given that the MLD is greater than the euphotic zone, so that phytoplankton cells spend much time mixed below the euphotic zone.

Finally, this study concludes that the north Indian Ocean (north of 10^0S) is not the only area that is affected by the summer and winter monsoons. The blooms occurring across the areas south of 10^0S may be directly influenced by the southeasterly tradewinds, with the monsoons playing an indirect role. However, further studies need to be done using wind data to confirm the exact effects of these winds on the blooms. Across NEM, the summer monsoon bloom is well spread over the area while the winter monsoon bloom is mostly coastal and of higher intensity than the bloom occurring during the summer monsoon. Across SEM, the summer monsoon bloom spreads from east to west while, the winter monsoon bloom spreads from west to east. The Mascarene Islands area is less productive with higher SSH and weaker eddies compared to the other areas. The MLD is deeper across the MI, thus less nutrients are injected into the euphotic zone. This study helps improve our understanding of the seasonal and interannual variability of the dynamics of the ADT and geostrophic velocities and SST and Chl-*a* and in these regions. Ultimately this should provide a basis for improved management of fishery resources using an ecosystem approach to fisheries in the region.

CHAPTER 6 REFERENCES:

Ali JR, Huber M. 2010. Mammalian biodiversity on Madagascar controlled by ocean currents. *Nature* 463: 653-656. doi:10.1038/nature08706.

Alvain S, Moulin C, Dandonneau Y, Bréon FM. 2005. Remote sensing of phytoplankton groups in case 1 waters from global SeaWIFS imagery. *Deep-Sea Research Part I: Oceanographic Research Papers* 52.

AVISO+. Satellite Altimetry Data. SSALTO/DUACS User Handbook: (M)SLA and (M)ADT Near-Real Time and Delayed Time Products. CLS-DOS-NT-06-034. 2015. Available at http://www.aviso.altimetry.fr/fileadmin/documents/data/tools/hdbk_duacs.pdf [accessed 25 July 2015].

Chandy JP, Al-Tisan I, Munshi HA, Ahd El Reheim H. 1991. Marine phytoplankton: A study on seasonal abundance and distribution in AL-JUBAIL. Technical Report No. SWCC (RDC) 17.

Conway DVP. 2005. Island-coastal and oceanic epipelagic zooplankton biodiversity in the southwestern Indian Ocean. *Indian Journal of Marine Sciences* 34(1): 50-56.

Crawford WR, Brickley PJ, Peterson TD, Thomas A. 2005. Impact of Haida eddies on chlorophyll distribution in the Eastern Gulf of Alaska. *Deep-Sea Research Part II: Topical Studies in Oceanography* 52: 975-989. doi:10.1016/j.dsr2.2005.02.011.

de Ruijter WPM, Van Aken HM, Beierc EJ, Johann RE, Lutjeharms JRE, Matanoc RP, Schouten MW. 2004. Eddies and dipoles around South Madagascar: formation, pathways and large-scale impact. *Deep-Sea Research Part I: Oceanographic Research Papers* 51: 383–400.

DiMarco SF, Chapman P, Nowlin WD. 2000. Satellite observation of upwelling on the continental shelf south of Madagascar. *Geophysical Research Letters* 27: 3965-3968.

Duncan RA, Backman J, Peterson LC.1990. $^{40}Ar/^{39}Ar$ Geochronology of basement rocks from the Mascarene Plateau, The Chagos Bank, and The Maldives Ridge. *Proceedings of the Ocean Drilling Program, Scientific Results,* 115: 43-51.

ETOPO2v2 (2006). Global gridded 2-minute database, national geophysical data center, national oceanic and atmospheric administration', U.S. Dept. of Commerce [accessed 12 May 2016].

European Commission DG Environment News Alert Service. 2010. Phytoplankton loss could spell disaster for marine ecosystems. Available at www.http://ec.europa.eu/environment/integration/research/newsalert/pdf/215na5_en.pdf [accessed 20 June 2014].

Fiedler PC, Talley LD. 2006. Hydrography of the eastern tropical Pacific: A review. *Progress in Oceanography* 69: 143–180.

Fisher RL, Johnson GL, Heezen BC. 1967. Mascarene Plateau Western Indian Ocean. [Abstract]. *The Geographical Society of America Bulletin* 78: 1247-1266.

Gallienne CP, Smythe-Wright D. 2005. Epipelagic mesozooplankton dynamics around the Mascarene Plateau and Basin, Southwestern Indian Ocean. *Philosophical Transactions of the Royal Society A* 363: 191–202. doi:10.1098/rsta.2004.1487.

Gao K, Helbling EW, Häder DP, Hutchins DA. 2012. Responses of marine primary producers to interactions between ocean acidification, solar radiation, and warming. *Marine Ecology Progress Series* 470: 167–189. doi: 10.3354/meps10043.

GlobalChange.gov. U.S. Global Change Research Program. Indicator: Ocean Chlorophyll Concentrations. Available at

http://www.globalchange.gov/browse/indicators/indicator-ocean-chlorophyll-concentrations [accessed 03 October 2015].

Hermes JC, Reason CJC. 2008. Annual cycle of the South Indian Ocean (Seychelles-Chagos) thermocline ridge in a regional ocean model. *Journal of Geophysical Research* 113: C04035. doi:10.1029/2007JC004363.

Ho CR, Zheng Q, Kuo NJ. 2004. SeaWiFs observations of upwelling south of Madagascar: long-term variability and interaction with East Madagascar Current. *Deep-Sea Research Part II: Topical Studies in Oceanography* 51: 59-67.

Hong L, Wang C, Zhou Y, Chen M, Liu H, Lin Z, Song X. 2012. The distribution of chlorophyll a in the tropical eastern Indian Ocean in austral summer. *Acta Oceanologica Sinica* 31: 146-159. doi: 10.1007/s13131-012-0244-6.

Huhn F, von Kameke A, Pérez-Muñuzuri V, Olascoaga MJ, Beron-Vera FJ. 2012. The impact of advective transport by the South Indian Ocean Countercurrent on the Madagascar plankton bloom. *Geophysical Research Letters* 39: L06602. doi: 10.1029/2012GL051246.

Interactive Media Center. Working with Windows Live Movie Maker. Available at http://library.albany.edu/imc/pdf/WindowsLiveMovieMaker.pdf [accessed 10 September 2015].

Jia F, Wu L, Qiu B. 2011. Seasonal modulation off eddy kinetic Energy and its Formation Mechanism in the Southeast Indian Ocean. *Journal of Physical Oceanography* 41: 657-665. doi:10.1175/2010jpo4436.1.

Kantha L, Clayson CA. 2003. Boundary Layers/ Ocean Mixed Layer. Available at www.http://curry.eas.gatech.edu/Courses/6140/ency/Chapter11/Ency_Atmos/BL_Ocean_Mixed_Layer.pdf [accessed 29 January 2015].

Lévy M, Klein P. 2004. Does the low frequency variability of mesoscale dynamics explain a part of the phytoplankton and zooplankton spectral variability? *Proceedings of the Royal Society A* 460: 1673-1683.

Lévy M, Shankar D, André JM, Shenoi SSC, Durand F, de Boyer Montégut C. 2007. Basin-wide seasonal evolution of the Indian Ocean's phytoplankton blooms. *Journal of Geophysical Research* 112, C12014. doi:10.1029/2007JC004090.

Longhurst A. 2001. A major seasonal phytoplankton bloom in the Madagascar Basin. *Deep-Sea Research Part I: Oceanographic Research Papers* 48: 2413-2422.

Lutjeharms JRE, Bang ND, Duncan CP. 1981. Characteristics of the currents east and south of Madagascar. *Deep-Sea Research Part A: Oceanographic Research Papers* 28: 879-899.

MathWorks. MATLAB. Available at http://www.mathworks.com/products/matlab/features.html [accessed 10 September 2015].

McDougall I. 1971. The Geochronology and evolution of the young oceanic island of Réunion, Indian Ocean. *Geochimica et Cosmochimica Acta* 35: 261-288.

McWilliams JC. 2013. The Nature and Consequences of Oceanic eddies. In: Hecht MW and Hasumi H (eds), *Ocean Modelling in an Eddy Regime*. American Geophysical Union, Washington, D.C., USA. pp 5-15. doi:10.1029/177GM03.

MODIS, NASA. Available at http://modis.gsfc.nasa.gov/about/design.php [accessed 7 September 2014].

Monticelli D, Ramos JA, Quartly GD. 2007. Effects of annual changes in primary productivity and ocean indices on the breeding performance of tropical roseate terns in the western Indian Ocean. *Marine Ecology Progress Series* 351: 273-286. doi:10.3354/meps07119.

Morrow R, Birol F, Griffin D, Sudre J. 2004. Divergent pathways of cyclonic and anti-cyclonic ocean eddies. *Geophysical Research Letters* 31: L24311. doi:10.1029/2004gl020974.

Narvekar J, Kumar SP. 2014. Mixed layer variability and chlorophyll a biomass in the Bay of Bengal. *Biogeosciences* 11: 3819–3843. doi:10.5194/bg-11-3819-2014.

New AL, Stansfield K, Smythe-Wright D, Smeed DA, Evans AJ, Alderson SG. 2005. Physical and biochemical aspects of the flow across the Mascarene Plateau in the Indian Ocean. *Philosophical Transactions of the Royal Society A* 363: 151-168.

Newell GE, Newell RC. 1977. Marine plankton: A practical guide (5th edn). London: Hutchinson Educational Ltd.

Ocean Color Forum, NASA. Available at http://oceancolor.gsfc.nasa.gov/forum/oceancolor/topic_show.pl?tid=4024 [accessed 7 September 2014].

OceanColor WEB, NASA. Products Definitions. Available at http://oceancolor.gsfc.nasa.gov/cms/products# [accessed 7 September 2014].

Pennington JT, Mahoney KL, Kuwahara VS, Kolber DD, Calienes R, Chavez FP. 2006. Primary production in the eastern tropical Pacific: A review. *Progress in Oceanography* 69: 285–317. doi:10.1016/j.pocean.2006.03.012.

Physical Oceanography Distributed Active Archive Center (podaac), NASA. Available at http://podaac.jpl.nasa.gov/SeaSurfaceTemperature [accessed 7 September 2014]

Qasim SZ. 1999. Some Unique characteristics of the Indian Ocean. *Qatar University Science Journal* 19: 11-116.

Quartly GD, Buck JJH, Srokosz MA, Coward AC. 2006. Eddies around Madagascar- The retroflection re-considered. *Journal of Marine Systems* 63: 115-129.

Raymont JEG. 1980. Plankton and Productivity in the Oceans (2nd edn). Volume I: Phytoplankton. Pergamon Press.

Reynolds CS. 2006. The Ecology of Phytoplankton. The Edinburgh Building, Cambridge CB2 2RU, UK: Cambridge University Press.

Saji NH, Goswami BN, Vinayachandran PN, Yamagata T. 1999. A dipole mode in the tropical Indian Ocean. *Nature* 401: 360–363.

Sarma YVB, Gopala Krishna VV, Rao DP, Sastry JS. 1990. Thermohaline circulation and water characteristics around Mauritius group of islands. *Indian Journal of Marine Sciences* 19: 196-200.

Schott FA, McCreary Jr JP. 2001. The monsoon circulation of the Indian Ocean. *Progress in Oceanography* 51: 1-123.

Schott FA, Dengler M, Schoenefeldt R. 2002. The shallow overturning circulation of the Indian Ocean. *Progress in Oceanography* 53: 57-103.

Schott FA, Xie SP, McCreary Jr JP. 2009. Indian Ocean circulation and climate variability. *Reviews of Geophysics* 47: RG1002. doi: 10.1029/2007RG000245.

Schouten MW, de Ruijter WPM, van Leeuwen PJ, Ridderinkhof H. 2003. Eddies and variability in the Mozambique Channel. *Deep-Sea Research Part II: Topical Studies in Oceanography* 50: 1987-2003.

Shankar D, Vinayachandran PN, Unnikrishnan AS. 2002. The Monsoon Currents in the North Indian Ocean. *Progress in Oceanography* 52: 63-120. doi:10.1016/S0079-6611(02)00024-1.

Smythe-Wright D, Boswell SM, Lucas CH, New AL, Varney MS. 2005. Halocarbon and dimethyl sulphide studies around the Mascarene Plateau. *Philosophical Transactions of the Royal Society A* 363: 169–185. doi:10.1098/rsta.2004.1485.

Sorokin YU-I, Sorokin YU-P, Zakouskina YU-O. 2003. Microplankton and its function in a zone of shallow hydrothermal activity: the Craternaya Bay, Kurile Islands. *Journal of Plankton Research* 25: 495-506.

Srokosz MA, Quartly GD, Buck JJH. 2004. A possible plankton wave in the Indian Ocean. *Geophysical Research Letters* 31: L13301. doi: 10.1029/2004GL019738.

Stramski D, Reynolds RA, Kahru M, Mitchell BG. 1999. Estimation of Particulate Organic Carbon in the Ocean from Satellite Remote Sensing. *Science* 285: 239-242. DOI: 10.1126/science.285.5425.239.

Sverdrup HU. 1947. Wind-driven currents in a baroclinic ocean; with application to the equatorial currents of the eastern pacific. *Geophysics* 33: 318-326.

Sverdrup HU. 1953. On Conditions for the Vernal Blooming of Phytoplankton. *Journal du Conseil / Conseil Permanent International pour l'Exploration de la Mer* 18: 287-295.

Thomas DN. 2013. Phytoplankton Growth – Literature for the basics. Bangor University, U.K. and Finnish Environment Institute, Helsinki, Finland. Available at http://www.mathclimate.org/sites/default/files/DavidThomas-PhytoplanktonGrowth.pdf [accessed 13 June 2014].

Tomczak M, Godfrey JS. 2003. Regional Oceanography: An Introduction (2nd edn). Delhi: Daya Publication House.

Vaulot D. 2006. Phytoplankton. *Encyclopedia of Life Sciences*. Available at http://sb-roscoff.fr/Phyto/Reprints/Vaulot_ELS_01.pdf [accessed 5 July 2014].

Volkov DL, Lee T, Fu LL. 2008. Eddy-induced meridional heat transport in the ocean. *Geophysical Research Letters* 35: L20601. doi:10.1029/2008gl035490.

Wiggert JD, Murtugudde RG, Christian JR. 2006. Annual ecosystem variability in the tropical Indian Ocean: Results of a coupled bio-physical ocean general circulation model. *Deep-Sea Research Part II: Topical Studies in Oceanography* 53: 644–676. doi:10.1016/j.dsr2.2006.01.027.

Wikipedia. Microsoft Excel. Available at: https://en.wikipedia.org/wiki/Microsoft_Excel [accessed 10 September 2015].

Wilson C, Adamec D. 2001. Correlations between surface chlorophyll and sea surface height in the tropical Pacific during the 1997–1999 El Niño-Southern Oscillation event. *Journal of Geophysical Research* 106: NO. C12, 31175–31188.

Woodberry KE, Luther ME, O'Brien JJ. 1989. The wind-driven seasonal circulation in the southern tropical Indian Ocean. *Journal of Geophysical Research* 94: No. C12, 17985–18002.

Xie SP, Annamalai H, Schott FA, McCreary Jr JP. 2002. Structure and Mechanism of South Indian Ocean Climate Variability. *Journal of Climate* 15: 864-878.

Zhang Z, Wang W, Qiu B. 2014. Oceanic Mass transport by mesoscale eddies. *Science* 345: 322-324. doi: 10.1126/science.1252418.

Zheng S, Du Y, Li J, Cheng X. 2015. Eddy Characteristics in the South Indian Ocean as inferred from surface drifters. *Ocean Science* 11: 361-371.

CHAPTER 7 APPENDIX

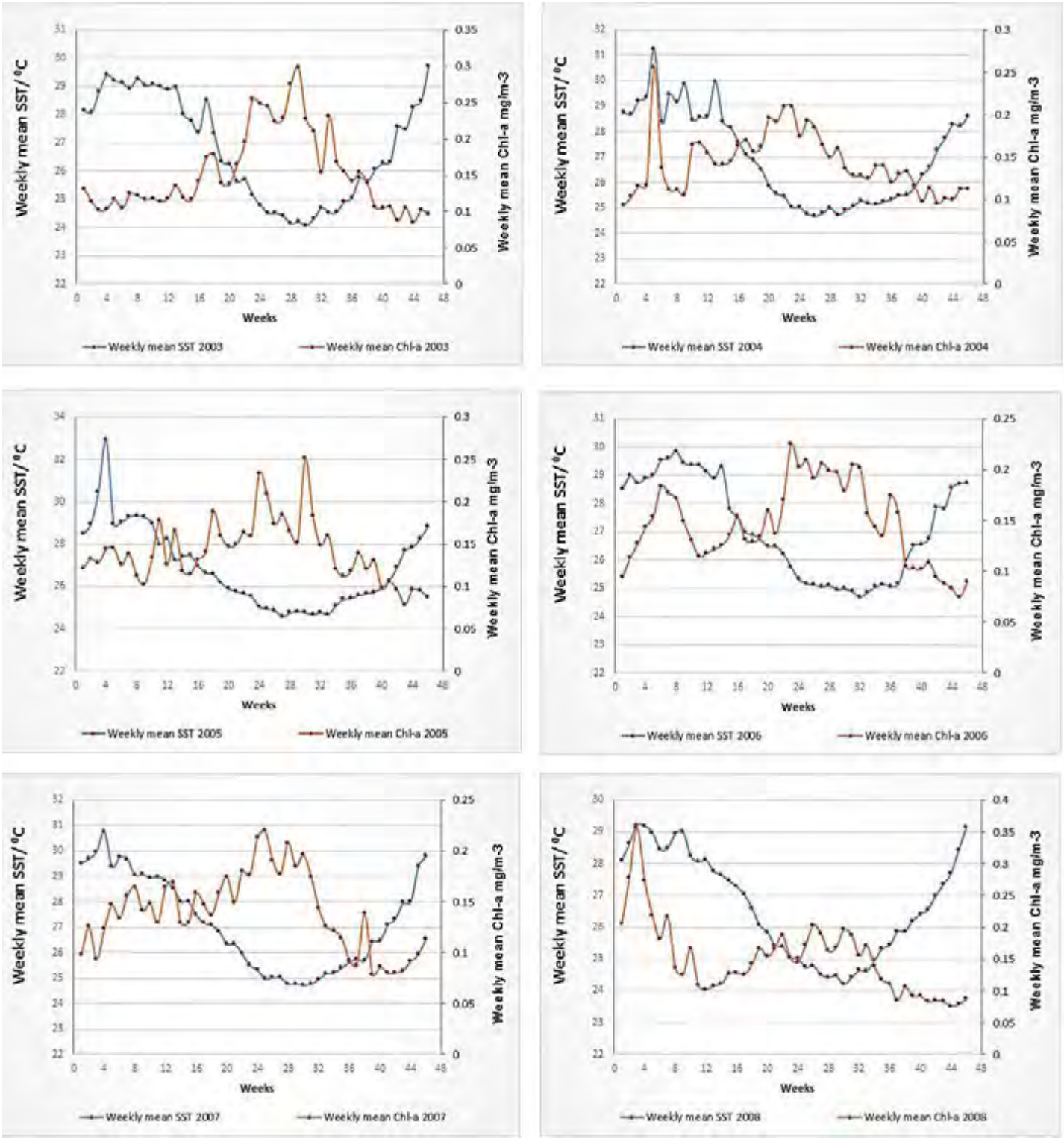

Figure A.7. Time series for the weekly Chl-a and weekly SST climatology for 2003-2008 for study Area 2 (Southeast Madagascar).

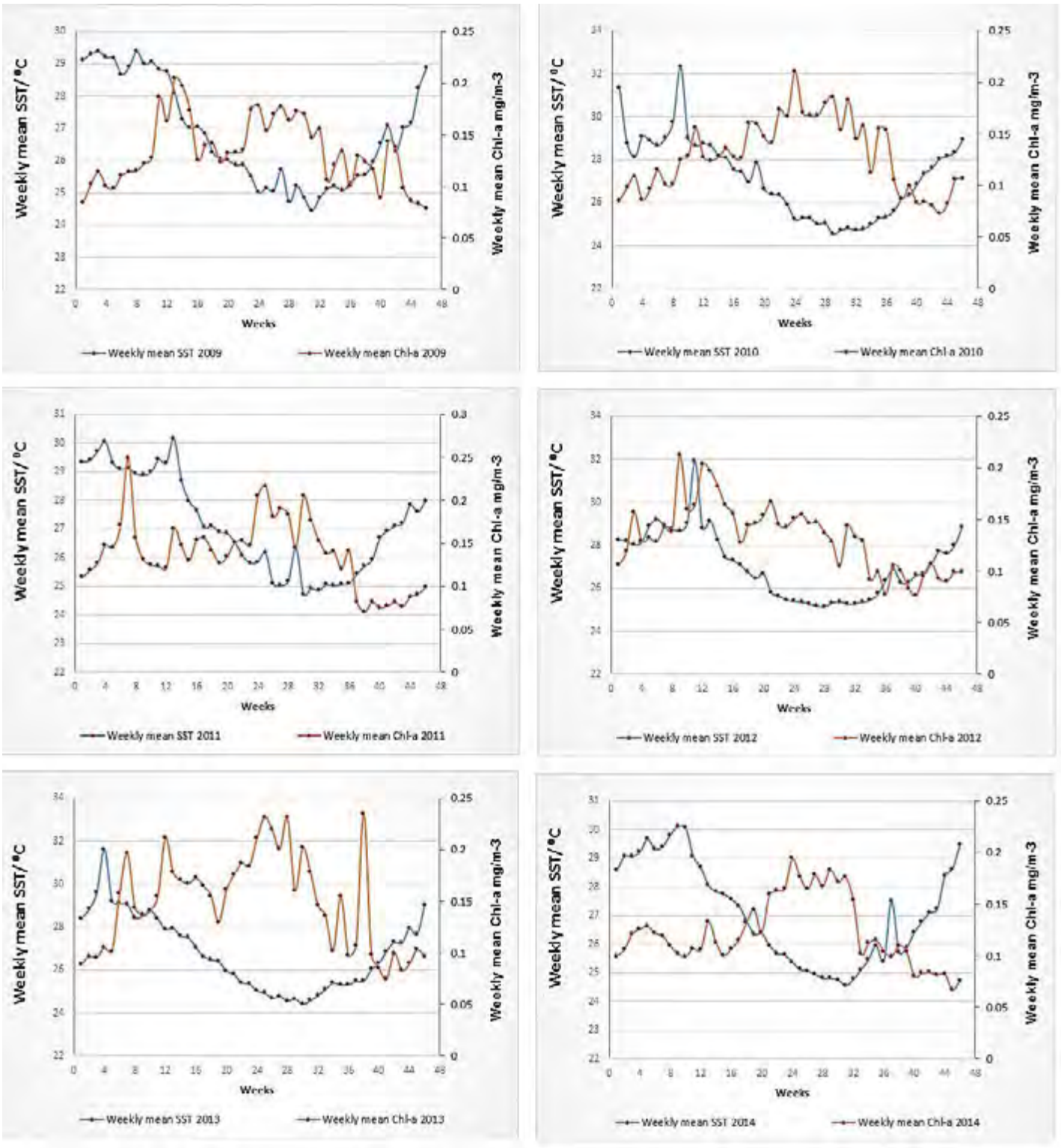

Figure A.8. Time series for the weekly Chl-a and weekly SST climatology for 2009-2014 for study Area 2 (Southeast Madagascar).